

# Development, Investigation, and Optimization of an Electrothermal Vaporization Unit with an Axially Focusing Convection Upstream for Analysis of Trace Elements

Inaugural-Dissertation  
zur Erlangung des Doktorgrades  
der Naturwissenschaften  
der Justus-Liebig-Universität Gießen  
Fachbereich 07 / Mathematik und Informatik, Physik, Geographie

vorgelegt von  
Alexander Trenin  
aus Kasan, Russische Föderation

I. Physikalisches Institut der Justus-Liebig-Universität Gießen  
Juni 2006

---

## Contents

---

<b>CONTENTS.....</b>	<b>2</b>
<b>SUMMARY.....</b>	<b>5</b>
<b>ZUSAMMENFASSUNG.....</b>	<b>10</b>
<b>LIST OF ABBREVIATIONS.....</b>	<b>16</b>
<b>1. INTRODUCTION AND PROBLEM STATEMENT.....</b>	<b>17</b>
<b>2. EXPERIMENTAL.....</b>	<b>24</b>
2.1 ETV-AFC INSTRUMENTATION.....	24
2.1.1 Principle .....	24
2.1.2 Construction and flow scheme.....	25
2.1.3 Temperature monitoring.....	27
2.1.4 External generator of gaseous additives to the internal flow .....	27
2.2 EXPERIMENTAL ARRANGEMENT.....	28
2.2.1 Experimental arrangement for intra-furnace ETV sampling.....	28
2.2.2 Principle of CFS spectrometry .....	29
2.2.3 Software for ETV-EP CS-CFS measurement controlling and data acquisition.....	31
2.2.4 Software for CS-CFS spectra evaluation.....	32
2.3 AEROSOL TRANSPORT, DIVIDING, AND DOSING .....	33
2.3.1 Principle .....	33
2.3.2 Electrostatic sampling.....	37
2.4 SAMPLES AND REAGENTS .....	38
2.5 OPERATIVE PARAMETERS AND PROCEDURES.....	39
2.5.1 Sample analysis with intra-furnace EP .....	39
2.5.2 Sample analysis with external 10-fold precipitation unit .....	40
2.5.3 Sample analysis with addition of aqueous and gaseous modifiers .....	40
2.5.4 Determination of analyte TEs.....	41
2.5.5 SEM and TEM investigations .....	42
2.5.6 Temperature measurements in the upstream .....	42
2.5.7 Determination of GF carbon losses.....	42
<b>3. INVESTIGATION AND OPTIMIZATION OF THE ETV-AFC SETUP: INFLUENCES OF GF CARBON, MODIFIERS, AND GASEOUS ADDITIVES ON THE TRANSPORT PROCESS OF SAMPLE ANALYTES.....</b>	<b>44</b>

3.1	ETV DEVELOPMENT .....	44
3.1.1	<i>Axially focusing convection (AFC) tube</i> .....	44
3.1.2	<i>Radiation shielding</i> .....	45
3.1.3	<i>Comparison of analytical performances for ETV-FT and ETV-AFC instruments</i> .....	47
3.2	OPTIMIZATION AND CONTROLLING OF THE GF HEATING CONDITIONS.....	48
3.3	OPTIMIZATION OF THE ETV FLOW DISTRIBUTION .....	50
3.4	MEASUREMENT OF TEMPERATURE DEPENDENCES ON THE AXIS OF THE AFC TUBE.....	51
3.5	INVESTIGATION OF THE INFLUENCE OF GF CARBON ON ANALYTE TE .....	57
3.6	SEM AND TEM INVESTIGATION OF GF CARBON PARTICLES .....	62
3.7	MODIFIER EFFECTS.....	66
3.7.1	<i>Determination of analyte TEs with addition of K, Mg, and Pd modifiers</i> .....	66
3.7.2	<i>Determination of analyte TEs with C<sub>6</sub>H<sub>12</sub> addition to the ETV internal gas flow</i> .....	68
3.7.3	<i>Determination of analyte TEs by combined use of C<sub>6</sub>H<sub>12</sub>, KNO<sub>3</sub> and Pd(NO<sub>3</sub>)<sub>2</sub></i> .....	70
3.7.4	<i>Behavior of the corona discharge current in presence of C<sub>6</sub>H<sub>12</sub></i> .....	75
<b>4.</b>	<b>PLATFORM-TO-PLATFORM SAMPLE TRANSFER, DILUTION, DISTRIBUTION, AND DOSING VIA ELECTROTHERMAL VAPORIZATION AND ELECTROSTATIC DEPOSITION .....</b>	<b>78</b>
4.1	PRECISION AND REPRODUCIBILITY OF MEASUREMENTS .....	79
4.2	FURTHER APPLICATIONS OF THE 10-FOLD PRECIPITATION UNIT .....	81
<b>5.</b>	<b>COMPUTER MODELING OF THE DYNAMICS OF SAMPLE ANALYTES AND GRAPHITE FURNACE CARBON IN THE AXIALLY FOCUSING CONVECTION UPSTREAM.....</b>	<b>83</b>
5.1	CONDENSATION PROCESSES .....	83
5.1.1	<i>Homogeneous analyte condensation</i> .....	83
5.1.2	<i>Heterogeneous analyte condensation</i> .....	84
5.2	KINETIC MODEL .....	86
5.2.1	<i>Rate of the carbon condensation process</i> .....	87
5.2.2	<i>Rate of the analyte condensation process</i> .....	89
5.2.3	<i>Attachment function</i> .....	90
5.2.4	<i>Analyte distribution function</i> .....	91
5.2.5	<i>Temperature dependence of the gas phase diffusion coefficients</i> .....	93
5.2.6	<i>Estimation of evaporation rates for analytes and carbon</i> .....	94
5.3	RESULTS AND DISCUSSION .....	96
5.3.1	<i>Carbon condensation</i> .....	97
5.3.2	<i>Analyte dynamics without condensation</i> .....	102
5.3.3	<i>Analyte dynamics with condensation</i> .....	102
5.3.4	<i>Influence of modifiers on analyte condensation</i> .....	109
5.3.5	<i>Comparison with experimental data</i> .....	109
<b>6.</b>	<b>CONCLUSIONS .....</b>	<b>112</b>
	<b>APPENDIX .....</b>	<b>116</b>

---

A.1	LIST OF FIGURES .....	116
A.2	LIST OF TABLES .....	121
A.3	CS-CFS SPECTRA EVALUATION SOFTWARE .....	122
A.4	ESTIMATIONS OF ANALYTE, MODIFIER, AND CARBON VAPOR SATURATIONS .....	125
<b>REFERENCES .....</b>		<b>126</b>
<b>LIST OF PUBLICATIONS .....</b>		<b>137</b>
<b>CURRICULUM VITAE .....</b>		<b>143</b>
<b>DANKSAGUNG .....</b>		<b>144</b>

---

## Summary

---

Flame and plasma based analytical techniques (e.g. flame atomic absorption and optical emission spectrometry, inductively coupled plasma optical emission and mass spectrometry) used for analysis of trace elements are originally designed for liquid sampling. However, samples submitted for analysis are often solids and need preliminary chemical decomposition. Decomposition methods (e.g. dry ashing and chemical digestion) are time-consuming and can lead to systematic and statistic errors with degradation of overall accuracy and precision of the measurements. There have been many attempts to adapt the techniques for direct analysis of solids by means of sample nebulization in the form of slurries and suspensions. However, nebulization has shown very low sample introduction efficiency and provides particles, which are then difficult to dissociate owing to their short residence times in the flame or plasma. The latter results in lower atomization efficiency and requires calibration against solid standards in equivalent matrices. Availability of solid reference materials is severely limited and makes this approach not always applicable.

Electrothermal atomization (ETA) in a graphite furnace (GF) is inherently more suitable for direct analysis of solid and liquid samples. With several commercially available and specifically designed instruments, samples can be directly introduced in the GF and then atomized under optimized operating conditions according to a stabilized temperature platform furnace concept with high efficiency. The method often allows calibration against aqueous standards but shows statistic errors caused by sample inhomogeneities as well as systematic errors caused by matrix effects.

A most powerful approach to avoid the problems with employing sample nebulization is electrothermal vaporization (ETV) of sample analytes and introduction of the aerosol formed by re-condensation into an analytical instrument. Compared with other sampling techniques, the ETV sampling offers exceptional advantages. Samples can be introduced into the ETV directly as solids or liquids, the sample preparation time and numerous possible risks of sample contamination and of analyte loss prior to analysis are reduced, and finally the ETV can be employed as an external sample pretreatment tool. Thus, the solvent and major components of the sample matrix are first externally removed by drying and pyrolysis and then the residual analytes are vaporized and transported by the argon flow where its condensation and aerosol formation occurs while being cooled down. The ETV sampling provides higher ana-

lyte transport efficiencies (TEs) to the analytical instrument than by nebulization and often enables calibration against liquid standards.

Different commercially available or specifically designed ETV units with vapor outlet through one of the ends of the GF tube (end-on flow-through ETV) have been initially used. Such ETV units have shown relatively low analyte TEs with pronounced dependence on element volatility. Volatile elements were transported with about two times higher efficiency than elements of lower volatility. Detailed investigations have shown that the major analyte losses occur owing to deposition on the colder outlet end of the GF tube. There have been many attempts to reduce the losses by means of construction modifications to obtain earlier cooling bypass gas admixture but they have given only moderate enhancement of analyte TEs. Then, upstream ETV configurations with the gas entering the furnace through its ends and flowing upwards through the hole in the GF tube center were employed to prevent the earlier analyte losses. These constructions have shown higher TEs with reverse dependence on element volatility. The analyte vapor in the upstream ETV units is released into a larger volume of a condensation chamber above the GF outlet hole. Thus, owing to the high buoyant force, the upstream velocity in the large gas volume becomes very fast that results in formation of whirls and turbulences leading to analyte deposition on colder walls.

The application of chemical modifiers for matrix separation and sensitivity enhancement is well established in GF atomic absorption spectrometry (GFAAS). In ETV sampling, matrix/carrier modifiers are a means to improve formation of a transportable aerosol and, thereby, to obtain higher and more homogeneous TEs. Generally, the modifier effect is to be explained due to co-vaporization of sample analytes with carrier forming constituents. Commonly used sample/carrier modifiers are  $\text{Pd}(\text{NO}_3)_2$ ,  $\text{Mg}(\text{NO}_3)_2$ ,  $\text{NaCl}$ ,  $\text{MgCl}_2$ , citric acid, and salt mixtures. Gaseous modifiers – mainly carbon-containing gases such as toluene, carbon tetrachloride, and freon – have been added to the ETV transport gas flow to enhance the TEs.

In our laboratory, investigations of analyte TEs using an end-on flow-through ETV unit based on the commercially available GF have been carried out. TEs have been determined using a laboratory made electrothermal atomization continuum source coherent forward scattering multielement spectrometer coupled to the ETV unit. The ETV generated aerosols have been quantitatively collected by means of electrostatic precipitation (EP) on the L'vov platform of the spectrometer as well as on external sample collectors. TEs of up to 19% for Cu, 21% for Fe and Mn, and 36% for Pb from the ETV boat to the L'vov platform of the

HGA-600 furnace have been obtained for the standard reference materials (BCR CRM 281, BCR CRM 189, and NIST SRM 1567) as well as for multielement standard solutions containing approximately the same element ratios as certified for the solid samples [Ber1, Ber2, Buc2]. Low analyte TEs and high dependence on analyte volatility motivated the scientific group to design a novel ETV unit with upstream configuration. The aim was to reduce the absolute analyte losses because their differences became reduced as well. Higher and more homogeneous TEs can be achieved by releasing the hot upstream into a narrow vertical convection tube (12-13 mm inner diameter) to prevent a counter flowing downstream at the tube walls leading to turbulences and analyte losses. This led to formation of a velocity profile with the hot outlet upstream on the axis of the convection tube where the analyte condensation occurs mainly apart from the colder walls. This design was designated as ETV with an axially focusing convection (AFC).

This work deals with further development, optimization, and investigation of the laboratory designed ETV-AFC unit. At the beginning of the work, TEs up to 25% for Ag, 27% for Pb, 30% for Mn, 25% for Cu, 31% for Fe, and 33% for Ni have been determined. The initially used quartz AFC tube has been sweated from the bottom through the GF radiation heating. An attempt to shield the tube with a tantalum sheet has led to its deformation and destroying. Then, a 7 mm thick copper shielding plate with sufficient heat capacity was mounted at a height of approximately 2.5 mm above the GF tube to one of the water-cooled copper flanges holding the graphite cones to cool off the plate between the ETV firings. Along with the use of the glass AFC tube, it allowed a significant increase of the axial temperature gradients above the GF outlet. Owing to this improvement, TEs up to 44% for Pb, 54% for Mn, 45% for Cu, 55% for Fe, and 59% for Ni were determined. To achieve more effective cooling of the upstream directly above the GF outlet, a 10 mm thick shielding plate with a ring slit for the admixture of a cold sluice gas to the upstream was mounted at the same height. With these means, TEs up to 48% for Ag, 51% for Pb, 60% for Mn, 53% for Cu, 68% for Fe, and 64% for Ni can be achieved. Temperature dependences on the axis of the AFC tube were measured using a rapid thermocouple and employed for the simulation of the condensation process.

Increasing TEs with the ageing of the pyrolytically coated GF tube were observed in this work. This effect was ascribed to the growing content of carbon particles released from older tubes. The tube losses during a single heating cycle (8 s, 2600°C) are in the range of 70-120 µg and increase up to 250 µg near the end of the tube lifetime. An estimate of the density

of C-vapor released from the tube showed high supersaturation already inside the GF, i.e. inside the tube the carbon is likely found as C-multimers and larger structures. SEM micrographs showed relatively large carbon particles already within the GF tube. At 2.5 mm above the GF outlet, SEM micrographs showed higher densities of larger C-particles. At 2.25 cm, SEM and TEM micrographs showed large amounts of carbon particulates with diameters around 10 nm, which begin to form chains and web-like structures. Thus, the analyte atoms are found in the environment of carbon particulates with higher density and significantly larger sizes. Thus, the work concludes that for typically used analyte contents (pico- and nanogram amounts) the condensation of the analyte atoms occurs mainly heterogeneously on carbon particulates before the analyte vapor achieves supersaturation via cooling. Hence, the homogeneous particle formation concept [Kan1], which is often used for larger analyte contents, is not applicable under ETV-AFC operating conditions.

Based on the heterogeneous particle formation concept, the condensation problem is numerically simulated for GF carbon and for six analytes of different volatilities Ag, Cu, Fe, Ni, Mn, and Pb. In the model, the measured temperature dependences within the AFC tube are used, the diffusion of the analyte atoms is taken into account, and the diffusion of the heavier carbon particles is neglected. The temperature dependence of the probability that a colliding analyte atom will be adsorbed by a carbon particle is described using an attachment function, which is formulated as a function of the analyte pretreatment temperature used by GFAAS with a statistical broadening of 15%. At the pretreatment temperature, the first losses of the analyte can occur in the GF. The calculated TEs are 45% for Ag, 43% for Pb, 55% for Mn, 51% for Cu, 67% for Fe, and 65% for Ni. The model shows a good agreement with the experimental data and reflects the dependence of the TEs on the analyte volatility.

The use of K and Pd modifiers added in microgram amounts in nitric acid solutions into the ETV boat increases the TE of volatile analytes. Addition of K results in TE increasing for Pb and Mn by about 5%. The acting of K as an analyte carrier is excluded because K begins to form particles by homogeneous condensation much later than the analytes.  $K^+$  ions and compounds may rather speed up the nucleated condensation of carbon. With addition of  $Pd(NO_3)_2$  modifier, higher and more homogeneous TEs for analytes of different volatilities are determined 63% for Pb, 62% for Mn, 69% for Fe, and 64% for Ni. The increase is achieved via co-vaporization of analyte atoms with higher carbon density. In the model, the modifier effect is taken into account via using higher pretreatment temperatures in the attach-



ment function. The calculated TEs are in good agreement with the experimental values: 61% for Pb, and 67% for Mn, 67% for Fe, and 65% for Ni. The combined use of  $\text{KNO}_3$  and  $\text{Pd}(\text{NO}_3)_2$  modifiers with  $\text{C}_6\text{H}_{12}$  (cyclohexane) added to the internal flow of the ETV unit results in significant enhancement of the TEs: 91% for Ag, 86% for Pb, 81% for Cu, 94% for Fe, and 90% for Ni.

In the context of an international research cooperation, a novel system for sample transfer, distribution, dilution, and dosing has been developed and investigated. The system combines the potential of the ETV-AFC unit as a sample pretreatment and introduction tool, possibilities of diluting, distributing, and dosing of the generated aerosols as gas carried slurries, and quantitative re-collection of the aerosol on one or a set of secondary boats by means of EP. Integration of these advantages provides a better way of coping with the problems associated with solid sampling. A primary solid sample can be weighed into the ETV boat in higher amounts in order to reduce dosing errors and effects caused by inhomogeneities of the sample, and thereby, to obtain higher precision and accuracy of the measurements. Due to the controlled splitting of the aerosol, the analyzed amount can be adapted to the dynamic range of the spectrometer. In addition, a set of platforms with equal analyte compositions from the same individual primary sample can be produced. Such multitudes are suited for control and supplementary measurements. The relative standard deviation (RSD) of the measurements with aerosol splitting into two sub-flows in 1:9 ratio is less than 5% (for  $n=4-5$  repetitions). The overall RSD for the measurements with 10-fold precipitation unit is below 12% ( $n=10$  platforms). Analyte compositions on secondary platforms are measured with a second ETV-EP process with intra-furnace deposition that results in the higher RSD.

---

## Zusammenfassung

---

Auf Flammen und Plasmen basierende analytische Verfahren, die zur Analyse von Spurenelementen geeignet sind, wie z.B. Flammenatomabsorptionsspektrometrie, optische Emissions- und Massenspektrometrie mit induktiv gekoppeltem Plasma, wurden ursprünglich für flüssige Proben entwickelt. Die zur Analyse verwendeten Proben sind oft jedoch in festem Zustand und benötigen somit eine vorausgehende chemische Behandlung. Behandlungsmethoden (wie beispielsweise trockene Veraschung und chemischer Aufschluß) sind zeitaufwendig und können zu systematischen und statistischen Fehlern führen, wodurch die Präzision und Richtigkeit der Messungen beeinträchtigt wird. Zahlreiche Versuche wurden unternommen, um die Verfahren zur direkten Analyse von Feststoffen anzupassen, etwa durch Zerstäubung der Probe in der Form von Aufschlammungen und Suspensionen. Die Zerstäubung zeigt oft jedoch sehr geringe Zufuhreffizienz, wobei die zugeführten Probenpartikel wegen der kurzen Aufenthaltsdauer im Plasma oder der Flamme schwer zu dissoziieren sind. Letzteres führt zur Minderung der Atomisierungseffizienz und erfordert eine Kalibrierung gegen Feststoffe in äquivalenten Matrices. Die Verfügbarkeit von festen Standardreferenzmaterialien ist begrenzt und macht dies nicht immer anwendbar.

Elektrothermische Atomisierung (ETA) in einem Graphitrohrfurnen ist zur direkten Analyse von festen und flüssigen Proben mehr geeignet. Mit einigen kommerziell verfügbaren als auch speziell für dieses Verfahren entwickelten Geräten können Proben direkt ins Graphitrohr eingeführt und anschließend unter optimierten Bedingungen (gem. Stabilized Temperature Platform Furnace, STPF-Konzept) mit hoher Effizienz atomisiert werden. Diese Methode erlaubt oft eine Kalibrierung gegen wässrige Lösungen, zeigt aber statistische Fehler, die durch Inhomogenitäten der Probe verursacht werden.

Das stärkste Verfahren, um die mit der Zerstäubung verbundene Problematik zu umgehen, ist die elektrothermische Verdampfung (ETV) von Probenanalyten und die Zuführung von dem durch Rekondensation entstehenden Aerosol in das Analysegerät. Verglichen mit anderen Probeneingabemethoden bietet die ETV-Probeneingabe außerordentliche Vorteile. Proben können sowohl in flüssiger als auch in fester Form direkt in die ETV-Einheit eingeführt werden. Die Probenvorbehandlungszeit und zahlreiche Risiken der Probenkontamination und der Analytverlust vor der Analyse sind geringer. Schließlich kann die ETV-Einheit auch als externe Vorbehandlungseinrichtung verwendet werden. Dadurch werden das Lö-

sungsmittel und wesentliche Teile der Probenmatrix zunächst extern durch Trocknen und Pyrolyse entfernt. Danach werden die verbleibenden Analyte verdampft und im Argonstrom zum Analysegerät transportiert, wobei die Kondensation und Aerosolbildung bei der Abkühlung erfolgt. Das ETV-Verfahren bietet höhere Transporteffizienzen zum Analysegerät im Vergleich zur Zerstäubung und oftmals ermöglicht eine Kalibrierung gegen wässrige Lösungen.

Unterschiedliche kommerziell verfügbare oder speziell entwickelte ETV-Anordnungen mit Analytdampfauslass durch eines der Enden des Graphitrohres wurden ursprünglich verwendet („End-on Flow-Through Prinzip“). Solche Anordnungen zeigten relativ geringe Transporteffizienzen der Analyten. Sie sind zudem sehr stark von der Volatilität des jeweiligen Elementes abhängig. Volatile Elemente werden mit einer etwa doppelt so hohen Effizienz transportiert als schwer volatile Elemente. Detaillierte Untersuchungen haben gezeigt, dass erhebliche Analytverluste am kälteren Auslass des Graphitrohres erfolgen. Es wurden zahlreiche Versuche unternommen, die Verluste durch frühes Vermischen mit kühlenden Beipassgasen zu reduzieren, diese lieferten aber eine nur mäßige Verbesserung der Transporteffizienz. Später wurden Upstream-ETV-Anordnungen verwendet, bei denen das Transportgas durch die Enden des Graphitrohres eintritt und durch das Loch in der Rohrmitte austritt, um frühe Analytverluste zu vermeiden. Diese Konstruktionen zeigten höhere Transporteffizienzen mit umgekehrter Abhängigkeit von der Volatilität. Der Analytdampf in den Upstream-Anordnungen gelangt in ein größeres Volumen der Kondensationskammer oberhalb des Auslasses des Graphitrohres. Der größte Nachteil dieser Anordnung besteht darin, dass wegen des starken Auftriebs die Konvektionsgeschwindigkeit sehr hoch wird, was zur Verwirbelung und zu Turbulenzen und somit zur Deposition des Analyten an den kälteren Wänden führt.

Die Verwendung von chemischen Modifiern zur Ermöglichung höherer Vorbehandlungstemperaturen zur besseren Matrixabtrennung und Sensitivitätssteigerung ist ein etabliertes Verfahren in der Atomabsorptionsspektrometrie (AAS). Beim ETV-Verfahren werden Modifier verwendet, um die Bildung von transportierbarem Aerosol zu steigern und somit höhere und von der Volatilität weniger abhängige Transporteffizienzen zu erhalten. Im Allgemeinen wird der Modifier-Effekt durch Kovaporisierung der Probenanalyten und der Trägerkonstituenten erklärt. Gebräuchliche Modifiern sind  $\text{Pd}(\text{NO}_3)_2$ ,  $\text{Mg}(\text{NO}_3)_2$ ,  $\text{NaCl}$ ,  $\text{MgCl}_2$ , Zitronensäure und Salzmischungen. Gasförmige Modifiern – hauptsächlich Kohlenstoffhalti-

ge Gase wie Toluol, Kohlenstofftetrachlorid und Freon – wurden zum ETV-Transportgas beigemischt, um die Transporteffizienz zu erhöhen.

In unserer Arbeitsgruppe wurden früher Untersuchungen der Analyttransporteffizienzen für eine kommerziell erhältliche ETV-Anordnung nach dem End-on Flow-Through Prinzip durchgeführt. Transporteffizienzen wurden mittels eines an die ETV-Anordnung angekoppelten Spektrometers bestimmt, das in der Arbeitsgruppe nach dem Verfahren der elektrothermischen Atomisierung und der kohärenten Vorwärtstreuung entwickelt wurde. Die durch ETV erzeugten Aerosole wurden mittels elektrostatischer Abscheidung quantitativ sowohl auf der L'vov Plattform des ETA-Ofens des Spektrometers als auch auf externen Probenträgern gesammelt. Transporteffizienzen bis zu 19% für Cu, 21% für Fe und Mn, und 36% für Pb vom ETV-Boot zum Spektrometer wurden bestimmt, sowohl für Standardreferenzmaterialien (BCR CRM 291, BCR CRM 189 und NIST SRM 1567) als auch für wässrig dosierte Multi-elementlösungen, die ungefähr die gleichen Elementmengen enthielten wie für die Standardreferenzmaterialien zertifiziert [Ber1, Ber2, Buc2]. Niedrige Analyttransporteffizienzen und hohe Abhängigkeit von der Volatilität der Analyte haben die Arbeitsgruppe zur Konstruktion der Upstream-ETV-Anordnung motiviert. Das Ziel war die absoluten Analytverluste zu mindern, damit die Differenzen zwischen ihnen ebenfalls gemindert würden. Hohe Transporteffizienzen mit geringer Abhängigkeit von der Volatilität können erreicht werden indem der Analytdampf in ein Konvektionsrohr entlassen wird. Damit durch hohe Aufwärtskonvektion keine Gegenströmung erzwungen wird, die zu Turbulenzen und Analytverlusten führen würde, darf der Durchmesser des Konvektionsrohres nicht zu weit sein (ca. 12-13 mm i.d.). Dabei entsteht ein Strömungsprofil mit der heißen Aufwärtsströmung auf der Achse des Konvektionsrohres. Die Kondensation des Analytendampfes erfolgt deshalb hinreichend wandfern. Diese Konstruktion wird als ETV-Anordnung mit einer axial-fokussierenden Konvektion (ETV-AFC) bezeichnet.

Diese Arbeit befasst sich mit der weiteren Entwicklung, Optimierung und Untersuchung dieser ETV-AFC-Anordnung. Anfangs wurden Transporteffizienzen bis zu 25% für Ag, 27% für Pb, 30% für Mn, 25% für Cu, 31% für Fe und 33% für Ni mit wässrigen Multi-elementlösungen gemessen. Das aus Quarz gefertigte AFC-Rohr wurde anfangs durch die Wärmestrahlung des Graphitrohres an der Stirnseite angeschmolzen. Eine Abschirmung durch ein Tantalblech führte zur Deformation und baldigen Zerstörung des Bleches. Danach wurde eine Abschirmung aus einer 7 mm dicken Kupferplatte gefertigt, die an einem wassergekühl-

ten Flansch, der auch zur Halterung des Kontaktkonens des Graphitrohres dient, und 2,5 mm oberhalb des Rohres montiert. Die Platte hat ausreichende Wärmekapazität, um eine Überhitzung innerhalb eines Heizzyklus zu vermeiden und ihre Wärme danach hinreichend schnell abgeben zu können. Überdies kann ein Konvektionsrohr aus Glas verwendet werden und eine wesentliche Erhöhung des Temperaturgradienten innerhalb der ersten Millimeter oberhalb des Auslasses des Graphitrohres erreicht werden. Dadurch kam es zur Erhöhung der Transporteffizienzen bis zu 44% für Pb, 54% für Mn, 45% für Cu, 55% für Fe und 59% für Ni. Weitere Verbesserung erfolgte durch Einarbeitung eines Ringschlitzes in einer später konstruierten 10 mm dicken Kupferplatte in Sandwichbauweise durch den ein kalter Schleusengasstrom zugeführt werden konnte. Dies bewirkte eine sehr effektive Kühlung der Aufwärtsströmung direkt oberhalb des Graphitrohres. Durch diese Maßnahmen wurden die Transporteffizienzen bis auf 48% für Ag, 51% für Pb, 60% für Mn, 53% für Cu, 68% für Fe und 64% für Ni erhöht. Der Temperaturverlauf auf der Achse des Konvektionsrohres wurde mittels eines schnell reagierenden Thermoelements gemessen und für die Modellierung des Kondensationsprozesses angewendet.

Das Altern des Graphitrohres führt zur Erhöhung der Transporteffizienzen. Der Effekt wird in dieser Arbeit mit der wachsenden Dichte der Kohlenstoffpartikel in Verbindung gebracht, die bei der Analytverdampfung vom gealterten Graphitrohr ausgelöst werden. Die Massenverluste des Rohres während eines Heizzyklus (8 s, 2600°C) wurden mit 70-120 µg bestimmt und erreichten 250 µg gegen Ende der Lebensdauer des Rohres. Eine Abschätzung der Dichte des aus dem Rohr ausgelösten Kohlenstoffdampfes zeigt Übersättigung schon innerhalb des Graphitrohres, d.h. innerhalb des Rohres liegt Kohlenstoff bereits in Form von C-Multimeren und größeren Strukturen vor. Rasterelektronenmikroskopische Aufnahmen zeigten relativ große Kohlenstoffpartikel schon innerhalb des Rohres. Bereits 2,5 mm oberhalb des Auslasses zeigten die Aufnahmen höhere Dichten von größeren Kohlenstoffpartikeln. Bei 2,25 cm zeigten rasterelektronenmikroskopische und transmissionselektronenmikroskopische Aufnahmen größere Dichten von Kohlenstoffpartikeln mit Durchmessern von ca. 10 nm, die zur Bildung von Ketten tendieren. Die Analytatoome kondensieren so in einer Umgebung von Kohlenstoffpartikeln mit wesentlich höherer Dichte und Größer. Für typisch verwendete Analytmassen im Pico- und Nanogrammbereich erfolgt die heterogene Kondensation der Analytatoome an diesen Kohlenstoffpartikeln insofern bereits bevor der Analytdampf durch Abkühlung die Übersättigung erreicht. Dadurch wird das homogene Partikelbildungskonzept [Kan1],

das oft zur Kondensation von größeren Analytmassen herangezogen wird, nicht mehr anwendbar.

Beruhend auf der heterogenen Partikelbildung wurde die Kondensation des Graphitrohrkohlenstoffes und der sechs Analyte der unterschiedlichen Volatilitäten Ag, Cu, Fe, Ni, Mn und Pb numerisch simuliert. Das Modell verwendet den gemessenen Temperaturverlauf innerhalb des Konvektionsrohres, berücksichtigt die Diffusion der Analytatom und vernachlässigt jedoch die Diffusion der schwereren Kohlenstoffpartikel. Ein Analytatom wird von einem Kohlenstoffpartikel mit einer temperaturabhängigen Wahrscheinlichkeit („Attachment-Funktion“) adsorbiert, wobei diese Wahrscheinlichkeit als eine Funktion der AAS-Analytvorbehandlungstemperatur mit einer statistischen Verbreiterung von 15% formuliert wird. Die berechneten Transporteffizienzen sind 45% für Ag, 43% für Pb, 55% für Mn, 51% für Cu, 67% für Fe und 65% für Ni. Die Modellierung zeigt gute Übereinstimmung mit den experimentellen Werten und spiegelt die Abhängigkeit von der Volatilität der Analyte wider.

Die Zugabe von einigen Mikrogramm Kalium- und Palladiumnitrat als Modifier erhöht besonders die Transporteffizienzen der volatilen Analyte. Die Zugabe von Kaliumnitrat bringt die Erhöhung um etwa 5% für Pb und Mn. Die Wirkung von Kalium als Analytträger ist nicht anzunehmen, weil Kalium die Partikelbildung durch homogene Kondensation viel später im Vergleich zu den weniger volatilen Metallen beginnt.  $K^+$ -Ionen und Verbindungen können eher die heterogene Kondensation von Kohlenstoff beschleunigen. Die Zugabe von Palladiumnitrat führt zu höheren und gleichmäßigeren Transporteffizienzen für Analyte mit unterschiedlichen Volatilitäten: 63% für Pb, 62% für Mn, 69% für Fe, und 64% für Ni. Die Erhöhung wird durch Kovaporisierung der Analytatom mit der höheren Kohlenstoffdichte erreicht. Im Modell wird dem durch Verwendung der höheren AAS-Vorbehandlungstemperaturen Rechnung getragen. Die resultierende Transporteffizienzen sind in gute Übereinstimmung mit den gemessenen Werten: 61% für Pb, 67% für Mn, 67% für Fe und 65% für Ni. Die kombinierte Anwendung von  $KNO_3$  und  $Pd(NO_3)_2$  Modifiern und von  $C_6H_{12}$  (Zyklohexan), das der internen Strömung des ETV-Gerätes beigemischt wird, hat eine weitere Erhöhung der Transporteffizienzen zur Folge: 91% für Ag, 86% für Pb, 81% für Cu, 94% für Fe und 90% für Ni.

Im Rahmen einer internationalen Forschungskoooperation wurde ein Verfahren zur Probenverdünnung, Aufteilung, und Dosierung entwickelt und untersucht. Das Verfahren nutzt neben der externen Probenvorbehandlung die große Homogenität der Analytdichte des

Aerosols zur Verdünnung, Aufteilung und Dosierung der Analyte. Eine Aufteilung und Dosierung auf eine oder mehrere Graphitplattformen ist durch elektrostatische Redeposition möglich. Mittels Verdünnung und dosierter Aufteilung des Aerosols kann die Analytmenge an den dynamischen Bereich des Spektrometers angepasst werden. Weiterhin kann eine primär feste Probe in größeren Mengen ins ETV-Boot eingebracht werden, um Dosierfehler und Effekte, die durch Probeninhomogenitäten entstehen, zu mindern, wodurch eine bessere Präzision der Messungen zu erzielen ist. Ebenfalls kann ein Probensatz gleicher Analytzusammensetzung aus einer Primärprobe gewonnen werden. Eine solche Vielzahl ermöglicht die sequentielle Multielementbestimmung mit Einelement-Verfahren oder Vergleichsmessungen mit unterschiedlichen Verfahren. Die relative Standardabweichung (RSD) der Messungen mit Aerosolaufteilung in 1:9 Verhältnis ist unter 5% (für n=4-5 Wiederholungen). Die RSD der Messungen mit dem 10-fach Abscheider ist unter 12% über n=10 Plattformen. Dabei wurden Analytzusammensetzungen auf den sekundären Plattformen mit Hilfe eines zweiten ETV-EP-Prozesses diesmal mit der Abscheidung im Ofen des Spektrometers bestimmt, dadurch wurde die RSD erhöht.

---

## List of abbreviations

---

<b>AAS</b>	<b>A</b> tomic <b>A</b> bsorption <b>S</b> pectrometry
<b>CFS</b>	<b>C</b> oherent <b>F</b> orward <b>S</b> cattering <b>S</b> pectrometry
<b>CS</b>	<b>C</b> ontinuum <b>S</b> ource
<b>EDX</b>	<b>E</b> nergy <b>D</b> ispersive <b>X</b> -ray <b>M</b> icroanalysis
<b>EP</b>	<b>E</b> lectrostatic <b>P</b> recipitation
<b>ETA</b>	<b>E</b> lectrothermal <b>A</b> tomization
<b>ETAAS</b>	<b>E</b> lectrothermal <b>A</b> tomc <b>A</b> bsorption <b>S</b> pectrometry
<b>ETV</b>	<b>E</b> lectrothermal <b>V</b> aporization
<b>ETV-AFC</b>	<b>E</b> lectrothermal <b>V</b> aporization – <b>A</b> xially <b>F</b> ocussing <b>C</b> onvection
<b>ETV-FT</b>	<b>E</b> nd-on <b>F</b> low- <b>T</b> hrough <b>E</b> lectrothermal <b>V</b> aporization
<b>FAAS</b>	<b>F</b> lame <b>A</b> tomc <b>A</b> bsorption <b>S</b> pectrometry
<b>FOES</b>	<b>F</b> lame <b>O</b> ptical <b>E</b> mission <b>S</b> pectrometry
<b>GF</b>	<b>G</b> raphite <b>F</b> urnace
<b>GFAAS</b>	<b>G</b> raphite <b>F</b> urnace <b>A</b> tomc <b>A</b> bsorption <b>S</b> pectrometry
<b>HGA</b>	<b>H</b> eated <b>G</b> raphite <b>A</b> tomizer
<b>ICP-OES</b>	<b>I</b> nductively <b>C</b> oupled <b>P</b> lasma – <b>O</b> ptical <b>E</b> mission <b>S</b> pectrometry
<b>ICP-MS</b>	<b>I</b> nductively <b>C</b> oupled <b>P</b> lasma – <b>M</b> ass <b>S</b> pectrometry
<b>LOD</b>	<b>L</b> imit <b>O</b> f <b>D</b> etection
<b>PLASATRADIS</b>	<b>P</b> latform-to- <b>P</b> latform <b>S</b> ample <b>T</b> ransfer, <b>D</b> istribution, <b>D</b> ilution, and <b>D</b> osing <b>S</b> ystem
<b>PRS</b>	<b>P</b> arameter and <b>S</b> pectra
<b>RSD</b>	<b>R</b> elative <b>S</b> tandard <b>D</b> eviation
<b>SEM</b>	<b>S</b> canning <b>E</b> lectron <b>M</b> icroscopy
<b>SD</b>	<b>S</b> tandard <b>D</b> eviation
<b>SSAAS</b>	<b>S</b> olid <b>S</b> ampling <b>A</b> tomc <b>A</b> bsorption <b>S</b> pectrometry
<b>STPF</b>	<b>S</b> tabilized <b>T</b> emperature <b>P</b> latform <b>F</b> urnace
<b>TE</b>	<b>T</b> ransport <b>E</b> fficiency
<b>TEM</b>	<b>T</b> ransmission <b>E</b> lectron <b>M</b> icroscopy



---

## 1. Introduction and problem statement

---

Many institutions including environmental, chemical and petrochemical, food and pharmaceutical, geological, and forensics are required to perform a variety of elemental determinations on various types of samples. The most commonly used analytical techniques include flame and electrothermal atomic absorption spectroscopy (FAAS and ETAAS), flame optical emission spectroscopy (FOES), inductively coupled plasma optical emission spectroscopy and mass spectrometry (ICP-OES and ICP-MS).

The major limitation of FAAS that significantly reduce the sensitivity of the technique is a relative inefficiency of the burner-nebulizer system as a sampling device: only a small fraction of the analytes reaches the flame, and the atomized analyte vapor passes quickly through the light path. With ETAAS, the sample is introduced into an electrically heated graphite tube, electrothermal atomizer (ETA), which is then heated in a programmed series of steps to remove the solvent and major matrix components and to atomize the remaining analytes. The atoms are within the tube for a certain time that results in significantly improved sensitivity and detection capability. Due to such inherent advantages, ETA is widely accepted as a versatile source for the production of atomic vapor that makes its application attractive for use with other specialized nonabsorption-based techniques such as atomic emission, atomic fluorescence, laser-enhanced ionization, and coherent forward scattering (CFS) spectrometry. The ICP-based instruments have generally an exceptional multi-element capability, a higher sample throughput, and a very wide analytical working range, but their costs are 3-4 times higher in comparison with ETAAS instruments [Per1].

The mentioned analytical techniques are used predominantly for the analysis of liquid samples. Unfortunately, most samples submitted for analysis are solids and thus conventional approaches require chemical decomposition of the sample prior to analysis. Decomposition methods such as with dry ashing and chemical digestion are time-consuming and can lead to systematic and random errors that will degrade the overall accuracy and precision of the analysis. There have been many attempts to adapt atomic spectrometric techniques to the direct analysis of solid samples. Solids, in the form of slurries or suspensions, have been nebulized into flames [Andr] and plasmas [Moch, Good]. However, nebulization provides very low sample transport efficiency and the particles that reach the flame or plasma are then more difficult to dissociate. This results in low sensitivities from slurries compared with calibration

standards in solution. It has been attributed to lower atomization efficiency from the solid particles due to their short residence in the flame or plasma. Nonuniform distribution of analytes throughout the particle size range should also be considered. The only way of successfully overcoming the above problems is to analyze the samples against solid calibration standards in similar matrices. However, this approach is not widely used for routine analysis because several calibration standards over an appropriate concentration range are required and the availability of solid reference materials is severely limited.

Compared with FAAS and ICP-OES/MS, ETAAS is inherently more suitable for the direct analysis of solid samples. This technique is known as solid sampling atomic absorption spectrometry (SSAAS). Solids may be weighed into an ETA boat [Kur1, Lück, Kri1, Kri2, Kri3] or a graphite cup [Carn, Wel1] and directly introduced into an electrothermal atomizer, and then atomized with high efficiency. Introduction of slurries [Mil1, Mil2, Kri4, Kri5] is also widely practiced. Under optimized operating conditions using stabilized temperature platform furnace (STPF) concept, solids and slurries have the same high atomization efficiencies that allow to use calibration standards in aqueous solutions without introducing systematic errors. A more likely source of errors by the direct analysis is an inhomogeneous distribution of the analyte through the sample. Many metal alloys contain undissolved trace components distributed inhomogeneously through the grains of the material or accumulated mainly at the grain boundaries. High inhomogeneity is revealed in geological and environmental samples, such as rocks, soils, sediments etc. Such samples are usually ground to a fine powder (less than 20  $\mu\text{m}$  particle diameter) in order to make them more homogeneous. A further source of systematic errors, producing scattered results, is the existence of rare particles of high analyte content (nuggets) in a powdered sample. This situation was described by Kurfürst [Kur3], who showed that these nuggets cause skewed distributions of analytical results. The large particle size influences the precision. Several authors [Full, Sato, Jac1] have demonstrated the improvement in precision obtained as the particle size is reduced. Detailed consideration on handling of solids and slurries using direct sample introduction has been done by Kurfürst [Kur2].

A most powerful approach to avoid the problems with low sample transport efficiency and incomplete atomization by FAAS and ICP-OES/MS as well as the most of occurring errors by direct analysis of solid samples is likely an interfacing an electrothermal vaporization (ETV) chamber to an analytical instrument. The use of an ETV unit has been established for

sample introduction into ICP-OES/MS [Kan2-Kan7, Sne1, Gre1, Dam1-Dam4, Hol1, Hol2, Kri6, Hass, Kur2]. Detailed information about the ETV as an instrument for sample introduction for analytical purposes is given in [Sne1, Kur2]. In comparison with the sampling techniques such as nebulization, laser ablation [Moen, Rus1-Rus3, Win1-Win2, Lam], sputtering [Mül1, Mül2] and other techniques resumed in [Sne1] the ETV sampling offers exceptional advantages. Samples can be introduced into the ETV unit directly as solids or liquids using the boat technique, the sample preparation time and possible risks of sample contamination and of analyte loss prior to analysis are reduced, and finally the ETV instrument can be employed as an external sample pretreatment tool. Thus, the solvent and major parts of the matrix are first externally removed by drying and pyrolysis and then the residual analyte is volatilized and carried away by the argon flow where its condensation and aerosol formation occurs while being cooled down. This approach can provide very high analyte transport efficiency and enable using liquid calibration standards.

The ETV sampling was successfully applied to flame (FAAS, FOES) and plasma techniques (ICP-OES/MS) but can be utilized for the graphite furnace (GF) analytical techniques such as ETAAS and CFS as well, by means of electrostatic precipitation (EP) of the ETV generated particle aerosols in a corona discharge [Sne2, Sne3, Buc1, Tor1, Tor2]. The investigation of point-to-plane coronas in different pure gas environments as well as in gas mixtures is presented elsewhere [Weis, Manm]. This approach offers very high particle collection efficiency [Buc1, Tors, Sne3]. For instance, by precipitation of airborne particles with aerodynamic diameters in the range of 300-500  $\mu\text{m}$  in a graphite tube [Tors], the collection efficiency is more than 99.9%. For particles with diameters less than 100 nm produced by laser ablation and deposited onto a L'vov-platform [Buc2], it is more than 99.7%. Thus, the analyte can be quantitatively re-collected on the platform of the same type using intra-furnace or external EP on the wall of a graphite tube [Tors] or on a secondary graphite boat [Ber1, Ber2, Buc2]. The generated particle aerosol can be also electrostatically or thermophoretically collected on suitable substrates for further investigation using high resolution scanning and transmission electron microscopy (SEM and TEM) [Her1]. Further advantage is that the content of both primary and secondary platforms can be analyzed with the same analytical instrumentation that makes the approach be excellently suited for direct determination of analyte transport efficiency (TE). Moreover, the ETV-EP procedure allows significant sample matrix reduction [Ber1] due to external thermal pretreatment of the sample and a complete

preceding sample pyrolysis and distillation cycle consisting of vaporization, condensation, and re-precipitation.

Different commercially available or specifically designed GFs with vapor outlet through one of the ends of the graphite tube, named as end-on flow-through ETV (ETV-FT), have been initially used as ETV devices [Dam2, Hol2, Kri6, Gre1, Gre2, Hass, Ber1, Buc2]. The analytical performance of every ETV instrument can first of all be quantitatively characterized by analyte TE that is defined as a percentage ratio of the analyte amount delivered to a spectrometer to the amount initially dosed into the ETV boat. Schäffer and Krivan [Kri6] have indirectly measured TEs for eight elements of different volatility with an ETV ICP-OES instrumentation using a radiotracer technique. As it follows from the study, up to 80% of total losses occur due to analyte condensation on colder outlet ends of the GF, on the graphite cones, and in the ETV-ICP connecting interface. To decrease the sedimentation, a cooling bypass gas that surrounds the outlet flow at the colder tube end has been introduced. Owing to this improvement, TEs between 26-37% for medium and low volatile analytes and 35-57% for volatile analytes have been reported. Another approach has been suggested by Hassler et al. [Hass]. An internal nozzle as a part of the graphite tube was used in this ETV design. In our laboratory [Buc2, Ber1, Ber2], TEs of 19-21% for medium volatile analytes (Cu, Fe, Mn) and 36% for the volatile analyte (Pb) have been obtained for organic certified reference materials vaporized with a commercially available ETV-FT unit (SM-30, Grün Analytische Mess-Systeme GmbH, Ehringshausen, Germany). Similar results have been also documented for multi-element standard solutions containing approximately the same metal contents as certified for the solid samples. The above discussion shows that the ETV-FT sampling has the following major problems: first the relatively low analyte TE from the ETV to the analytical instrument and second the noticeable dependence of the TE on analyte volatility. It makes the transport of the sample analytes highly nonuniform that significantly modifies the analyte content in the transported sample relative to the content in the initially dosed sample. Detailed investigations have confirmed that the major analyte losses occur due to their deposition onto the colder parts of the graphite tube [Kri2], connecting tubing [Hol2, Gre2], and under certain conditions within the ETV switching valve [Gre2]. It should also be pointed out that as it will be shown below the TE does not depend on physico-chemical properties of the analyte element only but also on sample matrix, vaporization temperature, GF heating rate etc.

A way to prevent analyte deposition on the colder ends turned out to be an upstream configuration with the gas entering the furnace through its ends and flowing upwards through the hole in the graphite tube center. The analyte vapor is released into a larger volume of a condensation chamber above the GF outlet hole. The main disadvantage of this construction is that, owing to a high buoyant force, the upstream velocity in the large gas volume became very fast and led to whirls and turbulences resulting in analyte vapor and aerosol deposition on colder walls. Such designs were first presented by Kántor and Záray [Kan2] for an indirect coupling to an ICP torch and by Lamoureux et al. [Gre1] for simultaneous measurement of the atomic absorption and mass spectrometric signals. Later, Kántor and Güçer [Kan6] determined the TEs for five elements in the upstream ETV. They reported 67-76 % for medium volatile (Cu, Mn, Mg) and 32-38 % for volatile analytes (Cd, Zn). The masses of the analytes applied were 4-10 µg for each analyte. Thus, using an upstream configuration, more efficiently transported are analytes with lower volatility and higher melting points. Comparisons carried out by Kántor [Kan7] have shown the superiority in analytical performance for the upstream configuration. Nevertheless, for both ETV unit constructions, an evident dependence of analyte TE and analyte losses on element volatility, sample mass, ETV operating conditions etc. is revealed.

Chemical modifiers are also often applied for ETA. Detailed consideration of modifier action mechanisms has been done by Ortner [Ort1]. In ETV sampling, matrix/carrier modifiers are a means to form a transportable aerosol as well. Modifiers are used as substances, which act additionally as physical carriers. Commonly used modifiers are  $\text{Pd}(\text{NO}_3)_2$  [Edig, Mil5, Mil6, Chan, Kara, Gre2, Gre3],  $\text{Mg}(\text{NO}_3)_2$  [Edig], NaCl [Edig, Gre2, Gre3],  $\text{MgCl}_2$  [Edig], citric acid [Edig], and salt mixtures as, for instance, diluted NASS-3 sea-water [Gre3, Gre4]. Their addition can support formation of a transportable aerosol and reduce the impact of the above mentioned factors on analyte transport. Besides, it may enhance and make more uniform the analyte TE distribution. Generally, the modifier effect is to be explained due to co-vaporization of sample analytes with carrier forming constituents that results in faster formation of stable particulates [Edig, Gre1, Kan1].

As sample/carrier modifiers are also often used gaseous additives to the transport gas flow. Záray and Kántor [Kan3, Kan4], Hassler et al. [Hass], and Krivan and Schäffer [Kri7] have reduced the transport losses by adding carbon-containing gases such as toluene, carbon tetrachloride, and freon. For example, by adding a carbon tetrachloride vapor [Kan6], the TEs

for the upstream ETV construction coupled to the ICP-torch were enhanced to 67-73% for all analytes studied. Another known application of the gaseous halogenated hydrocarbons is the supporting for quantitative vaporization of refractory elements and the preventing of carbide formation by some elements [Wann]. Further, an externally generated carbon particle aerosol produced by pyrolysis of hexane vapor [Hol3] was also used as a possible analyte carrier for the system ETV-ICP-MS. Signal enhancements were observed, but the effect was associated rather with changes in the plasma than with increased analyte transport. This conclusion was supported by the work [Merm] showing the signal enhancements with the addition of carbon-containing compounds into the plasma. The effect of carbon particulates released from the GF during the vaporization step was studied using ultrasonic slurry sampling ETV-ICP-MS [Mil5, Mil6]. They concluded that the increment in signal intensity is most likely the result of carbon particles released from the GF together with the analytes and increasing the analyte TE. It is expected that the GF carbon may play an important role in the analyte transport. A quantitative study of carbon losses for GF tubes with pyrolytic coating [Ort1, Ort2] showed differential mass losses of about 70-80  $\mu\text{g}$  per a heating cycle during the tube lifetime. The upper value is about 600  $\mu\text{g}$  for uncoated tubes when approaching to the tube lifetime. Evaluable losses are observed even during drying and pyrolysis steps for both tube types.

A theoretical description of the condensation of analyte vapors generated by ETV has been performed by Kántor [Kan1]. The concept is based on homogeneous formation of thermodynamically stable nuclei with sizes exceeding critical diameters, upon which further particle growth takes place. This theory is widely used for condensation of analytes dosed into the ETV in microgram and larger amounts (ppm range). In this case, the generated analyte vapor can often achieve supersaturation under experimental condition. For nano- and picogram amounts (ppb and ppt ranges), the analyte vapor in the gas phase is often unsaturated and cannot begin to form particles through homogeneous nucleation. Formation of a transportable aerosol in this case can occur through heterogeneous condensation on foreign particulates (carriers). There are neither theoretical nor empirical estimations of heterogeneous analyte condensation available.

In our laboratory, investigations of the analyte transport employing the ETV-FT unit based on the commercially available GF (SM-30, Grün Analytische Mess-Systeme GmbH, Ehringshausen, Germany) designed for SSAAS have been carried out. TEs have been determined employing a laboratory made electrothermal atomization continuum source CFS spec-

trometer (ETA-CS-CFS) [Her2-Her6] coupled to the ETV unit. By means of electrostatic precipitation (EP), the ETV generated aerosols have been quantitatively collected on the L'vov platform of the spectrometer as well as on external platform collectors. As mentioned above, TEs of up to 19% for Cu, 21% for Fe and Mn, and 36% for Pb have been obtained [Ber1, Ber2, Buc2]. Low analyte TEs and high dependence on analyte volatility motivated the scientific group to design a novel ETV unit with upstream configuration. The aim was to reduce the absolute analyte losses because their differences become reduced as well. Higher and more homogeneous TEs should be achieved by releasing the hot upstream into a narrow vertical convection tube in order to prevent a counter flowing downstream at the tube walls, which have led to turbulences and analyte losses by employing the upstream ETV designs mentioned above. Using the new convection tube, a velocity profile with the hot outlet upstream on the axis of the tube is formed. Under this condition, the analyte condensation occurs mainly apart from the colder walls. This design was named as an ETV unit with an axially focusing convection (AFC) upstream or shortly the ETV-AFC unit.

The purposes of this work are:

- (1) further development and optimization of the novel laboratory designed ETV-AFC unit with the aim to obtain higher analyte TEs with less dependence on volatility,
- (2) investigation of influences of different sample/carrier modifiers on analyte TEs,
- (3) understanding of the analyte condensation process in the AFC upstream with
- (4) subsequent development of a theoretical model of the analyte condensation.

## 2. Experimental

### 2.1 ETV-AFC instrumentation

#### 2.1.1 Principle

The principle of the developed ETV furnace with the AFC upstream is presented in Fig. 2.1. The velocity profile of the upstream flow in the AFC tube (the length of the tube is much longer than the diameter) has a parabolic form when the ETV is in the cold state. The profile looks completely different during the heating of the ETV. The internal flow passing into the AFC tube through the GF outlet hole becomes very fast by means of thermal gas expansion and high buoyant force exert by the surrounding cooling gas flow (the Archimedes' principle). By choosing appropriate ratio between the internal and cooling gas flows as well as the dimensions of the AFC tube, turbulences in the upstream and hence unnecessary contact of analytes with cold surfaces can be avoided and axially focused analyte condensation can be achieved. The idea of the AFC tube is taken from a simple experiment with a slightly smoking candle positioned under a long vertical tube. The hot upstream gas always ascends along the path of least flow resistance in the center of the tube independent on the positioning of the candle within the tube.

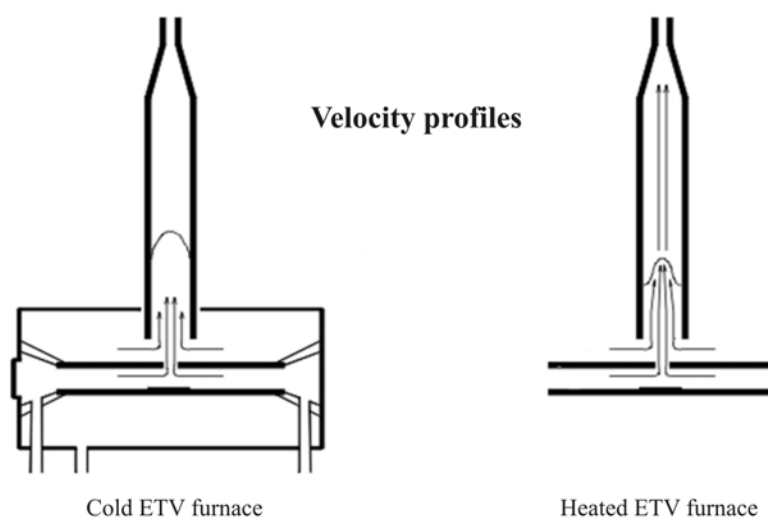


**Fig. 2.1:** Principle of the axially focusing of the upstream flow used in the development of the new ETV-AFC setup [Her8].



### 2.1.2 Construction and flow scheme

The cross-cut and the photograph of the ETV-AFC unit are given in Fig. 2.2(a,b). The ETV furnace has three gas inlets, one on the each side of the graphite tube for the internal gas

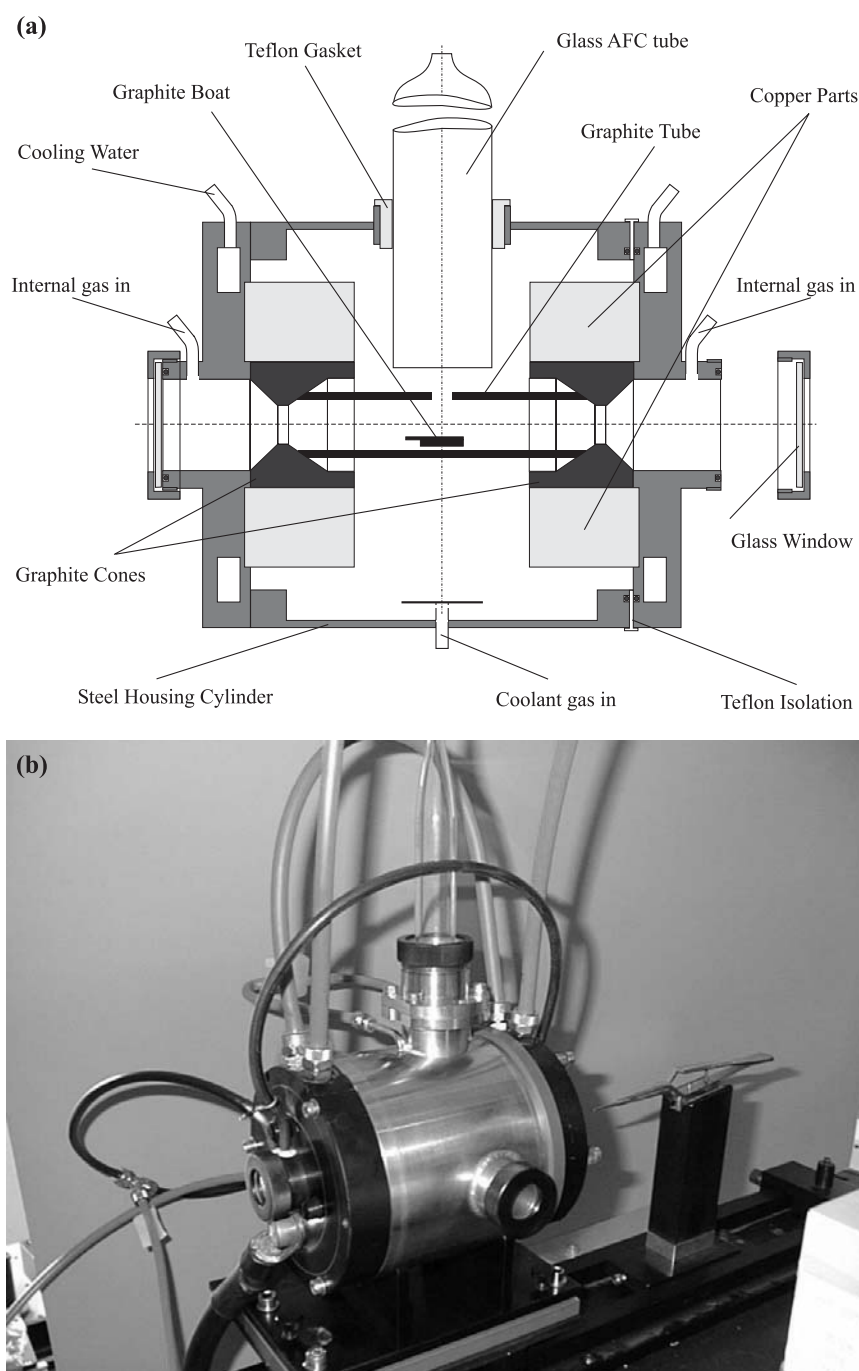


**Fig. 2.2:** A novel laboratory constructed electrothermal vaporization unit with an axially focusing convection tube (ETV-AFC): (a) schematic representation and (b) photograph.

flow and one on the bottom of the unit for the external cooling gas flow. The internal argon enters into the GF tube through the contact cones and carries out the vaporization products through a transverse hole in the tube center (diameter 2.5-3 mm). Directly above the GF outlet, the upstream is surrounded with several external coolant flows, which have additionally an upstream focusing effect. Longitudinally heated pyrolytically coated tubes (Schunk Kohlenstofftechnik GmbH, Heuchelheim, Germany) are used (length, outer, and inner diameter: 53, 10, and 8 mm, respectively). Both sides of the furnace are equipped with screwable windows to seal the furnace during the vaporization step. The boat introduction is performed by a pair of tweezers (see Fig. 2.2(b)) mounted on a sledge for reproducible transfer of the boat as a sample vessel into and out of the furnace, similar to that used in combination with the graphite furnace (SM-30, GRÜN Analytische Mess-Systeme GmbH) for SSAAS [Buc2, Ber1, Ber2]. The housing is equipped with four glass windows for longitudinal and transverse observation of the GF tube used for temperature measuring and controlling with optical methods.

Fig. 2.3 shows an improved ETV-AFC setup and a flow scheme that has become more sophisticated since first experiments. A radiation shield (a copper plate with sufficiently high

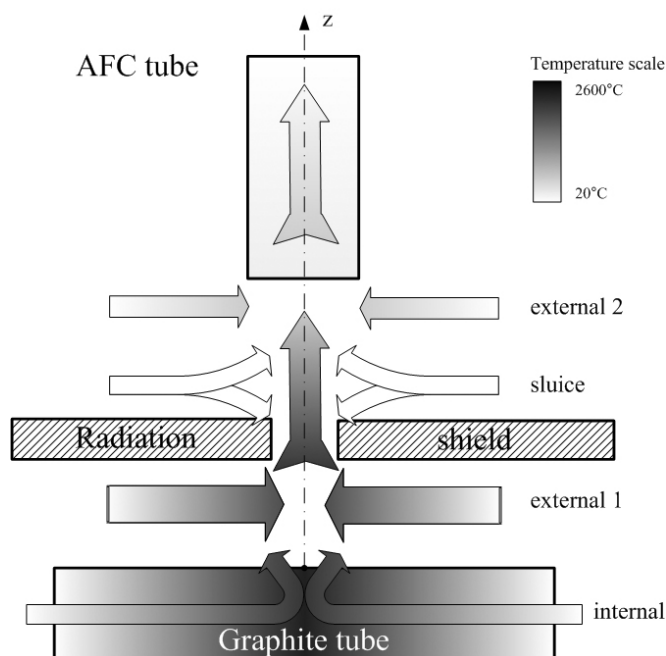


**Fig. 2.3:** Principle of the upstream shielding against incandescent radiation of the GF during ETV firing; the arrows show directions of internal, external, and sluice gas flows.

heat capacity) is mounted 2.5-3 mm above the GF tube to one of the water-cooled copper parts of the ETV furnace for cooling off the plate between the separate ETV firings. The rough plate dimensions are 70 mm length, 25 mm width, and 10 mm height with a cylindrical opening (diameter 7 mm) in the center. After this modification, the splitting of the external sub-flows 1 and 2 is adjusted via changing the distance between the radiation shield and the AFC tube.

An additional cooling sluice gas is introduced through the copper plate. Sluice gas outlet is situated as a ring slit within the cylindrical shield opening 1-2 mm above the bottom plane of the plate.

### 2.1.3 Temperature monitoring

High-temperature calibration of the ETV furnace is performed with optical pyrometer PB06F2 (Keller GmbH, Ibbenbueren, Germany) by observation of the area in the tube center inside and outside the tube through the windows in the ETV housing. The platform temperature is controlled in the same way. Alongside with the pyrometer, a photoconductive detector PIN-5D (UDT Sensors, Inc., Hawthorne, USA) in combination with a neutral filter is used for the monitoring of radiation intensity during vaporization. The photodiode is applicable for the spectral range from 350 to 1100 nm; the response time is 12 ns (for 632 nm, 10 V reverse bias, and 50  $\Omega$  series resistance).

Drying and pyrolysis temperatures are measured with digital thermometer based on the thermocouple GTH 1200 A (Greisinger Electronic GmbH, Regenstauf, Germany).

For temperature measurements in the upstream, a fast PtRh-PtRh thermocouple (type B, DIN IEC 584-1,  $\tau = 50$  ms, operating range 50 - 1800°C) is used. PtRh contents for positive junction are 70 to 30 % and for negative junction 94 to 4 %. The coordinate controlling is realized with a micrometer screw. The analogue data obtained from the thermocouple are digitalized and fed to a computer via an IEEE-488 bus.

### 2.1.4 External generator of gaseous additives to the internal flow

An external generator of gaseous additives to the ETV internal flow is constructed as shown in Fig. 2.4. An Ar flow rate from 75 to 200 mL min<sup>-1</sup> is maintained by a flow controller. On the first three-way valve, the flow is divided in a calibrated ratio by means of a screw-down valve. The smaller part (0.3-5 mL min<sup>-1</sup>) is delivered to an Erlenmeyer flask containing

approximately 100 mL of cyclohexane, whereas the other part is directed through a ballast flow resistor to the second three-way valve and after mixing with enriched first stream to the ETV inlet for the internal gas. The flask is found in a thermostat at a constant temperature between 15-20°C. The appropriate ballast flow resistor allows to make smoother the setting of the flow splitting ratio.

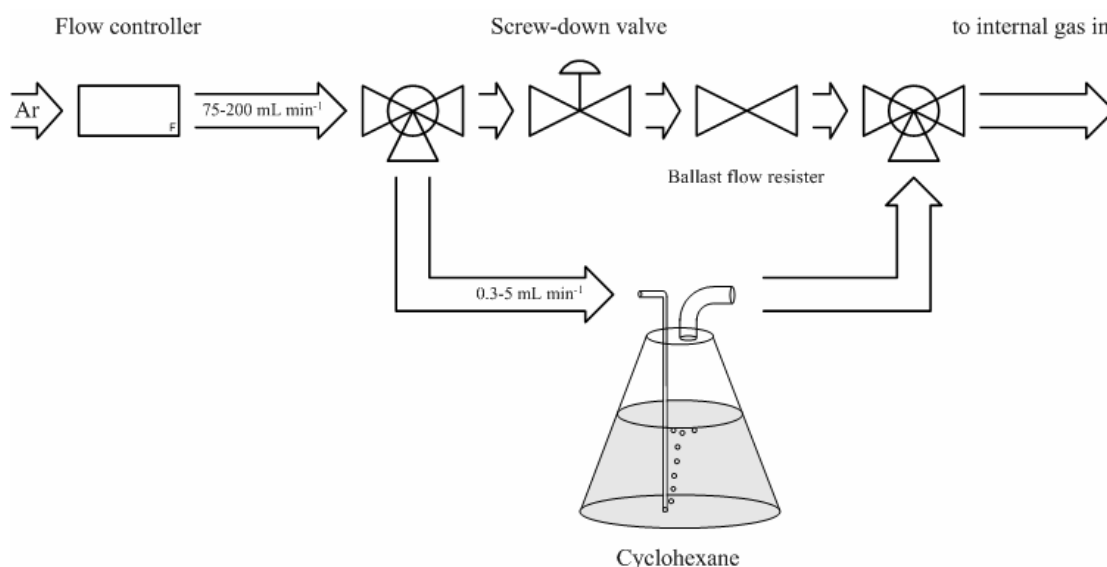


**Fig. 2.4:** Diagram of the external generator of gaseous additives to the internal flow of the GF.

The flow rate through the flask is estimated by means of a bubble frequency. Frequency fluctuations caused by the inner tubing volume are decreased by reducing both the total length and the thickness of the inlet tubing (0.5 m and 0.3 mm, respectively). The length of the outlet tubing is decreased as well to reduce a system reaction time. Under typical conditions, this time is about 10-30 min.

## 2.2 Experimental arrangement

### 2.2.1 Experimental arrangement for intra-furnace ETV sampling

The experimental arrangement for intra-furnace precipitation of the aerosol is schematically shown in Fig. 2.5. A laboratory-designed, computer-controlled continuum source CFS spectrometer (CS-CFS) is used for simultaneous multi-element analysis of the deposited particulates. The spectrometer is equipped with a continuum primary source (Xe short-arc

lamp, XBO 450 W/4, Osram GmbH, Germany), a longitudinally heated ETA graphite furnace (HGA-600 with autosampler AS-60, Bodenseewerk, Perkin-Elmer GmbH, Überlingen, Germany [Per2]), and an optical multi-channel analyzer (OMA, Model 1420 UV, EG&G,

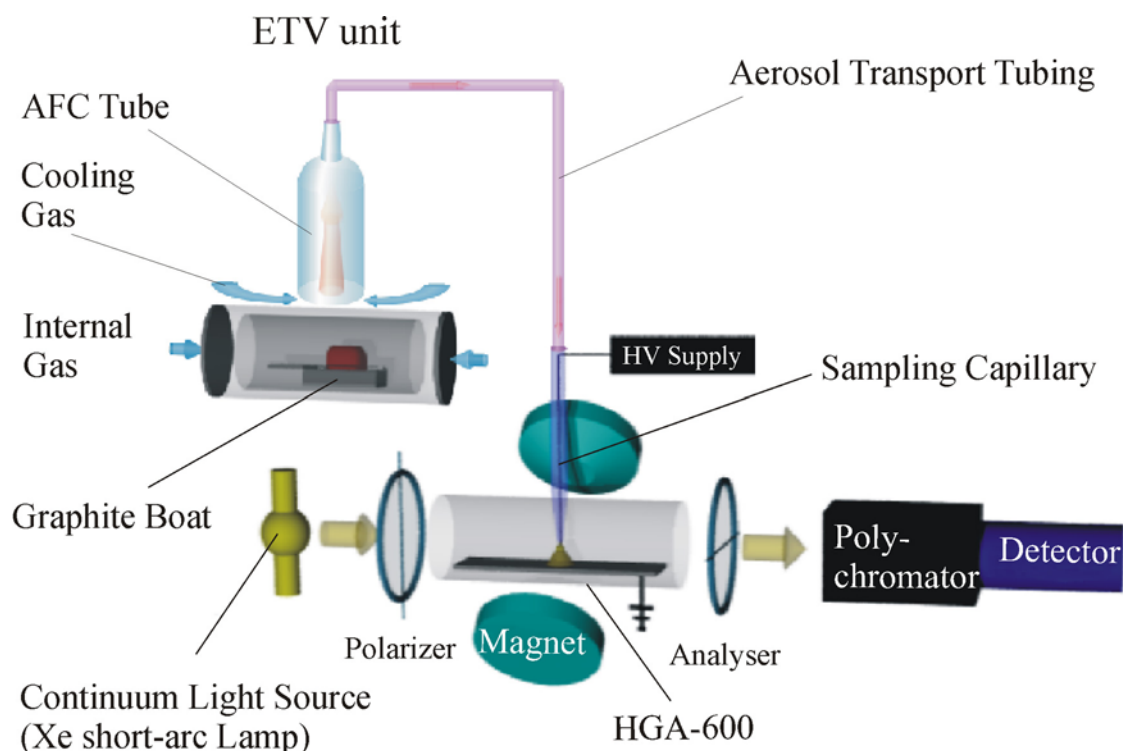


**Fig. 2.5:** Experimental arrangement for sample introduction into continuum source coherent forward scattering spectrometer (CS-CFS) using electrothermal vaporization with internal electrostatic precipitation (ETV-EP). Based on the idea of T. Buchkamp [Buc2].

Princeton Applied Research, USA). The detector is coupled to a 0.25 m polychromator (82-499, Jarell-Ash, Europe SA). This instrument has 3 gratings. With highest linear dispersion, it allows simultaneous detection of line intensities within approximately 50 nm wavelength interval. Further details of the spectrometer are reported elsewhere [Her7, Buc1, Buc2]

### 2.2.2 Principle of CFS spectrometry

The coherent forward scattering has been first studied and described by Corney et al. [Corn] with reference to double-resonance and level-crossing experiments. In a very general form, the authors discuss the interaction of polarized light with an atomic vapor in static transverse and longitudinal magnetic fields (Faraday and Voigt configurations).

The principle of CFS spectroscopy with the Voigt configuration is shown in Fig. 2.6 [Her2]. The analyte is vaporized between two crossed polarizers (the polarizer and the analyzer). The lamp may be a continuum spectrum or an atomic line source. Without anisotropic interaction, the light path is blocked by the crossed polarizers. Due to the applied longitudinal or transverse magnetic field, the atomic resonance lines split up into  $\sigma$  and  $\pi$  components. The angle between the first polarizer and the magnetic field is usually set as  $45^\circ$ , so that equal amounts of light are available for interaction with the  $\sigma$  and  $\pi$  components. The  $\pi$  components

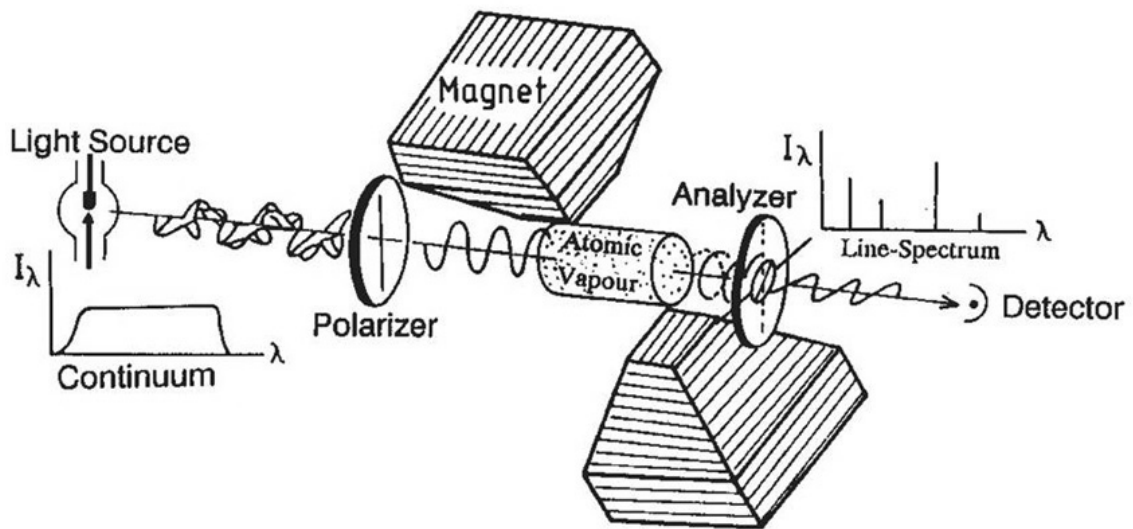


**Fig. 2.6:** Principle of CFS with a Voigt configuration and a continuum source [Her2].

are polarized parallel with the respect to the applied magnetic field, while the polarization of  $\sigma$  components is perpendicular to the field with a circular or linear state, depending on the direction of propagation parallel or perpendicular with respect to the magnetic field. Caused by the magnetically induced anisotropy, polarization of the incident light is changed in the spectral range of atomic resonance lines, and the resonance spectrum of the analyte vapor is transmitted.

In combination with a crossed polarizer-analyzer pair, CFS is a “zero-method”. This means that, under ideal conditions, the CFS line intensity is zero for zero atomic density in the analyte vapor. The signal is generated – like in OES – directly by optical means without

modulation and lock-in detection. Nevertheless, CFS is – like the AAS – an approach of atomic resonance interaction spectroscopy with probing the light from an external source. I.e. the CFS spectrum contains ground-state resonance lines and lines from populated lower levels, only. No lines from ions or excited state species are present. This greatly simplifies the dispersive requirements of the detection system, which can be remarkably low, permitting use of acoustooptic tunable filters and low-resolution monochromators, as well as imaging detectors. The spectral intensity of a continuum source generally exceeds that of a hollow cathode source for such weak transitions, because it does not depend on the oscillator strength of the related element line. Thus, not only is there a multielement capability associated with use of continuum sources, but also a multiline capability. CFS spectrometry offers the ability to make measurements with extremely weak atomic lines that allows to extend the analytical working ranges by many orders of magnitude and to determine major constituents of a sample simultaneously with traces. Thus, ETA-CFS with continuum sources can combine the high detection power usually associated with GF techniques with the capability to detect masses up to the higher microgram range simultaneously in the same sample, by use of lines of extremely different strengths.

Detailed theoretical descriptions of CFS as a physical effect and an approach of coherent forward scattering spectroscopy are given in [Corn, Ito, Davi, Her2-Her6, Ste1, Ste2, Kita, Yam1, Yam2, Win1, Win2, Ker1, Ker2, Hir1-Hir5].

### 2.2.3 Software for ETV-EP CS-CFS measurement controlling and data acquisition

Controlling programs for separate units of the CS-CFS spectrometer (HGA-600 with the autosampler, magnet, and OMA) are combined in a single software package for complete computer-controlling of the spectrometer. The communication with the computer is realized via an IEEE-488 bus card [Keit]. Further details are given in the literature [Her7, Buc1, Buc2, Buc3]. The data acquisition begins with the beginning of the atomization step. The pixels composing a spectrum in the 50 nm wavelength range are collected in the equidistant time intervals in the intermediate buffer and after the atomization step are saved in a temporary file and after that are converted and incorporated into the file in a laboratory-developed PRS-format (“**Pa**Rameters and **S**pectra”) [Lie1-Lie3] containing together with the spectra data the measurement satellite information such as concentrations of the pipetted solutions and their positions on the autosampler plate, the number of the repetitions, the temperature program as

well as the parameters of the resonance lines, the start time for the data acquisition, for the magnet switching-on etc.

Controlling programs for the ETV-EP instrumentation were developed by Thomas Buchkamp [Buc2, Buc3] and integrated into the software package of the CS-CFS spectrometer. The operating program for the ETV is realized analogously with the commercial controlling software for the GF of HGA-600 [Per2] with the exception of the following options as the temperature controlling circuit, the ramp increase of the temperature, and the controlling of the gas flows. The sub-program for the EP cell controls the position of the dosing arm of the autosampler and sends to the high-voltage power supply a command to apply a manually pre-set voltage to the precipitation electrode.

#### 2.2.4 Software for CS-CFS spectra evaluation

After the measurement cycle the obtained spectra can be observed with the spectra viewing program SPECVIEW 2.65 developed for the operation system OS/2. The selected spectrum is presented in two separate windows in orthogonal coordinates in dependence on the wavelength and the time. After the switching to the operating systems developed by Microsoft™, an equivalent program SPECVIEW 3.0 for Windows was developed by Marat Gafurov [Gafu] using the software package TestPoint™.

The first software package for the evaluation of CS-CFS spectra obtained by different spectrometers, the program package MULTI 2a, was developed by Thomas Liebner [Lie2, Lie3]. The software allowed several possibilities for the background correction and the signal evaluation as well as formation of the analytical calibration curves and determination of the analyte concentration in the unknown sample. The main disadvantages of this package are:

- (1) non-applicability for the analyte intensities near to the corresponding LODs;
- (2) insufficient accuracy for signal and background evaluation due to the linear approximation of spectral lines and temporal line profiles;
- (3) low resonance line resolving capability.

With the aim to eliminate these disadvantages, a novel software package has been developed by the author in Mathematica™. The algorithm with some examples is described in details in Appendix A.3.

The package contains the five separate steps.



(1) Determination of the parameters of resonance lines in the spectrum such as a relative line position in the 50 nm spectral window and a line half-height. These data are obtained only once and are further used for all measurement with the same position of the spectral window.

(2) – (3) Evaluation of resonance line intensities (with background subtraction) with the algorithm presented in Appendix 3 for calibration solutions and ETV-EP samples, respectively.

(4) Determination of transported analyte concentrations with the analytical calibration curve technique [Iup1] or with the bracketing technique [Iup2] and calculation of analyte TEs.

(5) Obtaining of temporal intensity profiles for analyte resonance lines of interest, for instance, to compare of the profiles for an analyte sampled in different matrices.

## 2.3 Aerosol transport, dividing, and dosing

### 2.3.1 Principle

The principle of aerosol transport, dividing, and dosing is shown in Fig. 2.7(a)-(c). The aerosol is carried by argon flow via a tygon® tubing R-3603 (Norton, Akron, OH, USA) with 4 mm inner diameter to electrostatic precipitators for internal (intra-furnace) or external deposition. The length of the transport path for both cases does not exceed 1-1.5 m. Fig. 2.7(b) shows a specially designed aerosol flow splitting system for reduction of the analyte amount transported to the precipitator to a pre-set fraction  $1/N$ . In this way, the aerosol flow is split into two sub-flows in a calibrated ratio:

$$1 : (N - 1). \quad (2.1)$$

The variation of the splitting ratio is realized by a specially designed flow valve with sufficiently long narrowing and widening parts to decrease occurring turbulences and to increase the precision of the flow splitting. In this work, a typically used splitting ratio is 1:9 with  $N = 10$ . Fig. 2.7(c) represents a scheme of aerosol dividing into  $N$  equal sub-flows using a highly-symmetric flow splitter with subsequent precipitation onto  $N$  different boats in an external precipitation unit consisting of  $N$  equal precipitators. The sub-flow through each precipitator is controlled with a flow reduction valve to achieve stationary sub-flow distribution.

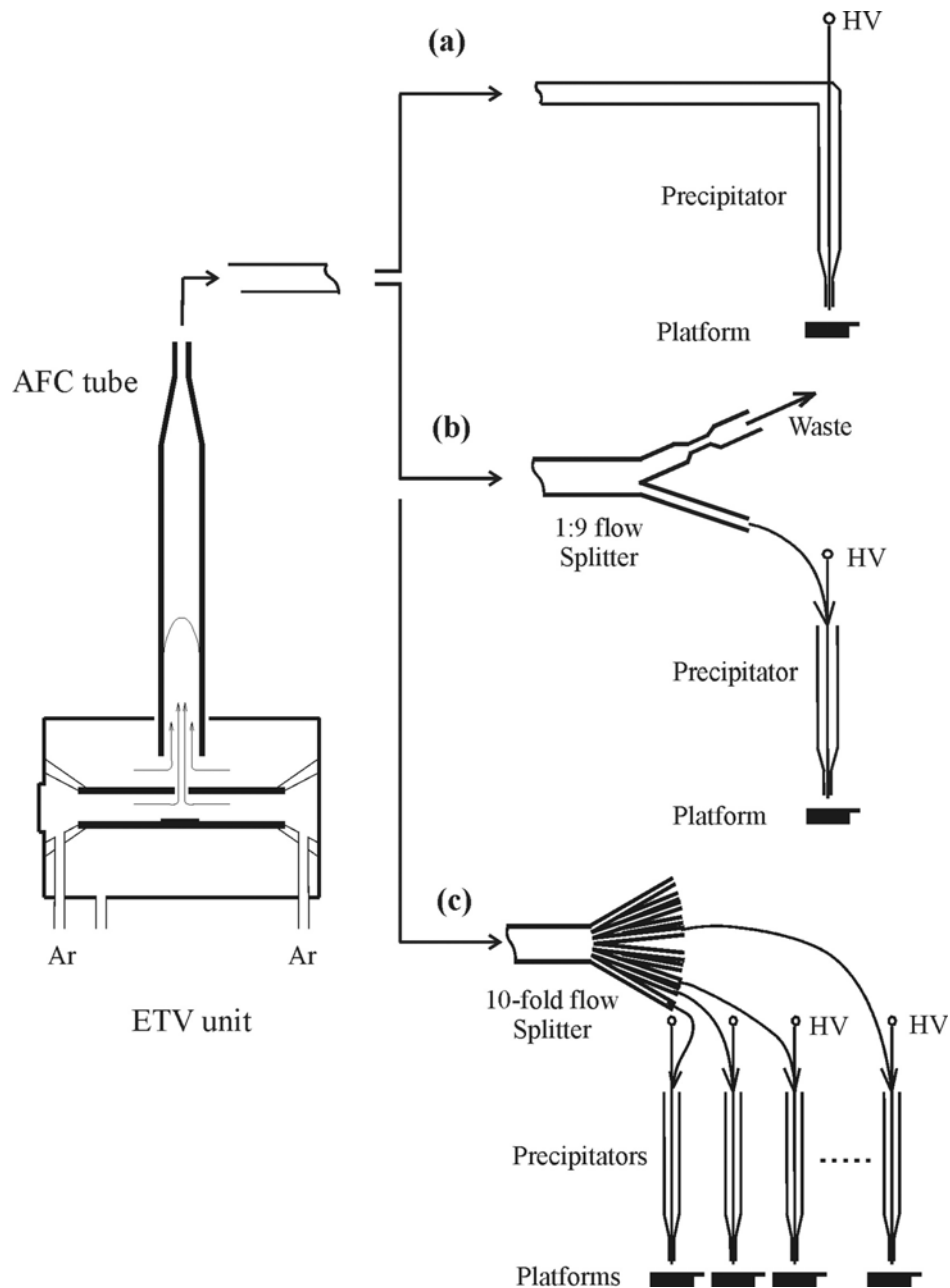


**Fig. 2.7:** Principle of aerosol transport, dividing, and dosing: (a) transport with internal/external EP dosing; (b) transport and dividing with internal/external EP; and (c) transport and dividing with external EP onto a set of sample collectors.

Fig. 2.8 shows technical realization of the EP equipment for internal aerosol deposition for both pre-divided and non-divided aerosol flows. A glass capillary with a Y-formed end piece combining electrical and gas flow connections is mounted on a laboratory modified

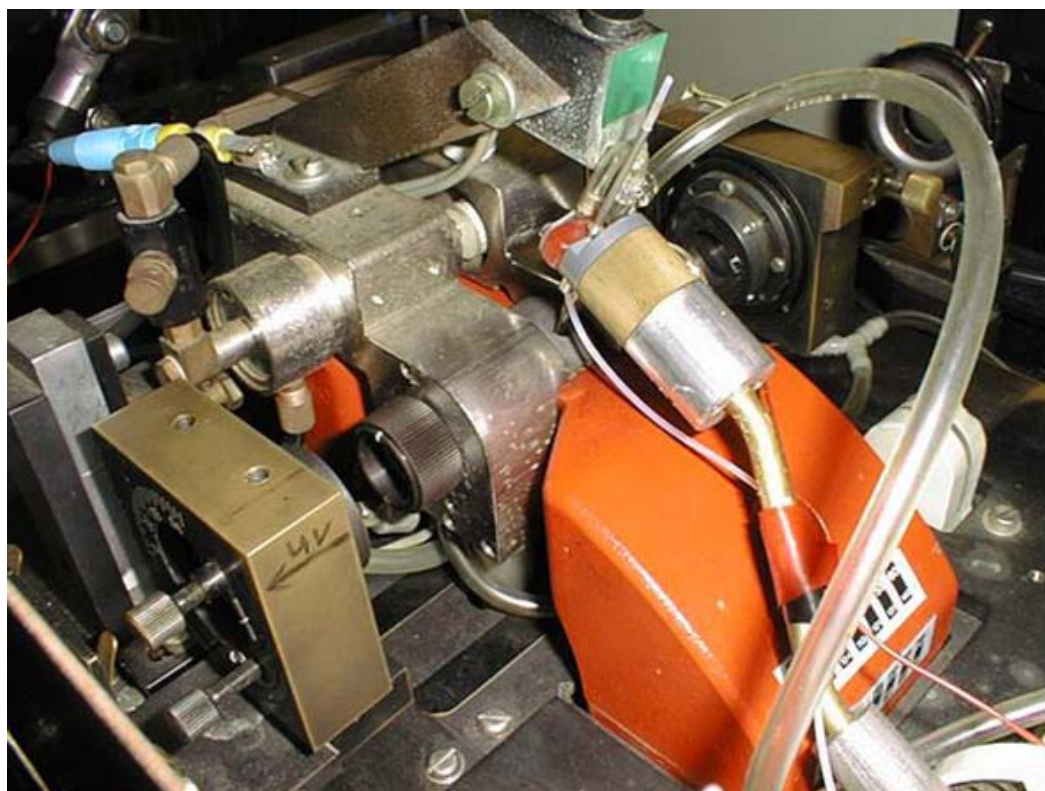
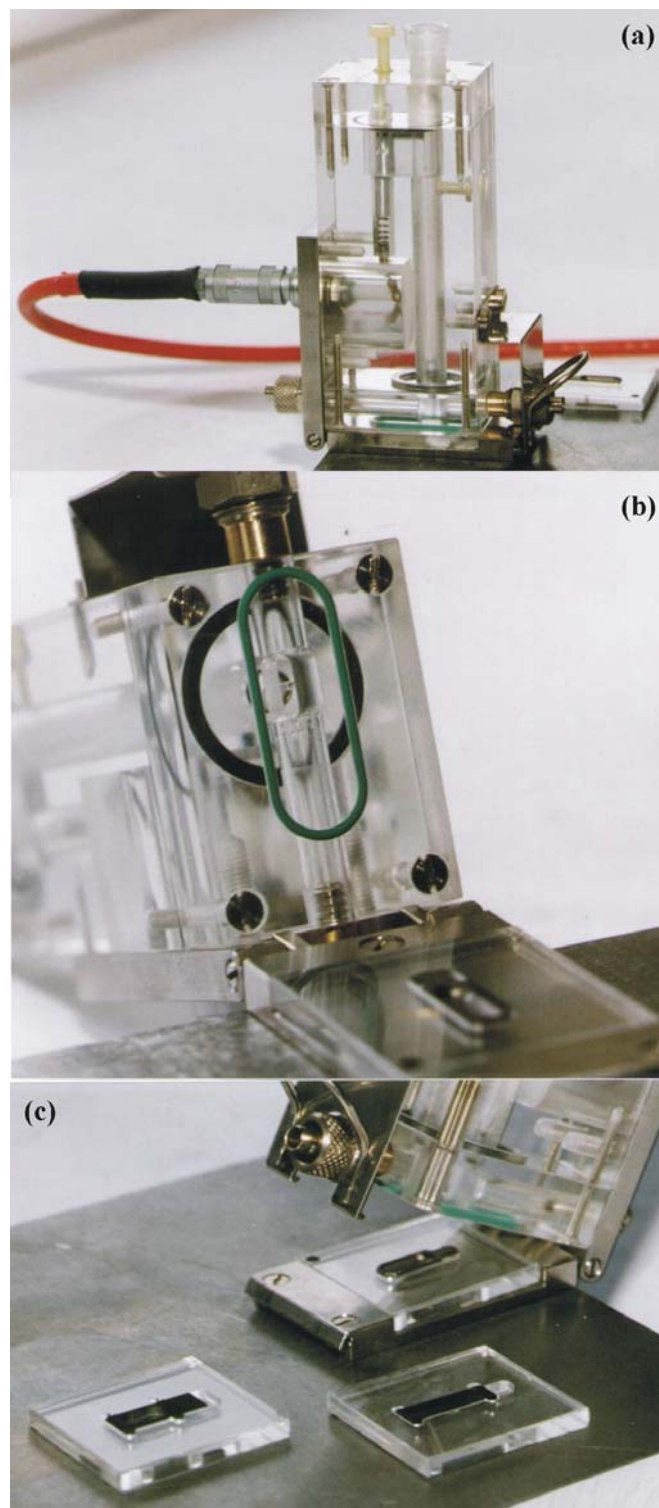


**Fig. 2.8:** Technical realization of internal EP directly onto the L'vov platform of the ETA furnace (HGA-600) with the AS-60 autosampler. The autosampler cap can be easily rotated by 180° between two pre-adjusted positions for sampling of aqueous solutions and ETV aerosols.

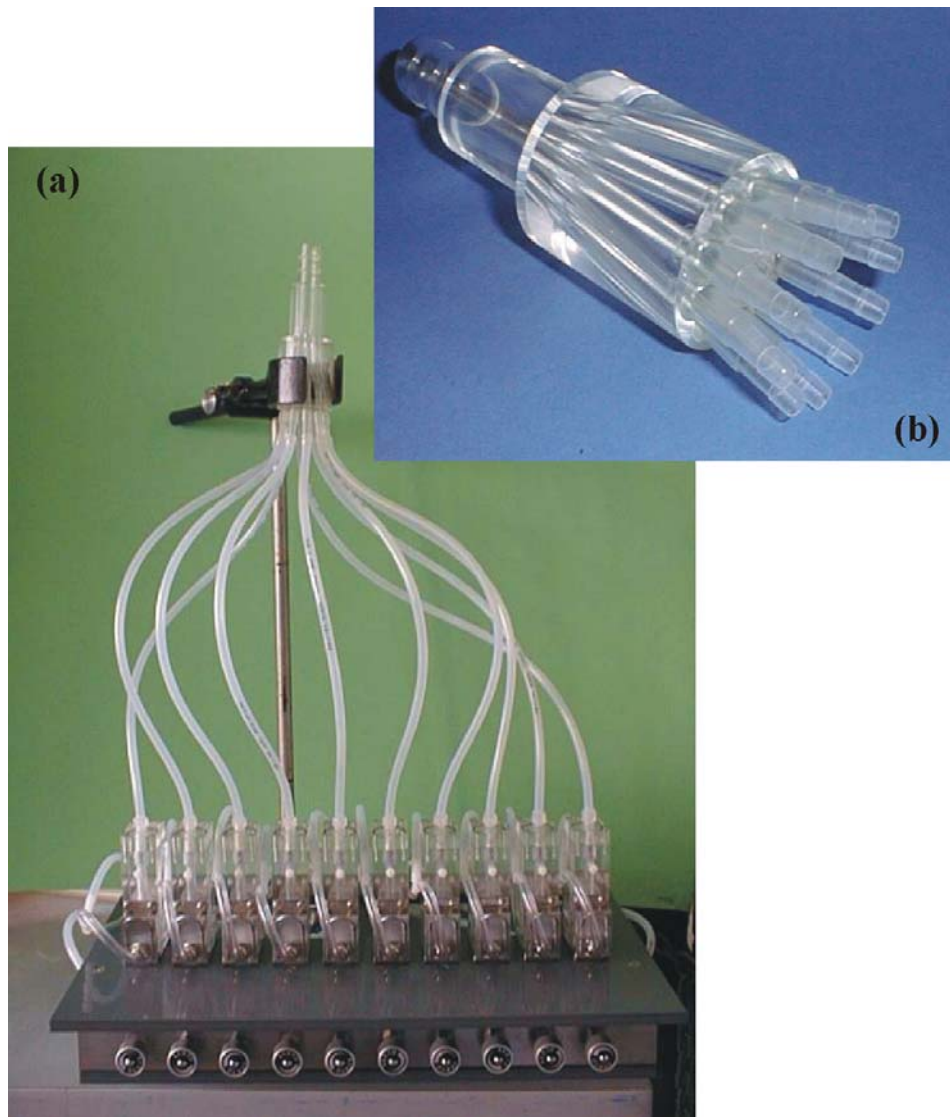
dosing arm of the AS-60 autosampler (Bodenseewerk PerkinElmer GmbH, Überlingen, Germany). After modification, the dosing arm is capable for sampling ETV aerosols and aqueous solutions. The autosampler with its mechanical precision inserts the sampling capillary into the ETA furnace through the dosing hole.

Fig. 2.9(a),(b) shows the laboratory-made equipment for external collection of the aerosol. The precipitation capillary is mounted and fixed in a housing. Position of the capillary and the wire relative to the substrate is controlled with adjustment screws. Fig. 2.9(c) shows adapters for secondary platforms for instruments of Analytik Jena AG, PerkinElmer, and Gruen AMS GmbH.

Photographs of the 10-fold precipitator and the highly symmetric 10-fold flow splitter are shown in Fig. 2.10. The calibration valves are in the bottom part of the precipitation unit.



**Fig. 2.9:** Technical realization of external EP onto GF boats [Her1]: (a) laboratory constructed external electrostatic precipitator; (b) electrostatic precipitator in open state; and (c) EP onto different platform types.



**Fig. 2.10:** Technical realization of (a) an external 10-fold precipitator and (b) a highly-symmetric 10-fold aerosol splitter [Her1].

### 2.3.2 Electrostatic sampling

Fig. 2.11 shows the principle and the variants of employing the electrostatic sampling used in this work. A deposition electrode (100- $\mu\text{m}$  tungsten wire) with a sharp tip is placed in the glass capillary and is located approximately 1.5-2 mm above the substrate for precipitation (platform collector) and directed transversely to it. The distance between the capillary and the substrate is 2-2.5 mm. The platform collector is grounded while negative voltage of 1.2-1.5 kV is applied via 30-40 M $\Omega$  pre-resistors to the deposition electrode to obtain a stable corona-

like discharge current of 1.2-1.6  $\mu\text{A}$ . By intra-furnace precipitation, the discharge area is partially protected against ambient air due to internal furnace gas ( $300 \text{ mL min}^{-1}$ ). For external precipitation, the deposition chamber is completely sealed.

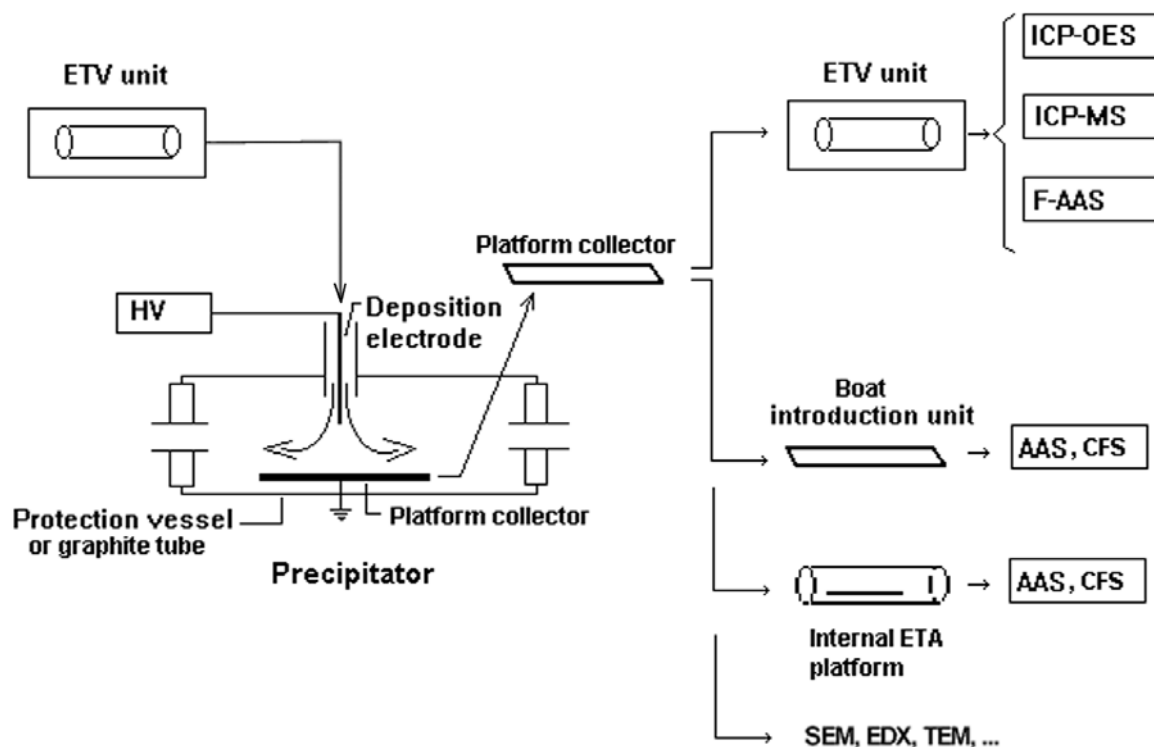


**Fig. 2.11:** Principle and capabilities of electrostatic sampling.

After deposition, the platform collector can be introduced into the ETV unit for ICP-OES/MS, FAAS, and CFS analysis as well as directly into the ETA furnace for AAS and CFS spectrometry [Ber1, Ber2]. By employing appropriate substrates, the collector can be analyzed with scanning electron microscopy (SEM), energy dispersive x-ray microanalysis (EDX), transmission electron microscopy (TEM) etc. Some of these methods are used for analysis of deposited particles in this work.

## 2.4 Samples and reagents

Aqueous multi-element solutions (dosing samples and solutions for calibration) are prepared by adequate dilution of standard stock solutions of metal nitrates ( $1000 \text{ mg L}^{-1}$ ) of Ag, Al, Cu, Fe, Mn, Ni, and Pb with double distilled water and acidified with nitric acid of

suprapur® grade to obtain 1% concentration (reagents produced by Merck KGaA, Darmstadt, Germany). Modifiers are prepared by adequate dilution of potassium standard stock solution (1000 mg L<sup>-1</sup>) and palladium modifier solution (Pd(NO<sub>3</sub>)<sub>2</sub>). Argon (99.996% purity, Messer Griesheim GmbH, Krefeld, Germany) is employed as internal, external, and sluice gas. By introducing the gaseous modifiers with the ETV internal gas, the final concentration in the range of 0.5-5% v/v C<sub>6</sub>H<sub>12</sub> is obtained.

## 2.5 Operative parameters and procedures

### 2.5.1 Sample analysis with intra-furnace EP

Temperature program for the ETV furnace is given in Table 2.1 (a). After adequate pre-dilution, an appropriate volume of the sample is injected manually into the ETV boat with a pipette (Eppendorf–Netheler–Hinz GmbH, Hamburg, Germany). Then, the boat is introduced into the ETV furnace. During drying and pyrolysis steps, the furnace is kept open and flushed with 1.5 L min<sup>-1</sup> argon flow. Gas enters from the rear end into the furnace, flows through the graphite tube and removes drying and pyrolysis products through the open fore end to avoid contamination of the transport tubing and sampling capillary. After pyrolysis, the ETV furnace is closed and the gas flows are tuned to the operative rates. The autosampler inserts the sampling capillary to the ETA furnace and, after a 5 s delay, high voltage is applied to the deposition electrode. The vaporization starts 10 s later to ensure a stable corona discharge. The flow rate through the capillary for optimal precipitation conditions should not

(a) ETV			(b) HGA-600		
Step	Temperature (°C)	Time (s)	Step	Temperature (°C)	Ramp time (s)
Dry	120	60	Dry	90	15
Pyrolysis	350	90	Dry	120	10
Cool-down	20	10	Pyrolysis	400	10
Vaporize	2600	7	Cool down	20	1
Cool-down I	1800	10	Atomize*	2500	0
Cool-down II	1300	10	Cool down	20	1
Cool-down III	800	10	Clean	2600	0
Cool-down IV	20	60			
Clean	2650	6			

\*gas-stop mode

**Table 2.1:** Temperature programs for (a) ETV and (b) HGA-600.

be higher than  $150\text{--}200\text{ mL min}^{-1}$ , at higher rates laminar flow becomes turbulent [Buc1, Buc2]. After the subsequent cool down step (stepwise during 60 s in order to prevent reverse flow owing to gas contraction), the EP process is completed. Before starting the optional cleaning step, the high voltage is switched off and the autosampler removes the precipitation capillary from the ETA. The whole ETV-EP measurement cycle takes about 4–5 min. Fig. 2.12(a),(b) shows schematic presentation of the measuring cycle for dosing of solid and aqueous samples into the HGA-600 furnace of the CS-CFS spectrometer.

### 2.5.2 Sample analysis with external 10-fold precipitation unit

A primary sample is vaporized into  $150\text{--}200\text{ mL min}^{-1}$  internal flow and transported to the 10-fold precipitator. The total flow remains constant at  $1.5\text{ L min}^{-1}$  in order to obtain the optimal flow rate through every precipitator after splitting into 10 sub-flows. When the precipitation is completed, the loaded secondary platforms are sequentially introduced into the ETV and analyzed by employing a second ETV-EP process this time with intra-furnace EP. Thus, the secondary samples are subjected to a tandem ETV-EP process. Calibration of the second ETV-EP process is performed against multi-element solutions dosed onto the ETV boat. Besides CFS, secondary samples are also analyzed with single- and multi-element analytical instruments (SSAAS, ETV-ICP-OES/MS, and ETAAS) in the context of international research cooperation after post mailing of the platforms in plastic containers.

### 2.5.3 Sample analysis with addition of aqueous and gaseous modifiers

Aqueous modifiers are dosed into the ETV boat after or prior to the sample and subjected to the same thermal pretreatment procedure.

The external generator of gaseous additives is allowed to run for a minimum of 30 min before any data is collected. After variation of the flow rate through the flask, an appropriate delay to stabilize the corona discharge is applied. The carbon concentration in the internal flow is estimated under the assumption of full saturation of the flow through the flask and controlled via bubble frequency as well as via corona discharge current.



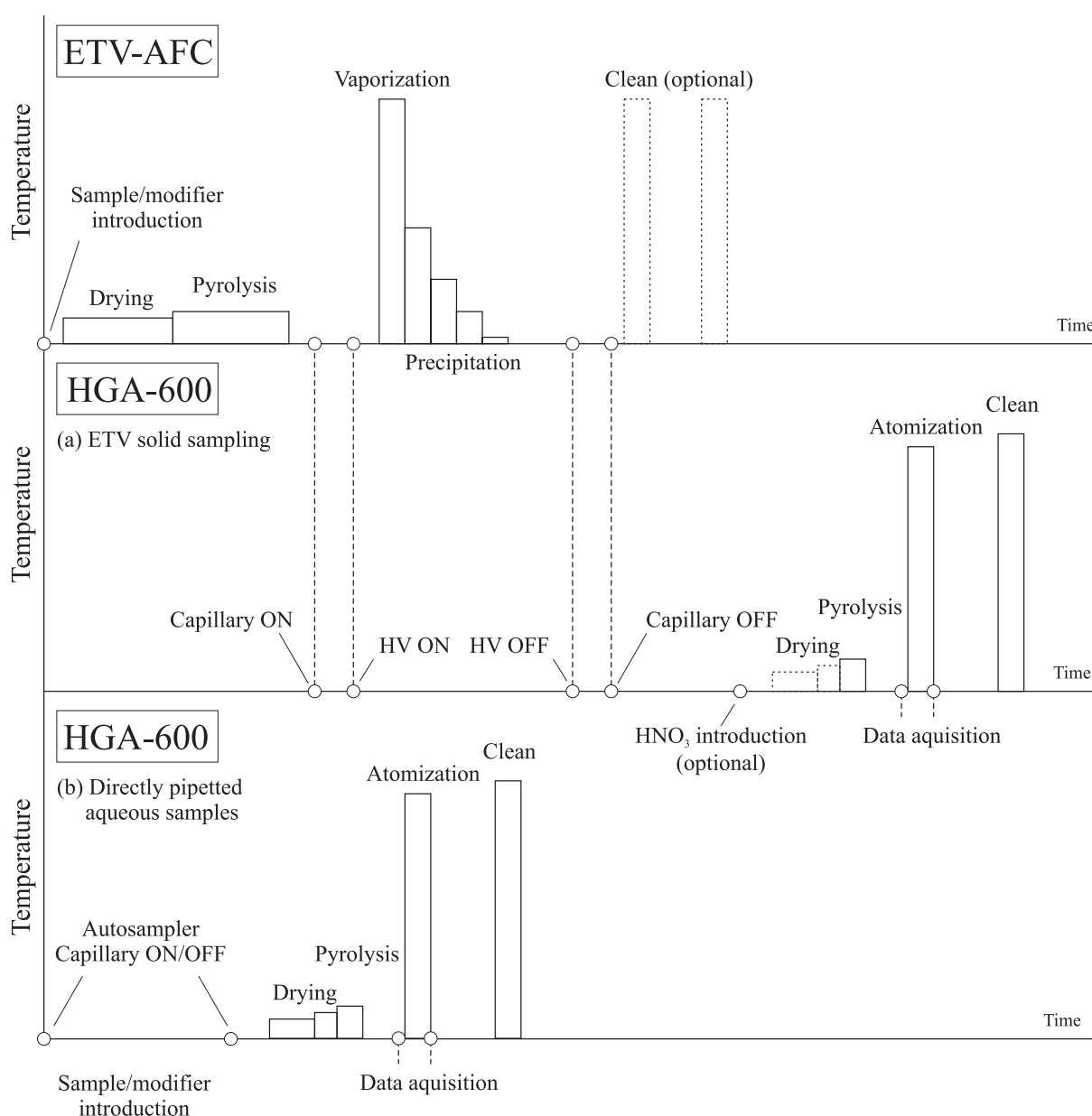


**Fig. 2.12:** Schematic presentation of the measuring cycle for the cases of (a) ETV-EP solid sample introduction and (b) aqueous sample introduction.

#### 2.5.4 Determination of analyte TEs

Analyte TEs for ETV-EP dosing are determined by means of the analytical calibration curve technique [Iup1] and the bracketing technique [Iup2] comparing analytical signals obtained by dosing the calibration multi-element standards in solutions directly into the ETA furnace of the spectrometer with signals obtained using the sample solutions subjected to the full ETV-EP CS-CFS procedure. The calibration is performed prior to or immediately after

the measurement series. Intensities of the analyte resonance lines obtained by ETA CS-CFS for transported samples as well as for calibration solutions are measured simultaneously.

Owing to the quadratic characteristic between transmitted intensity and atomic density [Her4], peak areas were preliminary linearized with coefficients that differ from line to line and then used as analytical signals. The algorithm of spectra evaluation is presented in Appendix A.3.

### 2.5.5 SEM and TEM investigations

Silicon wafers (20-25 mm<sup>2</sup>) after appropriate cleaning in 15% v/v HCl acid are used for SEM investigation of carbon and analyte particles produced by ETV using Philips XL 30 electron microscope. Nickel nets with carbon films (400 mesh, d=3.05 mm) are used for TEM. Particles are collected by external precipitation (SEM) as well as by thermophoresis in the upstream (SEM, TEM) and within the GF (SEM). Prior to analysis, the loaded silicon wafers are held in argon environment to prevent surface oxidation.

### 2.5.6 Temperature measurements in the upstream

Temperature measurements in the upstream are carried out during the step as for vaporization, however without sample dosed, and during subsequent cool down steps. The height is varied from 2.5 mm from the GF outlet until to the outlet of the AFC tube.

The calibration curve for PtRh-PtRh thermocouple used for the conversion of thermo voltages into the temperatures is shown in Fig 2.13.

### 2.5.7 Determination of GF carbon losses

For gravimetrical tracing of carbon losses during the tube ageing, the accumulative mass loss and the number of firings (including both vaporization and cleaning firings) are determined. After each series of measurement, the tube is weighted on a balance (Model M5SA, Mettler, Zurich, Switzerland). The differential losses are roughly estimated as an average of a weight difference per number of shots, when this weight changing takes place.

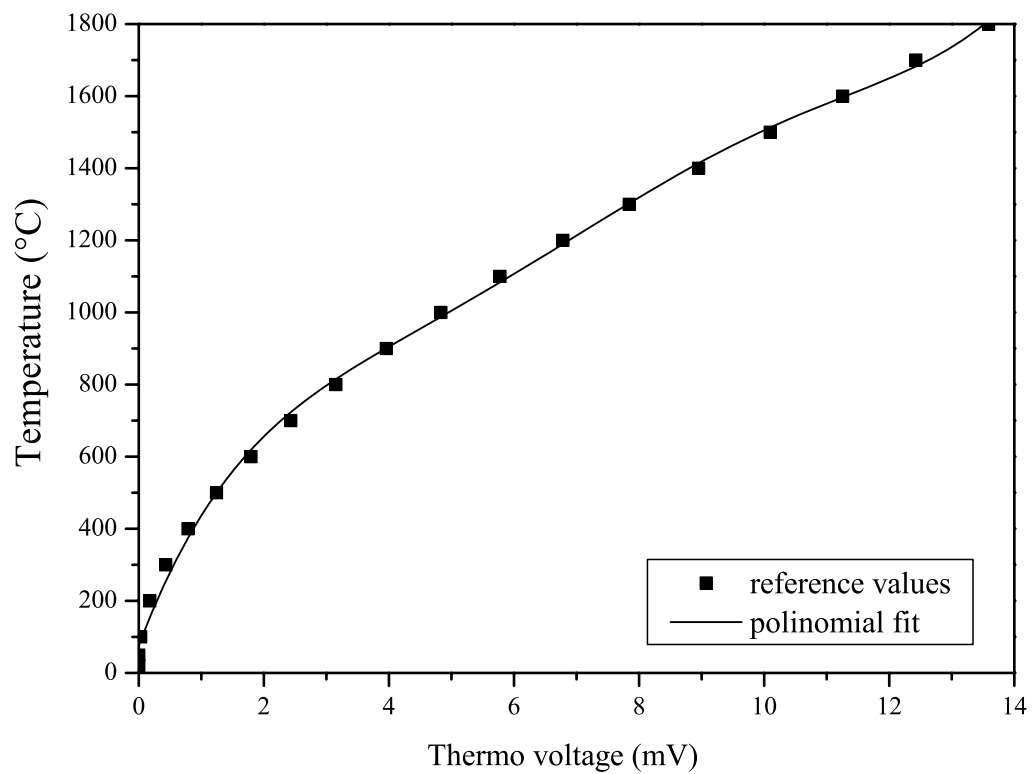


**Fig. 2.13:** Calibration curve for PtRh-PtRh thermocouple used for temperature measurements on the upstream axis.

---

### 3. Investigation and optimization of the ETV-AFC setup: influences of GF carbon, modifiers, and gaseous additives on the transport process of sample analytes

---

#### 3.1 ETV development

Results obtained with the former used end-on flow-through ETV in our working group [Buc2, Ber1, Ber2] were rather poor. The TEs turned out to be relatively low and very different for different elements, i.e. higher for volatile and low for medium and low volatile elements. It forced us to construct a new ETV unit with higher and with more homogeneous TEs because with the reducing absolute analyte losses their differences become reduced as well.

The principle of the construction is based on the upstream inside a vertically oriented glass tube that creates the AFC zone where the particle condensation occurs predominantly apart from the colder walls (see Sect. 2.1.). The use of the upstream configuration allows significant reduction of analyte losses within the GF tube while the use of the AFC tube reduces their loss during further transport. The aim of experimental efforts is the improvement of the ETV performance expressed in the analyte TE and the reduction of the total analyte losses. First test with the new ETV-AFC setup showed higher TEs, which were still different for different elements. TEs up to 24% for Cd, 25% for Ag, 27% for Pb, 30% for Mn, 25% for Cu, 31% for Fe, and 33% for Ni were determined for aqueous multi-element solutions with 3-4 times higher analyte concentrations compared with the later applied. To enhance the analytical performance, the construction is modified as described below.

##### 3.1.1 Axially focusing convection (AFC) tube

The efficiency of analyte-aerosol transformation is strongly affected by the flow structure within the AFC zone that is under given flow rates governed mainly by the convection tube geometry and its dimensions. Experiments confirmed that the tube form and the inner diameter play a key role to obtain optimal conditions for aerosol formation. Several bell-shaped tubes as well as convectors with cylindrical cross-sections were tested, and model vaporizations with smoking samples and gaseous additives to the internal gas flow were performed. The experiments showed the priority of the cylindrical tube with diameter reduction at the tube outlet for the proper junction with the 6 mm inner diameter transport tubing.

Further, at very large internal tube diameters, the upstream becomes very fast due to the low density of the hot flow and the high buoyant force exerted by the surrounding coolant gases that drives a counter-flowing downstream pressed against the cold AFC tube walls. At too low tube diameters, the wall condensation is coming to play the dominant role in the analyte loss. With optimal dimensions (13 mm inner diameter for  $1.5 \text{ L min}^{-1}$  gas flow), a stream with a laminar-like behavior can be obtained within the AFC tube where the cooling gases create a shield layer to the inner AFC tube surface. Thus, these optimizations should decrease the analyte loss during condensation and enhance the total ETV-EP TE.

### 3.1.2 Radiation shielding

The second point is that the longitudinal temperature gradients in the upstream right above the outlet of the GF should be as high as possible in order to facilitate aerosol formation. It was found that the emission of the incandescent ETV walls is a major cause for increased temperatures of the condensing particulates. With the aim to reduce the heating, the upstream is shielded against furnace radiation with a specifically designed radiation shield (see Sect. 2.1.2).

First experiments were performed before this work began with a 1 mm thin tantalum plate with a 7 mm opening for the upstream flow. This first approach was unsuccessful. Despite the high melting-point of tantalum (about  $3000^{\circ}\text{C}$ ), the shield was completely deformed and destroyed after several measurement cycles. Nevertheless, the obtained empirical data were useful for getting some basic information on required properties of the radiation shielding.

Then, a 7 mm thick copper plate with a conical opening (with diameter widening in the upstream direction, 7 mm and 14 mm bottom and top diameters) in the center was mounted to one of the water-cooled copper flange holding the graphite cone of the ETV furnace. The plate had sufficient heat capacity to collect the thermal radiation of the GF during the fast heating cycle and good thermal contact to the cooled flange for rapid cooling down between the firings. The conical geometry of the opening should reduce the analyte diffusional losses within the plate prior to mixing with the second flow of the cooling gas.

Besides the thermal shielding, the plate allowed to improve the heat exchange between the hot ETV internal flow and the surrounding external cooling gases in the AFC upstream. The surrounding in this construction occurs directly above the GF outlet. These two factors

gave rise to a considerable increase of the longitudinal temperature gradients (up to 3000 K  $\text{cm}^{-1}$ , Sect. 3.4) causing faster particle condensation. These improvements led to a significant enhancement of the analyte TEs for all analytes studied. Fig. 3.1 illustrates this effect for the ETV operating conditions with 1.5 L  $\text{min}^{-1}$  total gas flow and 1:9 flow splitting prior to EP. With taking into account the effect of the analyte mass on analyte TE shown by Buchkamp [Buc2] for the flow-through ETV, it should be noted that measurements with the improved ETV are performed with much lower analyte amounts that repeatedly clearly signifies the advantages of the improved ETV construction.

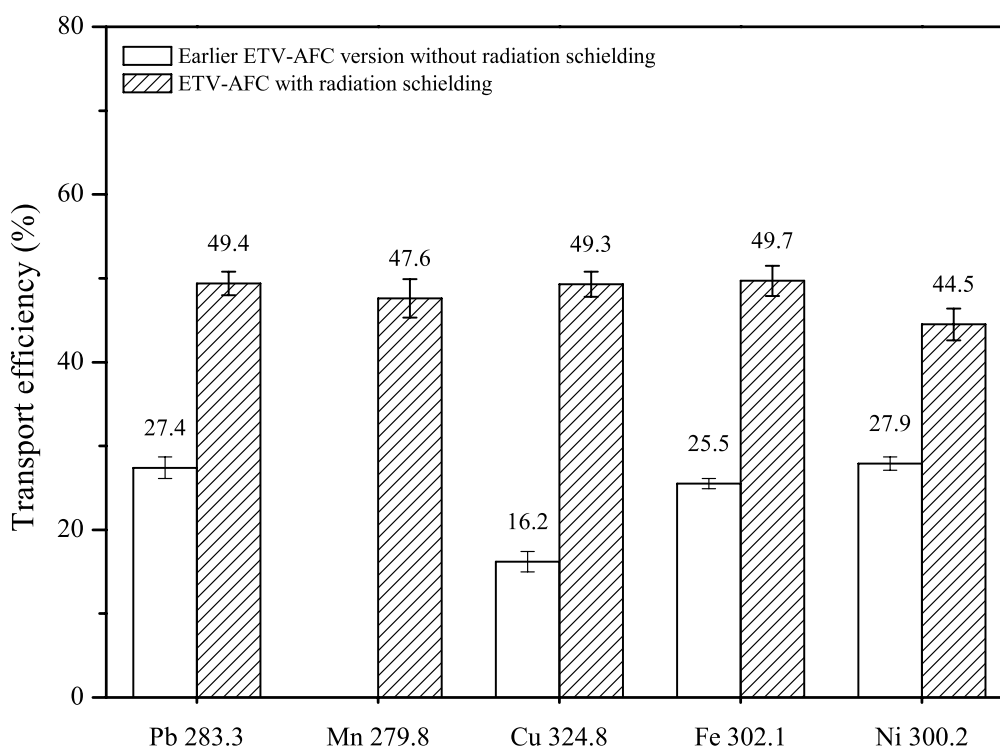


**Fig. 3.1:** Effect of upstream shielding against incandescent GF tube radiation on TEs for Cu, Fe, Mn, Ni, and Pb dosed as liquid solutions into the ETV boat. Analyte masses: 64 ng Cu, Fe, Pb, and 640 ng Ni (ETV without radiation shielding) and 4 ng Mn, 20 ng Cu, Fe, Pb, and 100 ng Ni (ETV with radiation shielding); flow conditions 200/1300 mL  $\text{min}^{-1}$  (internal/external flow) with 1:9 splitting; standard deviations for  $n=5$ .

The further step in the improvement of the ETV setup is introduction of an additional “cold” cooling gas – the sluice flow (Fig. 2.3) – through the cooled copper plate. It allows particularly to avoid flow heating prior to admixture to the upstream in contrast to the other

external cooling flows subjected to the GF heating. For this purpose, the plate was modified as it was described in Sect. 2.1.2. The flow was admixed to the upstream to achieve besides the cooling the reduction of the amount of graphite particles originating from the outer GF surface and carried by the external flow 1 (Fig. 1.3). In order to reduce possibly occurring turbulences in the upstream flow, the total cross-section of the arranged outlet ring slit was made as large as possible to decrease the linear velocity of the stream. The optimization of the gas flow distributions is presented in details in Sect. 3.3.

### 3.1.3 Comparison of analytical performances for ETV-FT and ETV-AFC instruments

The analytical performance of the improved ETV-AFC device was tested by using aqueous multi-element solutions and compared with that for the end-on flow-through ETV [Ber2]. Fig. 3.2 shows the comparison of the TEs for Ag, Al, Cd, Cu, Fe, Mn, Ni, and Pb, elements of widely differing volatilities. The ETV-AFC system presents much higher TEs, which are additionally more uniform for the analytes with different volatilities.

Some observed features of this setup have to be mentioned. In the upstream system the analyte losses will be decreased with the decreasing the analyte volatility in contrast to the all known flow-through systems [Kan7, Ber2, Kri6, Hol2]. For example, using radiotracer technique, Schäffer and Krivan [Kri6] showed that the elements with high boiling points were retained by more than 40% in the GF while the more volatile ones were retained in much lower amounts. The deposition increased with decreasing temperature in the gas flow direction from 3-4% (percentage of total deposition) on the GF center (the hottest part), where the platform was placed, and reached the maximum value (~80-85%) on the coolest outlet part of the GF. Therefore, one can conclude that the upstream construction is inherently more suitable for handling with analytes with widely differing volatilities: under optimal ETV working conditions (flow distribution, GF heating conditions, applied modifiers etc.) a major part of analyte atoms doesn't have any contact with colder surfaces and, hence, the analyte losses can be significantly reduced.

Though the ETV-AFC instrumentation provides higher TEs, at least a half (see Fig. 3.1) of dosed sample analytes is still lost by transporting to the analytical instrument at present state of the development. This figure for flow-through ETVs is even worse; only 10-50% [Dam3] of the analyte mass introduced into the ETV boat can reach an analytical instrument

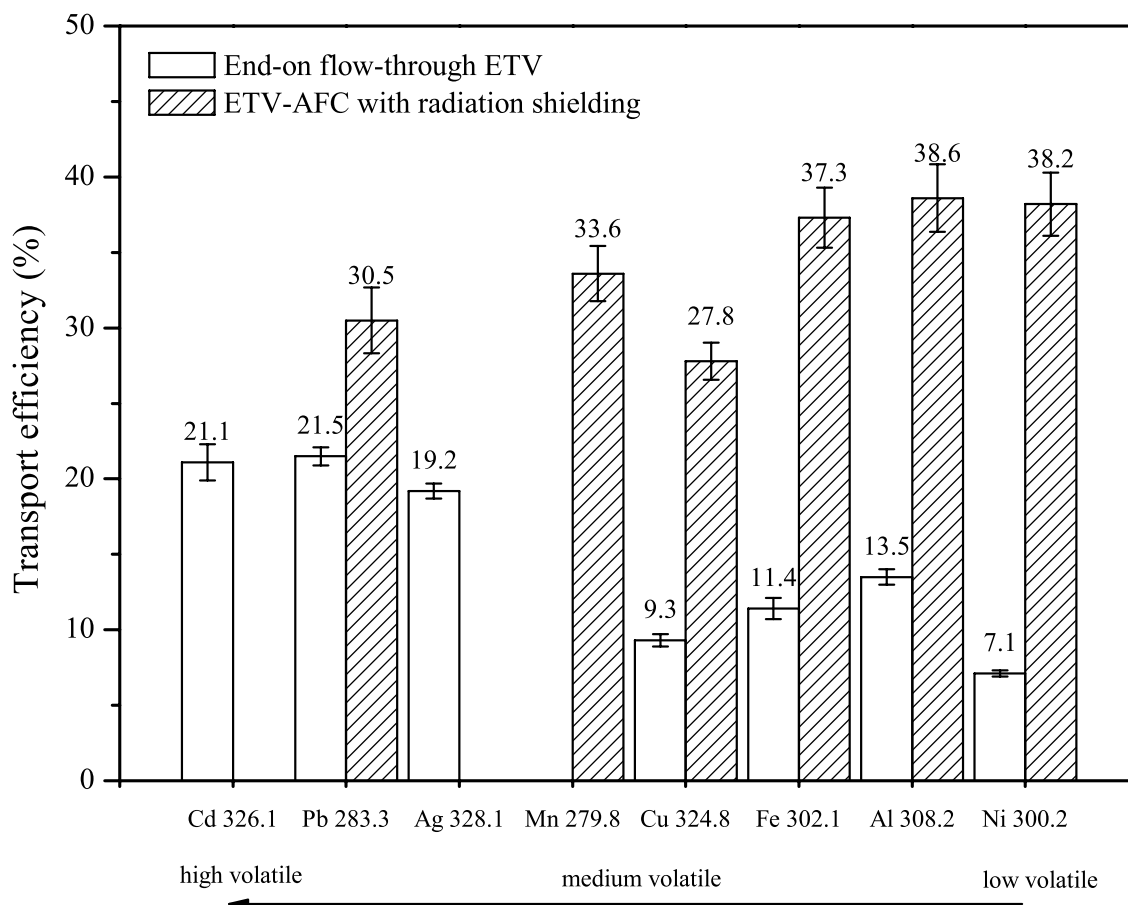


**Fig. 3.2:** ETV-EP analyte TEs for high, medium, and low volatile elements with end-on flow-through ETV and ETV-AFC, determined simultaneously, calibrated against aqueous standard solutions dosed into ETA-CFS furnace. Sample for end-on flow-through ETV measurements: 2 ng Ag, 6.4 ng Al, Cu, Fe, Pb, and 64 ng Cd, Ni; total flow: 150 mL min<sup>-1</sup> [Ber2]; sample for ETV-AFC measurements: 0.4 ng Mn, 2 ng Al, Cu, Fe, Pb, and 10 ng Ni; total flow 220 mL min<sup>-1</sup>.

after sample vaporization, condensation, and aerosol transport. The problems of flow-through ETVs are relatively good investigated by different groups [Kri6, Hol2, Buc2, Ber1, Ber2]; the typical sites of the analyte loss are localized and the systems are optimized with the goal to enhance the analytical performance.

### 3.2 Optimization and controlling of the GF heating conditions

Temperature programs that have been use by Buchkamp [Buc2] for the end-on flow-through ETV have included a pre-vaporization step (temperature 600°C, duration 6 s) with the aim to prepare the GF for rapid temperature increase with the thermal expansion of the GF



tube material. The same temperature programs were later employed for the ETV-AFC unit as well. The pyrometrical investigation of the GF heating process performed with the ETV-AFC unit showed that the GF reaches the pre-set temperature 3-4 s after the beginning of the vaporization step, which continues typically 6-8 s. In this case, the GF platform that is heated mostly through the furnace radiation achieves the vaporization temperature with a 5-6 s delay. Such conditions extend the analyte vaporization time and can lead to incomplete evaporation of analytes with higher melting points. Besides, high, medium, and low volatile elements are co-vaporized with carbon amounts differing in the orders of magnitude. In this case, the transport of analytes with lower volatility is more supported by carbon particulates acting as analyte carriers. As a result, we obtain completely different transport conditions for different analytes.

With the aim to obtain more similar vaporization conditions for analytes with widely differing volatilities, a pre-vaporization step with maximal power (“max. power”) of the ETV power supply is introduced into the temperature program. The fast heating temperature is set via the step duration because the used power supply is not equipped with an optical temperature controlling circuit. The effect of the “max. power” step on the heating rate of the GF and the platform is shown in Fig. 3.3(a). With the improvement of the heating program, the central area of the GF achieves the pre-set temperature 1-2 s faster. The platform heating occurs in this case rapidly (the rate is slightly faster than with the GF heating without “max. power” step). However, the time delay between platform and wall is remained. This delay is well known as “the platform effect” owing to the STPF concept where the analytes are released into the hot furnace [Wel2]. Fig. 3.3(a) illustrates it for our ETV-AFC system.

With the “max. power” step, the TEs for all analytes studied are increased by up to 3-4% without any remarkable dependence on volatility. The optimal heating conditions derived from this investigation are used for all further measurements.

Fig. 3.3(b) shows the transverse emitted radiation intensity of the GF center in normalized form used for controlling of the ETV heating conditions during the analytical GF tube lifetime. These measurements are performed together with the measuring of the electrical power dissipated on the GF (typically 5.9-6.1 kW) and are employed as a template for possible correction of the temperature program with the ageing of the GF tube in order to obtain the stabilized temperature conditions.

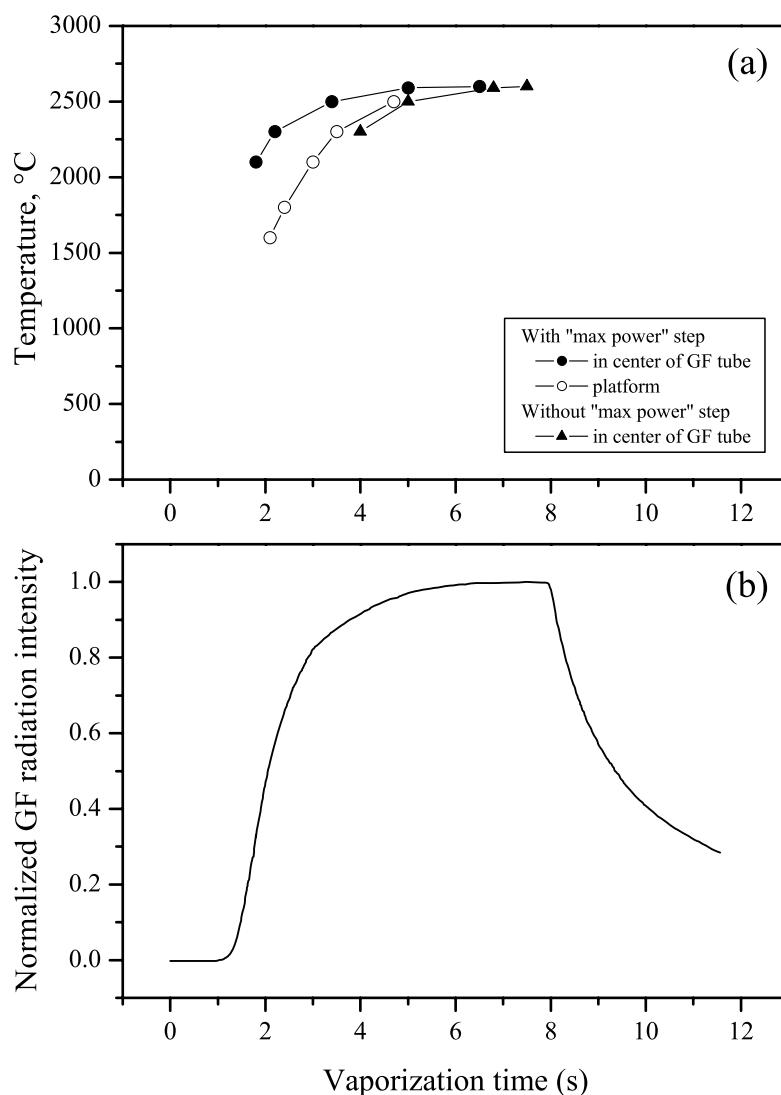


**Fig. 3.3:** Optimization and controlling of the ETV vaporization conditions: (a) pyrometrically (longitudinal observation through the housing side window) and (b) by means of a photodiode (transversal observation) for applied GFs of larger size; 2600°C vaporization temperature, 8 s hold time. Influence of the maximal power step on the ramp time, presentation of the “platform effect”.

### 3.3 Optimization of the ETV flow distribution

The introduction through the cooled copper plate of an additional cooling gas, here named sluice gas (see Sect. 2.1.2), has the following objectives. First, this bypass flow should prevent analyte deposition on the surface of the radiation shield and facilitate the upstream cooling down by laminar-like surrounding of the hot upstream close to the GF outlet. Besides,

the sluice gas should reduce unnecessary contamination of the transport gas with contaminants released from the outer GF wall.

With the introduction of the sluice gas, the distribution of the flows in the condensation zone had to be optimized again, in order to maintain the upstream focusing effect. Fig. 3.4(a) illustrates the dependence of the CS-CFS temporal peak areas in the normalized form for Pb, Mn, Cu, Fe, and Ni on the total flow dividing between the internal, sluice, and external gases. The first column in the diagram represents the ETV operating conditions without sluice gas addition. Optimal mode for analyte condensation and transport are found for 200/200/1100 mL min<sup>-1</sup> internal/sluice/external gas flow rates. Higher sluice gas flows cause obviously turbulences in the upstream leading to analyte adsorption on the walls.

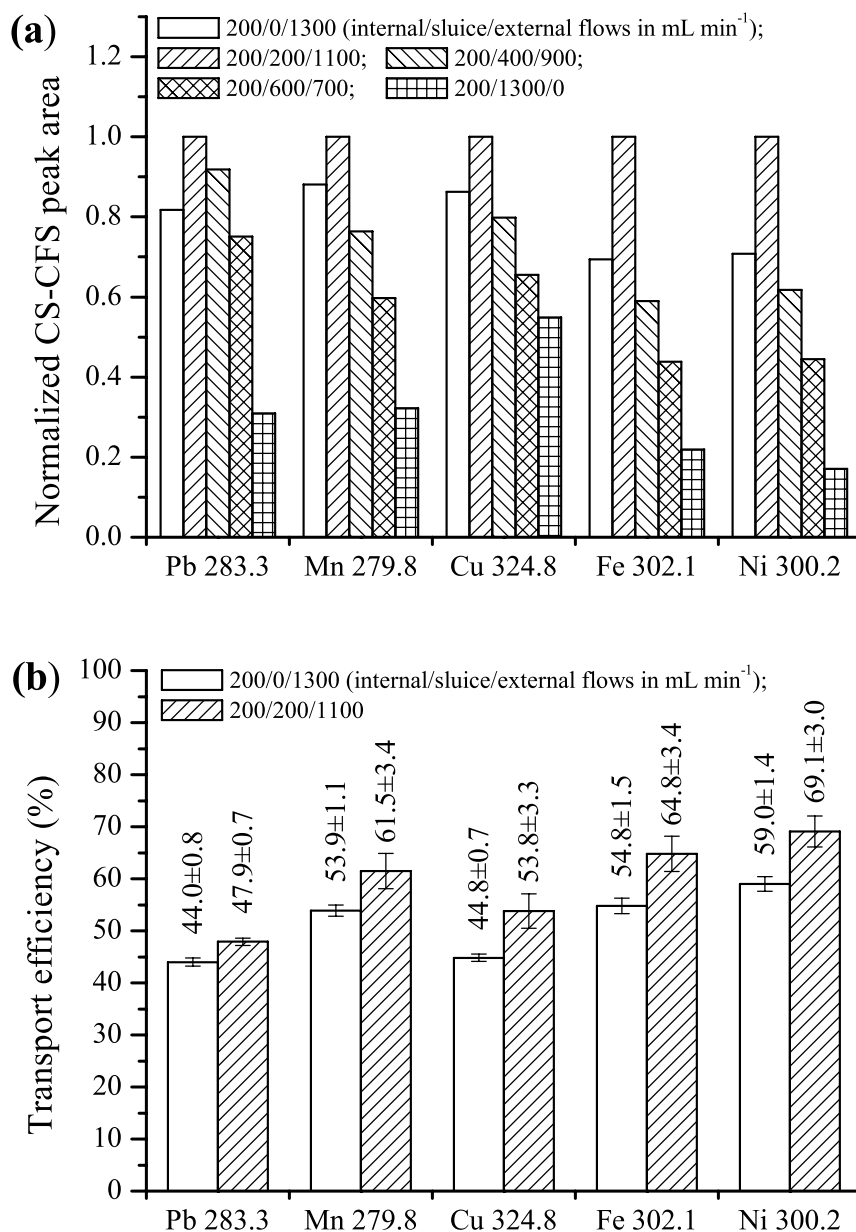
Fig. 3.4(b) shows the quantitative evaluation of the effect of the sluice gas introduction on the TE enhancement. The improved ETV setup shows up to 10% higher TEs for the five analytes studied. However, the losses of volatile analytes as well as the non-uniformities in the TEs remain to be high. The obvious discrepancies between the CS-CFS signals and the corresponding TEs for all analytes are possibly caused by fluctuation of the analyte TE, vaporization conditions etc. with the ageing of the GF tube. Fig. 3.4(b) represents more reliable results.

The same procedure of optimization of the flow distribution has to be performed after each modification in the ETV construction (such as variation GF outlet hole diameter, geometries of the radiation shield and the AFC tube etc.).

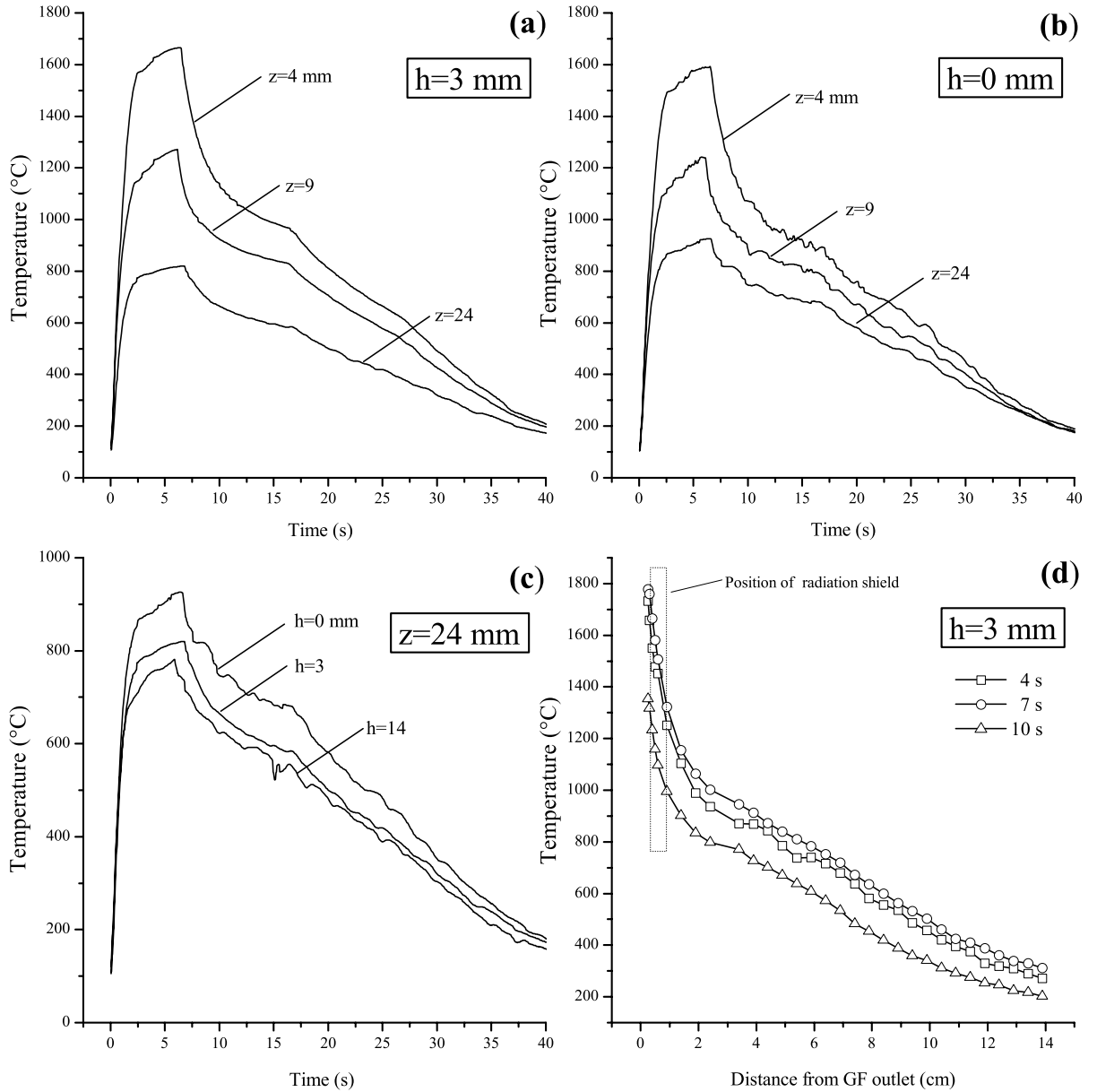
### 3.4 Measurement of temperature dependences on the axis of the AFC tube

The estimation of the longitudinal temperature gradients in the upstream especially at small distances from the GF outlet hole plays a key role in the understanding of the processes occurring by analyte condensation. The temperature behavior on the axis of the AFC tube during vaporization and cool-down steps is studied. The measurements are performed with flow distribution 200/1300 mL min<sup>-1</sup> (internal/external flow) without sluice gas addition and with the 3 mm diameter of the GF outlet hole. The temperature dependences for optimized and non-optimized flow distributions (Figs. 3.5(a) and 3.5(b), respectively) for different cut-offs of the vertical axis ( $z = 4$  mm,  $z = 9$  mm, and  $z = 24$  mm) are presented. The noise on the curves in Fig. 3.5(b),(c) is very likely caused by a turbulent behavior in the upstream. This

assumption is confirmed by observing the upstream flow with additives forming by decomposition visible soot particulates. The shape of the decay is defined by the stepwise cool-down (Table 2.1(a)) of the ETV that should prevent a reverse flow owing to the thermal gas contraction.



**Fig. 3.4:** Influence of the ETV flow conditions on analyte transport: (a) normalized CS-CFS temporal peak areas as a function of ETV flow conditions; (b) TEs with and without additional sluice gas. Analyte masses dosed into ETV boat: 4 ng Mg, 20 ng Pb, Cu, Fe, and 100 ng Ni.



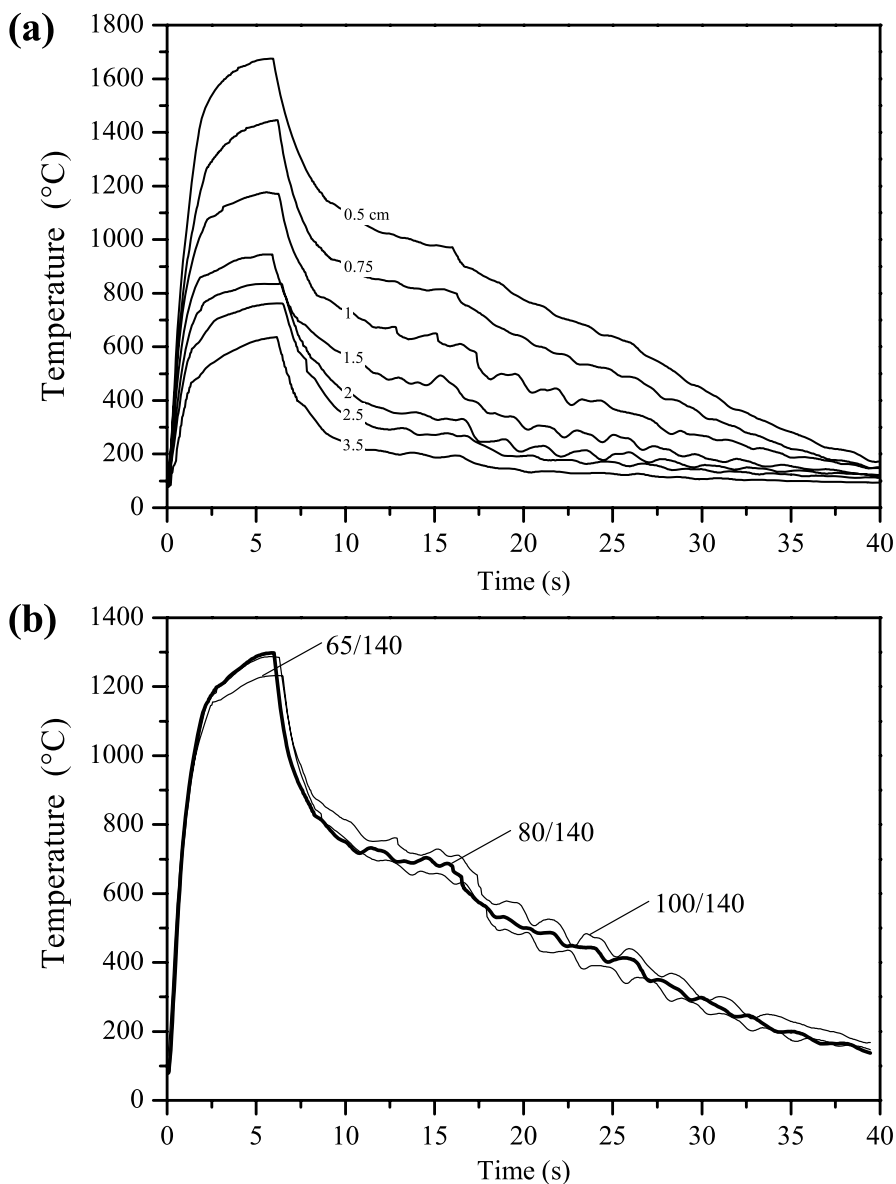
**Fig. 3.5:** Temperature dependences on the axis of the AFC tube during the ETV firing and subsequent cool-down steps: (a-c) temporal and (d) spatial. The plots (a) and (d) corresponds to the optimal flow conditions and the plot (b) for turbulent behavior in the upstream (noise on the curves). Obtained for the same vaporization temperature ( $2600^{\circ}\text{C}$ ) and flow distributions  $200/1300 \text{ mL min}^{-1}$  (internal/external), for different distances between the radiation shield and the AFC tube ( $h$ ) and for different vertical coordinates ( $z$ ) with the beginning at the GF outlet (at  $z=0$ ).

Fig. 3.5(c) shows temperature distributions for different splitting ratios ( $h = 0$  mm,  $h = 3$  mm, and  $h = 14$  mm) of the external flow into the external flow 1 and the external flow 2 (see Fig. 2.3) at the same vertical coordinate ( $z = 24$  mm). When the AFC tube is positioned

directly onto the top of the radiation shield ( $h = 0$  mm), the upstream temperatures are higher during the complete vaporization step that results in decreased temperature gradients along the condensation zone. It is caused by the fact that the external flow 1 that surrounds the upstream under the shield and hence is more heated than the external flow 2 that is admixed to the upstream above the plate. This effect along with the occurring whirls makes the condensation process slower and can probably enhance the analyte losses through the wall adsorption. At too large distances between the radiation shield and the convection tube ( $h = 14$  mm), the temperature gradients are slightly higher (at least above the shield) obviously due to the colder part of the external flow. Nevertheless, the turbulent behavior of the upstream eliminates this advantage.

Fig. 3.5(d) shows the temperature profiles in the upstream for the optimized flow conditions ( $h = 3$  mm, 200/1300 mL min<sup>-1</sup> internal/external gas flow rate) at different times during the vaporization and cool-down steps. The upper curve (7 s) corresponds to the maximal achieved temperatures in the upstream by current flow conditions. These curves reflect not only the dependence on the coordinate, but also the hidden ones on the flight time because by the data processing the delay times (occurring due to the limited propagation velocity of the upstream flow) were removed. These delay times are up to 0.1-0.3 s depending on the GF outlet hole diameter. Hence, the presented temperatures correspond to the temperatures of an analysis volume traveling along the AFC tube under current flow conditions. As it is seen from the Fig. 3.5(d), right above the GF outlet, the temperature gradient can achieve values up to 3000 K cm<sup>-1</sup>, whereas within the AFC tube they are much lower (about 60 K cm<sup>-1</sup>). These data are further applied for the modeling of the analyte condensation process in the ETV-AFC (Chapter 5).

The same experiments are also performed for the ETV operating conditions for direct platform-to-platform intra-furnace sampling with 220 mL min<sup>-1</sup> total gas flow and without flow splitting prior to EP. The temperature dependencies illustrated in Fig. 3.6(a) show more turbulent behavior of the upstream flow despite of the fact that they were obtained for the optimized for analyte transport operating conditions. This fact can partially explain the considerably lower ETV performance for the sampling with 150-220 mL min<sup>-1</sup> total gas flows. Fig. 3.6(b) shows the dependencies for different flow distributions. As it is clearly seen from the diagram, a deviation from the optimal conditions makes the upstream flow more turbulent. The AFC tube should be narrower to prevent turbulences at lower ETV flow conditions.



**Fig. 3.6:** Temporal temperature dependences on the axis of the AFC tube for the ETV mode with direct platform-to-platform sampling without splitting: (a) for different distances from the GF outlet hole with optimized on the maximum of the TE flow distributions 80/140 mL min<sup>-1</sup> (internal/external) and (b) for different ETV flow distributions; both obtained for the same vaporization temperature 2600°C.

Fig. 3.7 shows the comparison of the upstream temperatures against the vertical coordinate and estimated flight time of the analysis volume along the vertical axis obtained for the different ETV flow conditions: 80/140 and 200/1300 mL min<sup>-1</sup> (internal/external flow rates). Sample transportation under lower flows represents in higher spatial temperature gradients

(Fig. 3.7(a)) but in the coordinates against the flight time the temperature decrease (i.e. the heat exchange with the surrounding cooling gases) is more or less similar for the both modes.

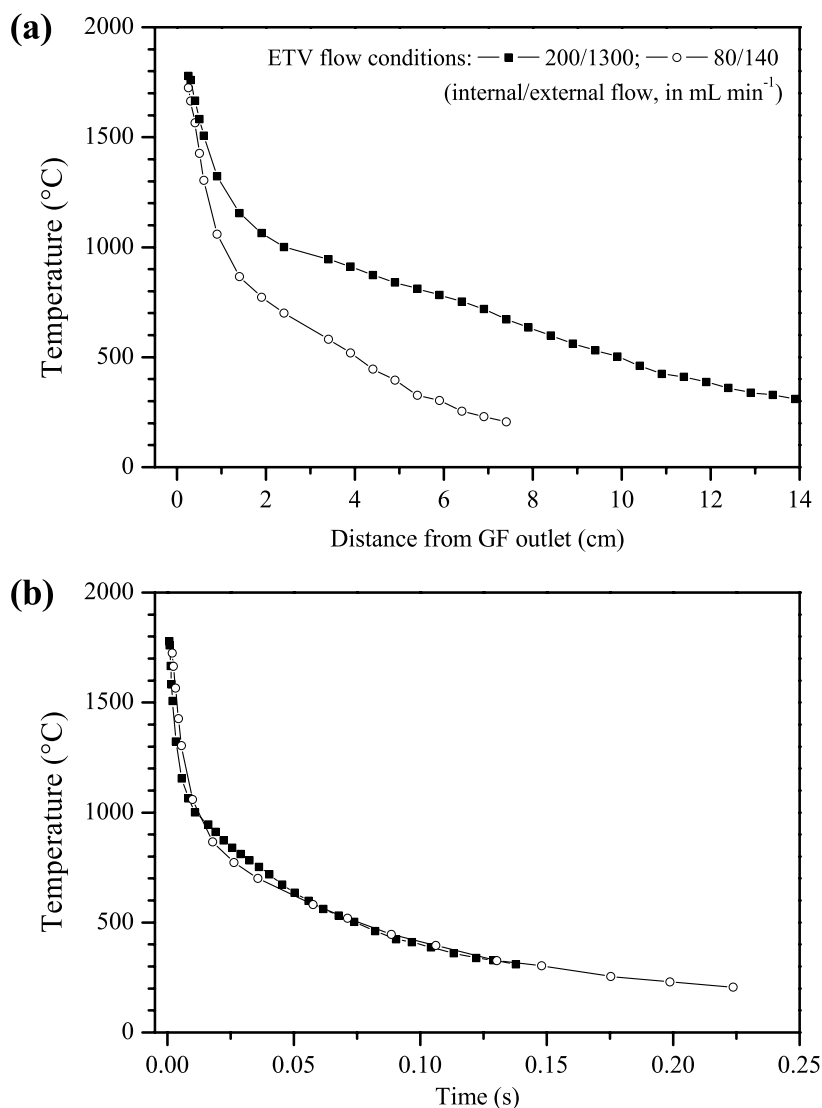


**Fig. 3.7:** Comparison of (a) spatial and (b) temporal temperature distributions on the axis of the AFC tube obtained by different ETV flow distributions: 80/140 mL min<sup>-1</sup> and 200/1300 mL min<sup>-1</sup> (internal/external). All the curves correspond to the 7<sup>th</sup> s of the vaporization step. The flight times obtained for the GF outlet diameter 3 mm; vaporization temperature 2600°C.

From Fig. 3.7(b) it is very difficult to estimate the influence of the rate of upstream cooling on the analyte condensation process. During the first milliseconds of the flight, the upstream is cooled slightly faster at higher ETV flow rates. Possibly, it is one of the reasons of superiority in the ETV performance for ETV-EP sampling with higher flow rates.



### 3.5 Investigation of the influence of GF carbon on analyte TE

Variation of analyte TEs with the ageing of the GF tube is investigated by performing a series of identical measurements for different GF tube ages. The weight of the tube is controlled after each series. Fig. 3.8(a) shows the accumulative and the differential material loss of the GF. The differential mass loss with the GF ageing does not suffer significant variations and is about 80-100  $\mu\text{g}$  per shot. An enhancement of the losses up to 200-250  $\mu\text{g}$  per single ETV firing is observed with the approaching to the end of the analytical tube lifetime. This curve is good reproducible under constant experimental conditions and is in agreement with the data given by Ortner et al. for the smaller 5 mm diameter tube [Ort2].

An influence of the vaporized material composed mainly of carbon particulates on the TE of Pb, Mn, Cu, Fe, and Ni is shown in Fig. 3.8(b)-(f). Increasing TE with the tube ageing is observed for most analytes studied and is presumably associated with the increased density of carbon particulates co-vaporized with the analytes. With the aim to prove this hypothesis, theoretical estimations of carbon densities based on the experimentally obtained GF tube losses per a single firing (see Table A.4.1) were performed for different temperatures by upstream cooling. The calculations show that the carbon vapor is highly supersaturated even within the GF at the vaporization temperature. This can signify that inside the tube the carbon can be probably found in the form of relatively large polyatomic structures. The hypothesis is also supported by SEM and TEM investigations of the carbon particles within the GF and in the upstream flow (see Sect. 3.5.2). These results clearly demonstrate the presence of the carbon particulates in the GF and further in the upstream but not the fact that analytes are completely or partially co-vaporized with the carbon because of the large gap between the melting points of carbon (3652°C sublimation) and analytes (e.g. 1535°C for Fe) [Weas]. The platform effect of the GF boat makes this gap shorter and at the same time supports the co-vaporization. The difference in the platform and the GF heating rates in the ETV-AFC furnace was investigated using the pyrometrical tracing of the platform and GF temperatures during the vaporization step (see Fig. 3.3). The platform achieves the pre-set temperature 1-2 s later than the GF tube. Other known mechanisms of carbon appearance at lower temperatures are presented in Refs. [Mil5, Mil6]. Similar estimations of analyte densities in the ETV upstream at different temperatures (see Table A.4.1) show that the analyte vapor achieves saturation

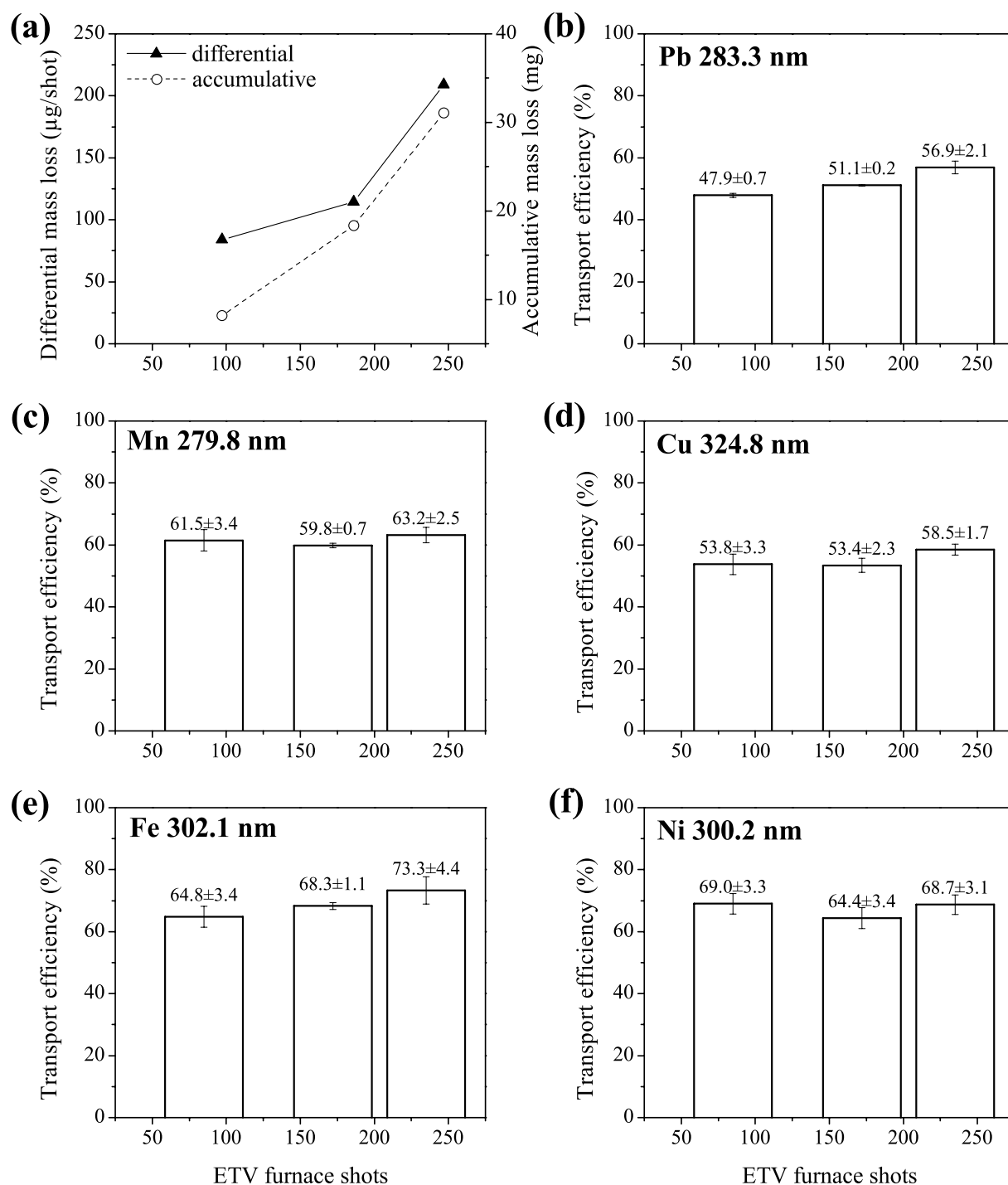


**Fig. 3.8:** (a) Differential and accumulative mass losses of the GF with incomplete protection against ambient air and (b-f) respective TEs for 4 ng Mn, 20 ng Pb, Cu, Fe, and 100 ng Ni, both as functions of the GF tube age. Flow conditions: 200/200/1100 mL min<sup>-1</sup> (internal/sluice/external).

(equilibrium between evaporation and condensation) at much lower temperatures in comparison with the vaporization temperature. Therefore, analyte self-nucleation (homogeneous condensation) cannot be considered as a predominant mechanism of analyte condensation. The commonly used condensation theory of ETV generated particles [Kan1] can be obviously applied only for larger analyte amounts (micrograms). Thus, the nucleated condensation (heterogeneous condensation) of analytes as a process promoted by the presence of condensation nuclei seems to be a main mechanism of the analyte condensation and transport in the case of typically used analyte amounts for ICP-OES/MS and ETAAS measurements. Analyte atoms can be adsorbed by the carbon aerosol composed of growing carbon particulates. This mechanism probably leads to the packing of the analytes into the carbon particulates.

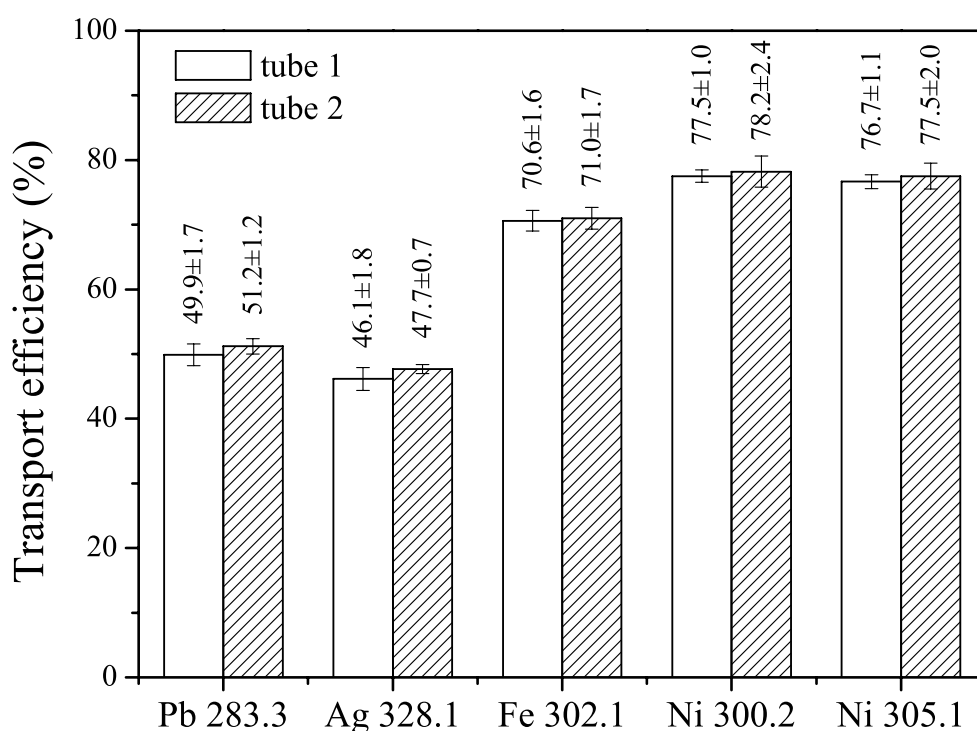
The behavior of the analyte TEs is very likely defined by several competitive impact mechanisms. The TE increasing is possibly reduced by intercalation of metals and metal-containing molecular species into the interplanar space of the graphite sheets when the pyrolytic coating is coming to be destroyed [Moor, Jac2]. If an analyte is intercalated, its release to the gas phase may require additional time for diffusional transport of the metal through the graphite to the surface. It is also known [Jac2] that strong acids do not directly attack the graphite surface. They rather cause oxygen to be bound within the graphite lattice, causing the expansion of the last, swelling, and eventually exfoliation. As it is observed during the measurements, relatively short contact of the GF tube with ambient air before or during the measurement cycle leads to the evaluable growth of the graphite losses that can further enhance the analyte TEs. With the aim to avoid such fluctuations, the ETV unit is sealed between the measurements under a small overpressure that should prevent diffusion of air molecules into the ETV volume. These impurities have also an impact on the corona discharge current. After flushing of the housing with argon during 10-20 min, the corona current achieves its maximal value that is 20-30% higher than the initial one. Each contamination of the gas flow results in current decreasing.

Fig. 3.9 presents some of ETV-EP analyte TEs obtained using different GF tubes of the same series and at the same analytical tube age. The goal of the study is to demonstrate the reproducibility of the analyte TEs by changing of the GF tube. The study shows very high correlation between the TEs for different sample analytes and corresponding tube ages.

Fig. 3.10 shows more detailed investigation of GF electrical properties and mass losses during the complete analytical tube lifetime. After a short condition stage (20-30 shots), when

the tube properties are still unstable, the tube comes into the age (200-300 shots) suitable for the analytical measurements. During this period, the GF shows more or less steady dissipation power (Fig. 3.10(a)) with its rapid decrease prior to the tube break. This character is caused by material vaporization from both surfaces of the GF resulting in GF tube impedance enhancement. Variation of the dissipation power during the analytical tube lifetime is less than 2% according to the experimental estimations. Simple calculation also shows that the temperature variation caused by GF tube impedance increase is lower than 1%. Therefore, the temperature variation caused by changing of tube electrical properties during the analytical tube lifetime is of less importance.

The measured differential mass losses have also a constant character with slight enhancement at the end of the lifetime. It should be noted that in contrast to the study presented in Fig. 3.8(a), this measurements are carried out with completely sealed ETV furnace during and between the measurements in order to reduce the influence of ambient air. In order to



**Fig. 3.9:** TEs for two different tubes from the same series and in the same analytical age (15-35 furnace shots); analyte masses: 4 ng Ag, 20 ng Pb and Fe, 100 ng Ni; improved sluice gas inlet. Flow conditions: 200/200/1100 mL/min (internal/sluice/external), 1:9 splitting.

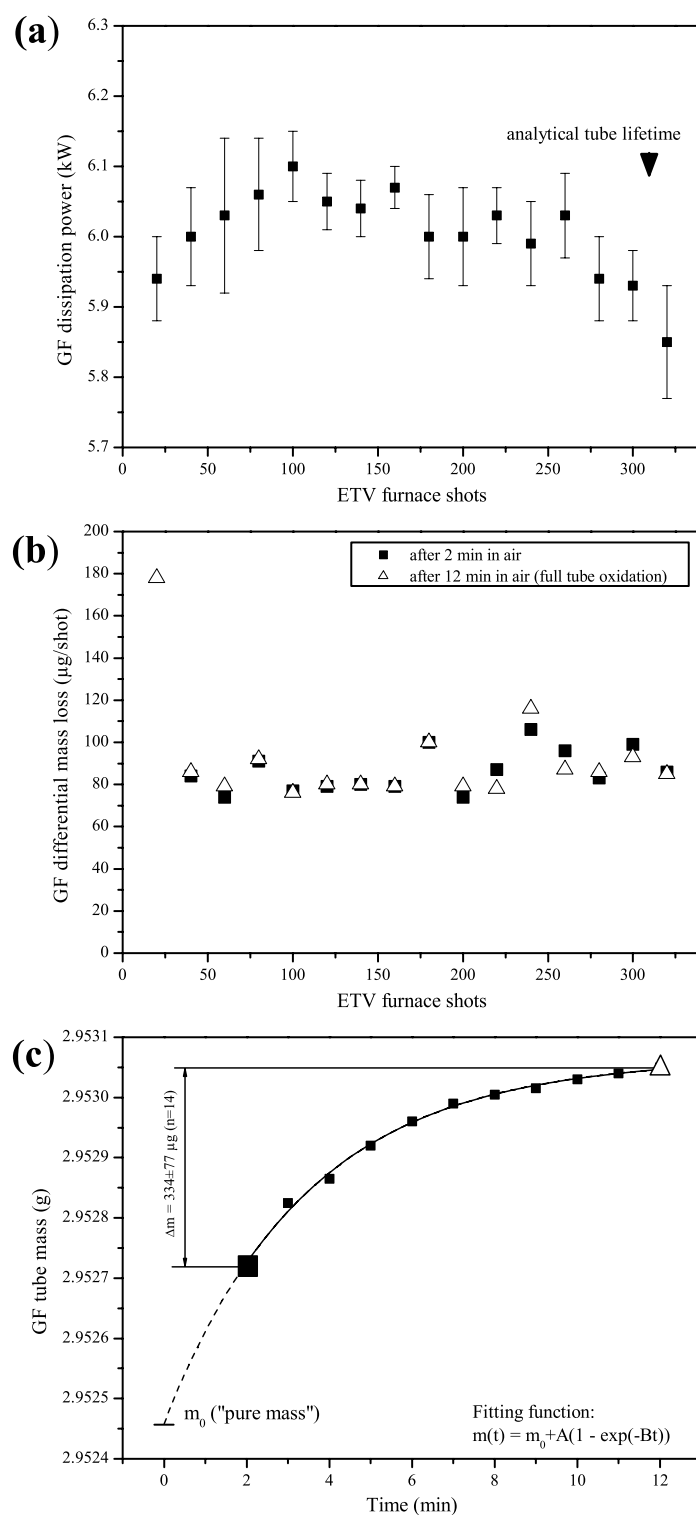


**Fig. 3.10:** Monitoring of the GF tube characteristics during the tube ageing: (a) dissipation power and (b) differential mass loss of the GF (with sufficient inert gas protection) both as functions of the tube ageing and (c) tube mass increase during weighing in ambient air; obtained without sample introduction, vaporization temperature 2600°C. Additional information see in the Text.

demonstrate the rates at which the “pure” GF tube can accommodate the ambient air molecules, the tube after extraction from the ETV is weighed during a certain time interval with a minute tact. Fig. 3.10(c) shows that the mass increase within 10-12 min is more than 300  $\mu\text{g}$ . Because of such unexpected time dependence of the tube mass measurements, the differential losses (Fig. 3.10(b)) are presented for two different weighing times: 2 min (solid rectangle) and 12 min (empty triangle, the tube is fully oxidized) after ETV dismount.

### 3.6 SEM and TEM investigation of GF carbon particles

With the appearance of the hypothesis about a significant role, which possibly plays carbon in the analyte transport process, the particles in the upstream flow and inside the GF are collected on appropriate materials by means of thermophoretic and electrostatic deposition for investigations with SEM and TEM methods. Fig. 3.11(a)-(c) illustrates particulates within the GF collected by different vaporization temperatures. By ETV firing with 1800°C (optimal vaporization temperature for Pb and Ag) no carbon particles are observed. EDX investigations in different areas on the wafer showed only strong Si signal. By vaporization at 2200°C, fine particulates cover the whole surface of the Si wafer. In this case, the EDX clearly shows a strong C signal together with the Si signal. At 2600°C (vaporization temperature for medium and low volatile analytes as Fe and Ni), the carbon particulates are deposited on the surface with higher density. It is difficult to estimate the diameters of the particles from these images, but it is clear that at higher temperature (higher C masses) the particles are slightly larger. Light-grey spherical agglomerates above the C layer are very likely Si particulates originating from the molten bordering areas of the wafer. In order to avoid the partial or complete destroying of the wafers, the latter collections are made at the larger distances from the center of the GF tube.

Fig. 3.11(d) shows the carbon particulates collected outside the GF at 2.5 mm from the GF tube outlet. The carbon particles are slightly finer and their density seems to be higher. Determination of particle diameters is still impossible because of too low resolution of SEM method for such applications.

Higher resolution can be obtained using TEM investigation. Fig. 3.12 illustrates TEM images of carbon particulates collected in the upstream flow at 2.25 cm from the GF outlet

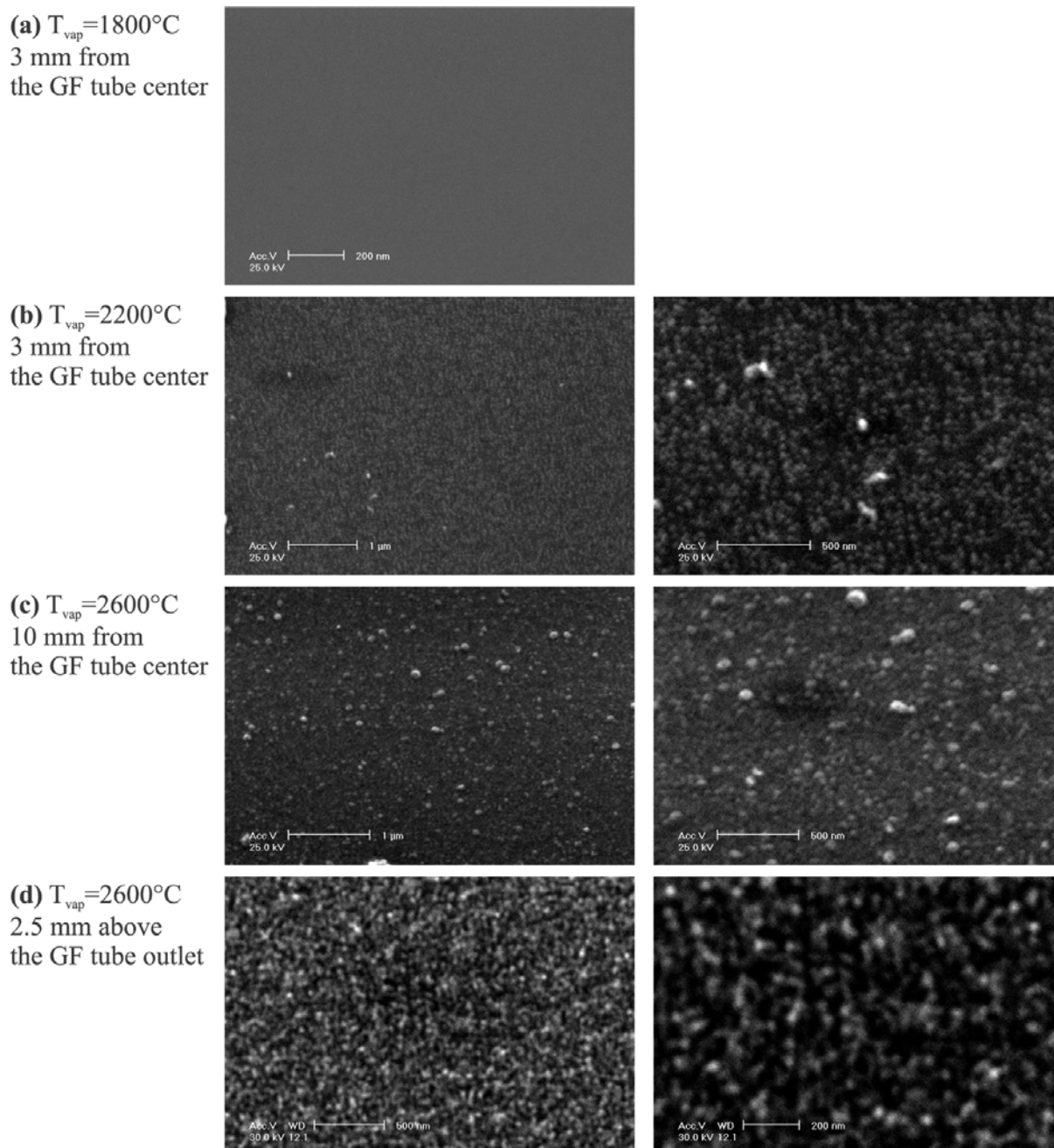


**Fig. 3.11:** SEM images of carbon particles released from the ETV furnace by different vaporization temperatures during 6 s vaporization time and thermophoretically collected on silicon wafers (a-c) inside the GF, flows 150/0/0 mL min<sup>-1</sup> (internal/sluice/external) and (d) directly above the GF outlet hole, flows 150/150/1200 mL min<sup>-1</sup>.

hole by 2400°C (at higher temperatures or shorter distances TEM nets are destroyed). These images allow to derive a lower estimate of the mean diameters of carbon particulates at least at one cut on the axis of the AFC tube. Single large particulates with diameters 5-15 nm as

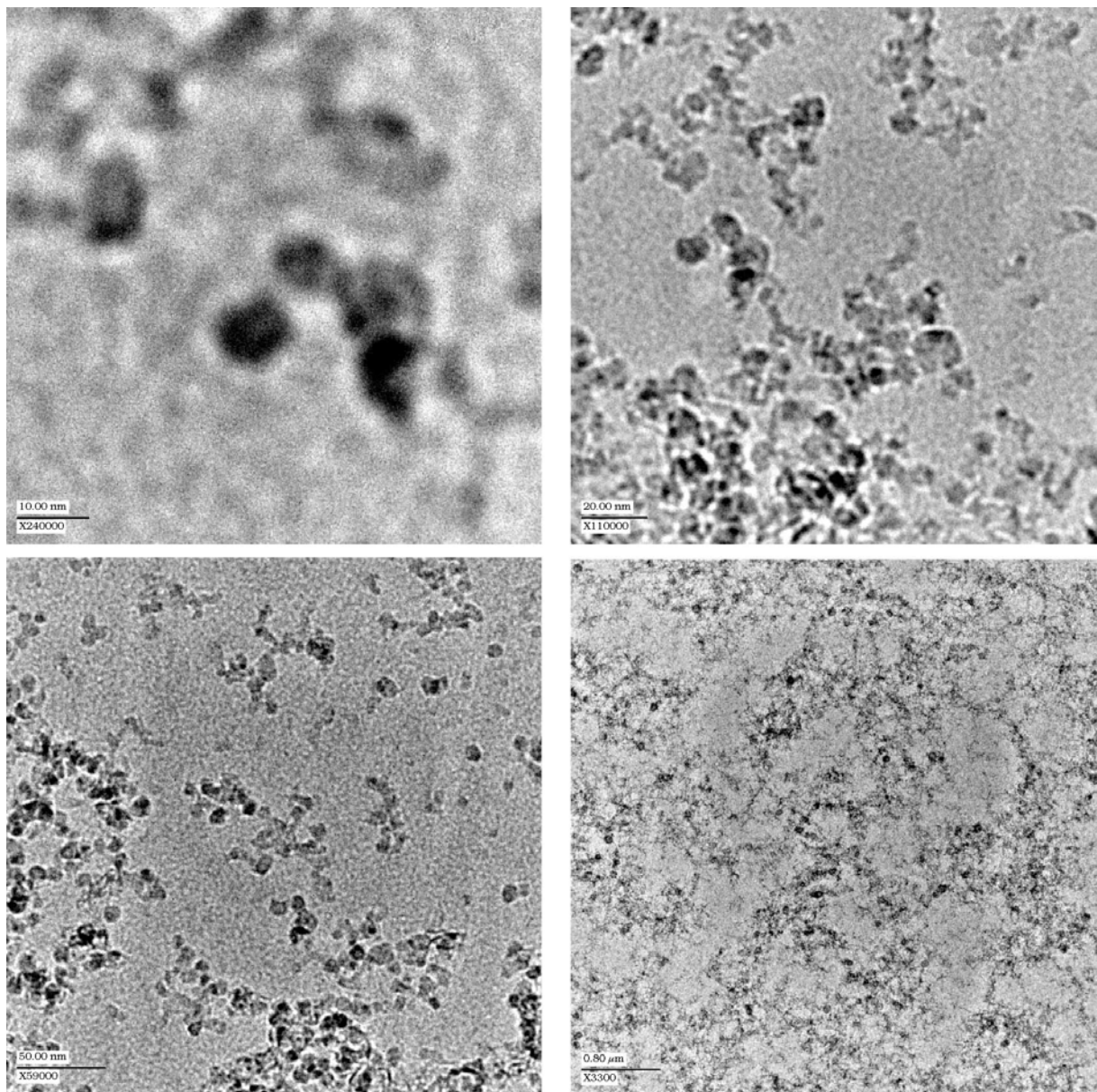


**Fig. 3.12:** TEM images of carbon particles released from the ETV furnace during vaporization and thermophoretically collected at 2.25 cm above the GF outlet hole on nickel nets (400 mesh, 3.05 mm diameter, with carbon coating), obtained by vaporization temperature 2400°C (6 s hold time) with flows 150/150/1200 mL min<sup>-1</sup> (internal/sluice/external).

well as the finer particles are coming to form chains and web-like structures even at such short distances from the C particle source. Fig. 3.13(a) shows the SEMs obtained for the same distance but at higher vaporization temperature. A compact layer with a carpet-like surface formed by chains and web-like structures composed of fine carbon particulates is obviously seen. The same structures obtained by electrostatic collection of the carbon aerosol presented



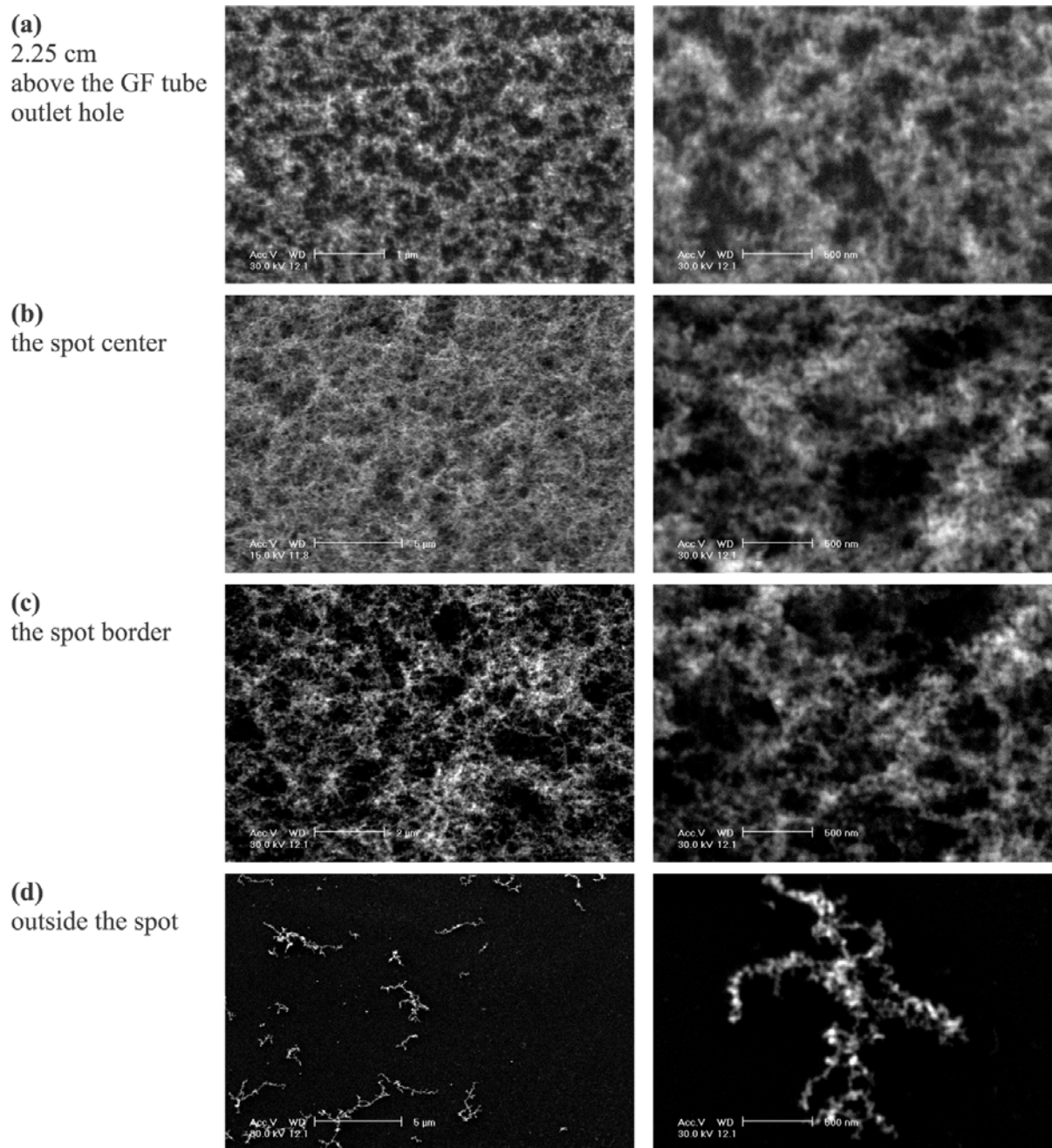


**Fig. 3.13:** SEM images of carbon particulates released from the ETV furnace by vaporization at 2600°C during 6 s and collected on silicon wafers (a) thermophoretically 2.25 cm above the GF outlet hole and (b-d) electrostatically in different areas of the precipitation spot; flows 150/150/1200 mL min<sup>-1</sup> (internal/slucie/external), 1:9 flow splitting prior to particle collection.

in Fig. 3.13(b). The tubing length between these two positions is more than 1 m and as it follows from the comparison of the images, the mean diameter of a single particle in the chain is not increased but the total length of the chains in the separate agglomerate is without any

doubt enhanced. The comparison of the particulate structures directly above the GF outlet and on the end of the transport path proves the supposition that such shapeless structures are formed not by the electrical field in the corona discharge but possibly by means of charged particles in the upstream flow.

Fig. 3.13(b)-(d) show precipitation spot in different areas: in the center, in the border, and outside. A decrease of the density of the layer is obvious with approaching to the spot border. Separate components of the layer with the carpet-like surface can be observed in the area outside the spot (Fig. 3.13(d)).

### 3.7 Modifier effects

#### 3.7.1 Determination of analyte TEs with addition of K, Mg, and Pd modifiers

For investigation of the influence of  $\text{KNO}_3$ ,  $\text{Mg}(\text{NO}_3)_2$ , and  $\text{Pd}(\text{NO}_3)_2$  modifiers on analyte transport process from the ETV-AFC unit to the ETA furnace of the CS-CFS spectrometer, TEs for Cu, Fe, Mn, Ni, and Pb are determined. TEs are obtained for different ETV operating conditions:  $80/140/0 \text{ mL min}^{-1}$  (internal/sluice/external) and  $200/200/1100 \text{ mL min}^{-1}$  with 1:9 flow splitting prior to EP.

Fig. 3.14(a) shows the effect of modifier addition on the TEs for ETV-EP ETA-CFS process for ETV operating mode with lower flow rates. TEs in the range of 31-40% are measured for the analytes studied. Addition of the modifiers increases the TEs by 7-12% for volatile analytes (Pb and Mn) and by 1-5% for medium and low volatile analytes (Cu, Fe, and Ni). The differences between the TEs measured with addition of K and Pd modifiers are within the standard deviations. As it follows from these results, the application of K and Pd modifiers lead to more uniform transportation of sample analytes.

Fig. 3.14(b) shows the effect of K, Mg, and Pd modifiers on TEs for the ETV with higher flow conditions. TEs in the range of 51-68% are obtained without modifier additions. The use of K enhances the TEs by 4-6% for analytes higher volatility (Pb and Mn) and has no influence on the TEs of medium and low volatile analytes (Cu, Fe, and Ni). Possible explanation of the influence of K on the analyte TEs is that  $\text{K}^+$  ions and compounds serve as the nuclei for the soot particulates [Donn, Mann] and accelerate the formation of the carbon aerosol. According to this supposition, K should play an important role at the beginning of the carbon

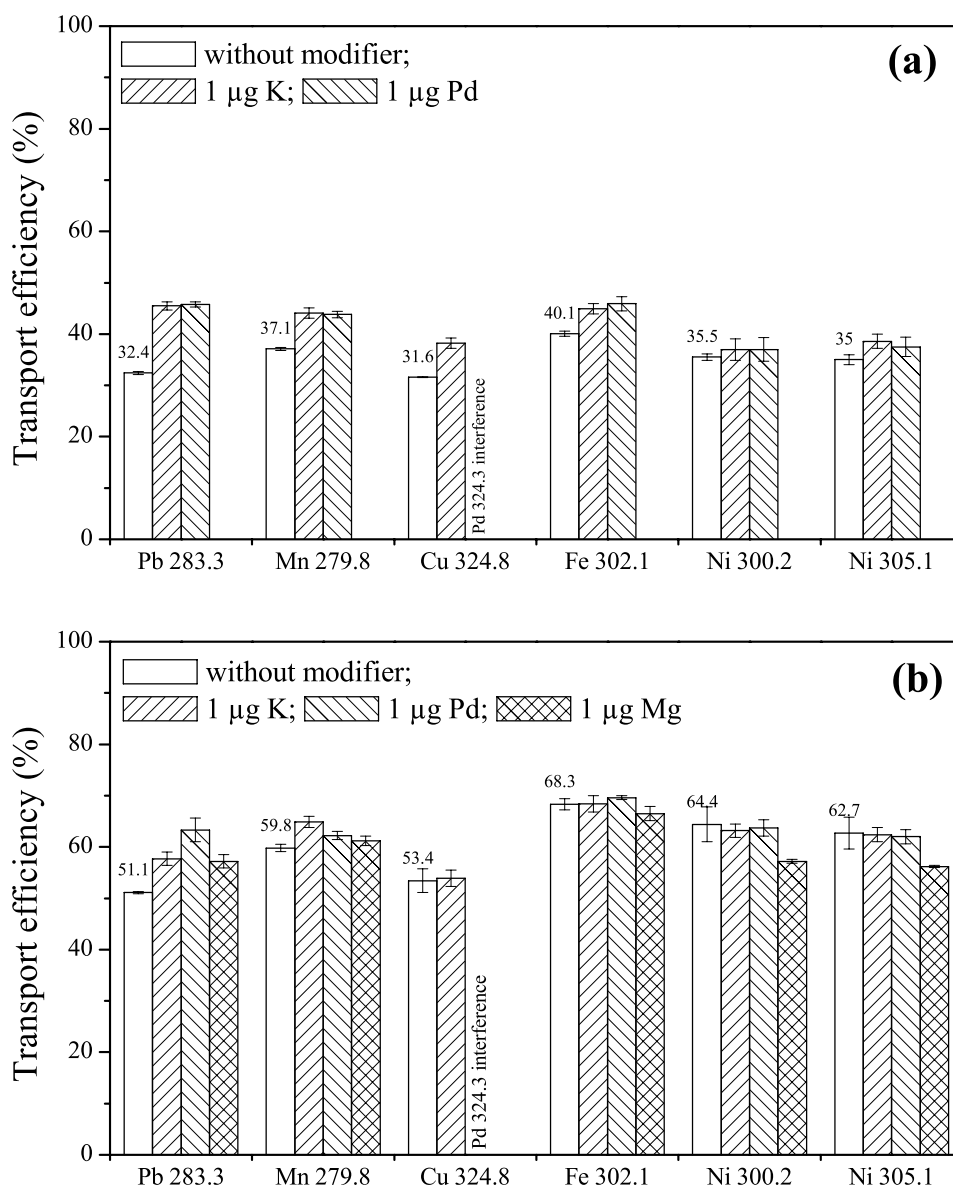


**Fig. 3.14:** Effect of  $\text{KNO}_3$ ,  $\text{Pd}(\text{NO}_3)_2$ , and  $\text{Mg}(\text{NO}_3)_2$  modifiers on TEs of Pb, Mn, Cu, Fe, and Ni for different ETV-AFC operating conditions: (a) flow distribution 80/140/0 mL min<sup>-1</sup> (internal/slucie/external) without dilution, sample: 0.4 ng Mn, 2 ng Cu, Fe, Pb, and 10 ng Ni; and (b) 200/200/1100 mL min<sup>-1</sup> with 1:9 flow splitting, sample: 4 ng Mn, 20 ng Cu, Fe, Pb, and 100 ng Ni. Obtained by GF tube ages 150–180 shots, carbon loss ~ 100 µg shot<sup>-1</sup>.

condensation and indirectly increase the TEs of more volatile species. Certainly, K can act as a carrier by itself, but this mechanism is less probable, because K begins to form particles by self-nucleation much later than the other metals with higher melting points (see Table A.4.1).

With the addition of diluted  $\text{Pd}(\text{NO}_3)_2$  modifier, the TEs of volatile analytes are increased by 3-12%. No influence on the TEs of Fe and Ni is observed. The effect of the  $\text{Pd}(\text{NO}_3)_2$  modifier is that the last increases the vaporization temperature of the analytes studied. As a result, the volatile analytes (Pb and Mn) are released at higher temperatures and with higher carbon densities. The modifier can also act as an analyte carrier by itself owing to the early-achieved saturation (see Table A.4.1). However, the presence of the carbon particulates in much higher densities very likely makes this influence negligible. Some outcomes of the modifier effect on the analyte TEs should be further investigated. Until now, we do not have any satisfactory explanation for the behavior of the TE of Cu with the addition of modifiers, although the positive effect of K has been already documented [Her1]. With the addition of Mg modifier, the TEs of all analytes studied undergo no significant variations. In the case of Ni, the TE even decreases. Nevertheless, according to these measurements, we can conclude that the use of the sample/carrier modifiers makes the TEs more uniform and less dependent on the analyte volatility.

Generally, the modifier effect is to be explained due to co-vaporization of sample analytes with carrier forming constituents that results in faster formation of stable particulates [Edig, Gre1, Kan1]. In this thesis, we consider the GF carbon as a predominant analyte carrier and the role of the modifiers is only to provide convenient conditions for analyte vaporization and condensation. Detailed consideration of action mechanisms of modifiers in ETAAS has been done by Ortner [Ort1].

### 3.7.2 Determination of analyte TEs with $\text{C}_6\text{H}_{12}$ addition to the ETV internal gas flow

For investigation of the influence of  $\text{C}_6\text{H}_{12}$  (cyclohexane) addition to the internal flow of the ETV furnace on analyte transport process, TEs for Ag, Cu, Fe, Ni, and Pb are determined. TEs are determined with and without  $\text{C}_6\text{H}_{12}$  for ETV flow conditions 200/200/1100  $\text{mL min}^{-1}$  (internal/sluice/external) with 1:9 flow splitting prior to EP.

Fig. 3.15 shows the analyte TE variation for different carbon amounts produced by cyclohexane decomposition in the ETV furnace by vaporization. Without additives, TEs in the range of 41-45% are obtained for volatile analytes (Ag, Cu, and Pb) and between 73-78% for Ni and Fe. The addition of small amounts of cyclohexane (carbon content  $\sim 2 \mu\text{g s}^{-1}$ , for comparison, the mean carbon losses of the GF during vaporization are 6-10  $\mu\text{g s}^{-1}$ ), TE decrease is measured for all analytes studied. For volatile analytes it sinks up to 34-39% and for

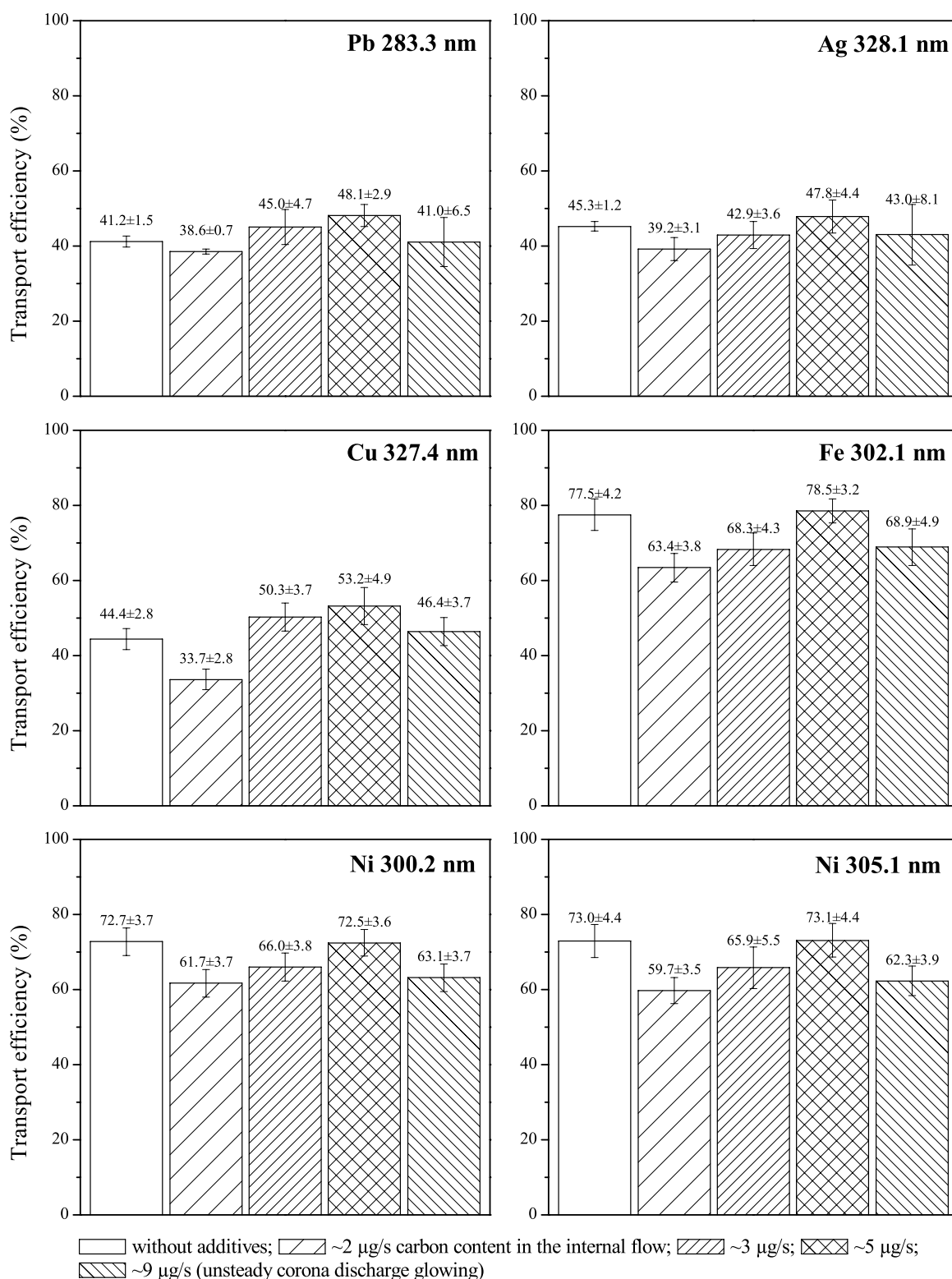


**Fig. 3.15:** Effect of C<sub>6</sub>H<sub>12</sub> (cyclohexane) addition to the ETV internal flow on TEs of 4 ng Ag, 20 ng Cu, Fe, Pb, and 100 ng Ni, obtained by ETV flow conditions 150/150/1200 mL min<sup>-1</sup> (internal/sluice/external) with 1:9 splitting. GF tube ages are 50–90 shots.

medium and low volatile up to 60-63%. With the increasing of the carbon content in the internal flow up to  $\sim 3 \mu\text{g s}^{-1}$ , an enhancement of the TEs is observed for all analytes studied. Further increase of the carbon content ( $\sim 5 \mu\text{g s}^{-1}$ ) leads to a further enhancement of the TEs. The measured TEs for this case are 45-50% for Ag, Cu, and Pb and 73-79% for Ni and Fe. Thus, the mean increase of the TEs for Ag, Cu, and Pb is around 6% and for Ni and Fe is around 0.3%. Further increase of the carbon content in the internal flow results only in decreasing of the TEs. The data obtained for carbon content  $\sim 9 \mu\text{g s}^{-1}$  show 41-46% for volatile and 62-69% for medium and low volatile analytes. As it follows from these measurements, the optimal carbon content in the internal flow is  $\sim 5 \mu\text{g s}^{-1}$ .

It should be pointed out that the addition of the cyclohexane has also an impact on the properties of the corona discharge. With the presence in the discharge zone of  $\text{C}_6\text{H}_{12}$  molecules and their decomposition products ( $\text{H}_2$ ,  $\text{C}_2$ ,  $\text{C}_3$ ,  $\text{C}_5$  etc.), the mean current of the corona discharge suffers an increase by up to 5-6  $\mu\text{A}$  and by higher  $\text{C}_6\text{H}_{12}$  fractions (with carbon content more than  $5 \mu\text{g s}^{-1}$ ) obtains an unstable behavior (spontaneous pulsations within the range between 20-30  $\mu\text{A}$ ). In this case, an erratic movement of the corona glow from one spot on the EP electrode tip to another in rapid succession can also be seen with a mirror through the tube side. The same phenomena have been observed by Weissler [Weis], during investigation of the point-to-plate corona in Ar with additions of  $\text{H}_2$  (up to 1%). The motion of the discharge resulted in production of irregular pulses, which were observed oscillographically. Thus, it can be not excluded that due to unsteady discharge glowing the precipitation efficiency of the ETV aerosol can be significantly reduced. The behavior of the mean corona discharge current with addition of cyclohexane is presented below.

### 3.7.3 Determination of analyte TEs by combined use of $\text{C}_6\text{H}_{12}$ , $\text{KNO}_3$ and $\text{Pd}(\text{NO}_3)_2$

The influence of  $\text{C}_6\text{H}_{12}$ ,  $\text{KNO}_3$ , and  $\text{Pd}(\text{NO}_3)_2$  modifier combination on TEs for Ag, Cu, Fe, Ni, and Pb is presented in Fig. 3.16. The TEs are also obtained for the ETV operating mode with higher flow rates of internal, sluice, and external gases (200/200/1100  $\text{mL min}^{-1}$  respectively) and with 1:9 flow splitting prior to deposition.

The use of  $\text{C}_6\text{H}_{12}$  together with  $\text{Pd}(\text{NO}_3)_2$  produces a significant increase in TE for Cu and Pb, up to 72% and 78%, respectively. For Ag this effect is much lower, only 56.9%. An enhancement is also measured for medium and low volatile analytes Fe and Ni (83.7% and 80.8%,

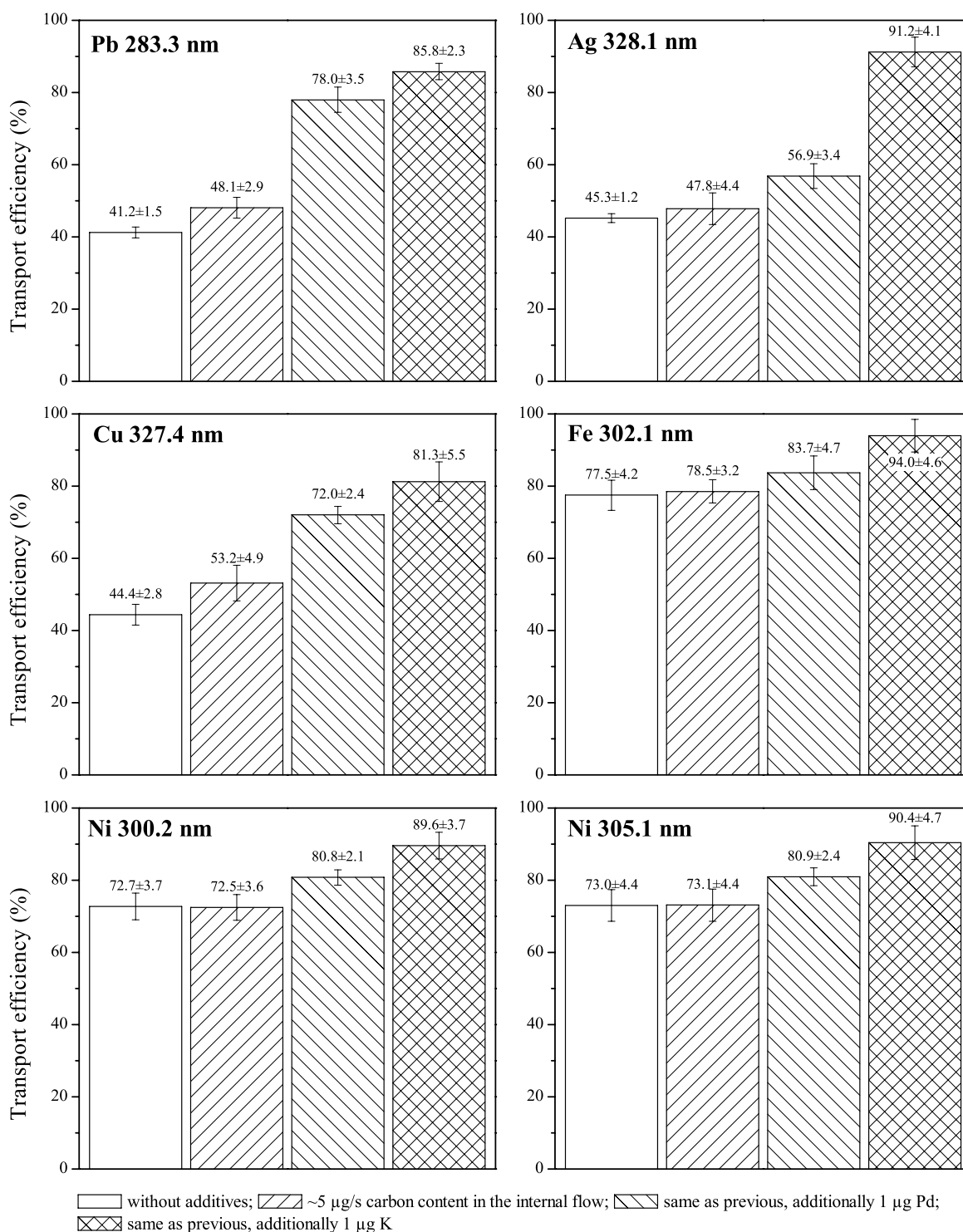


**Fig. 3.16:** Effect of combined use of  $C_6H_{12}$  added to the ETV internal flow,  $KNO_3$  and  $Pd(NO_3)_2$  modifiers to the ETV boat on TEs of 4 ng Ag, 20 ng Cu, Fe, Pb, and 100 ng Ni, obtained by flow distribution 150/150/1200 mL min<sup>-1</sup> (internal/sluice/external) with 1:9 splitting, GF tube ages 50–90 shots.

respectively). By using all modifiers together, very similar figures for all analytes without strong dependence on volatility are obtained. The determined TEs are 91.2% for Ag, 81.3% for Cu, 94% for Fe, 90% for Ni, and 85.8% for Pb. The standard deviation for  $n=5$  are not higher than 5-6%.

The use of  $C_6H_{12}$ , K, and Pd modifiers also leads to changing the signal appearance time by analyte atomization in HGA-600. Fig. 3.17 shows the results of comparative measurements for the same samples dosed directly into the HGA-600 as a solution and by ETV-EP sampling as an aerosol with and without modifiers. The appearance times of the signals for analytes subjected to the ETV-EP sampling without additives are shifted with respect to those with the aqueous dosed sample: to earlier times for volatile (Ag and Pb) and to the later times for medium and low volatile analytes (Cu, Fe, and Ni). The ETV aerosol once subjected to the vaporization contains the analytes predominantly as metals in contrast to metal oxides obtained after drying and pyrolysis of the aqueous sample in the ETA furnace. Atomization of metals needs lower excitation energies than that of metal oxides and occurs generally by lower temperatures and earlier times. Thus, the analytes after ETV-EP sampling should be released at earlier times. A possible explanation is that the analytes in the ETV aerosol are packed into the carbon particulates and need more time for diffusional transport to the particle surface. The shift on different times is very likely due to different starting points of the analyte condensation (typically, melting point or maximal pyrolysis temperatures).

The use of  $C_6H_{12}$  results in a shift to a lower appearance time for Ag and Pb probably due to the increase of the carbon particle diameters caused by additional C content in the upstream. The addition of  $Pd(NO_3)_2$  modifier alone and with  $C_6H_{12}$  leads to a pronounced shift in the signal appearance toward later times (except for Ni) and a significant narrowing of the signal profiles. Later vaporization (first of all for volatile analytes) leads to more convenient conditions for further analyte condensation in presence of higher densities of carbon particulates.

Addition of  $KNO_3$  can probably speed up the carbon condensation process and support the growth of carbon particulates especially at the beginning of the condensation. The combined use of  $C_6H_{12}$  and  $Pd(NO_3)_2$  modifiers produce a further increase of the TEs but no shifts of the appearance times are observed. By application of  $KNO_3$  alone, a slight shift in the signal appearance towards earlier times is detected for all analytes studied.



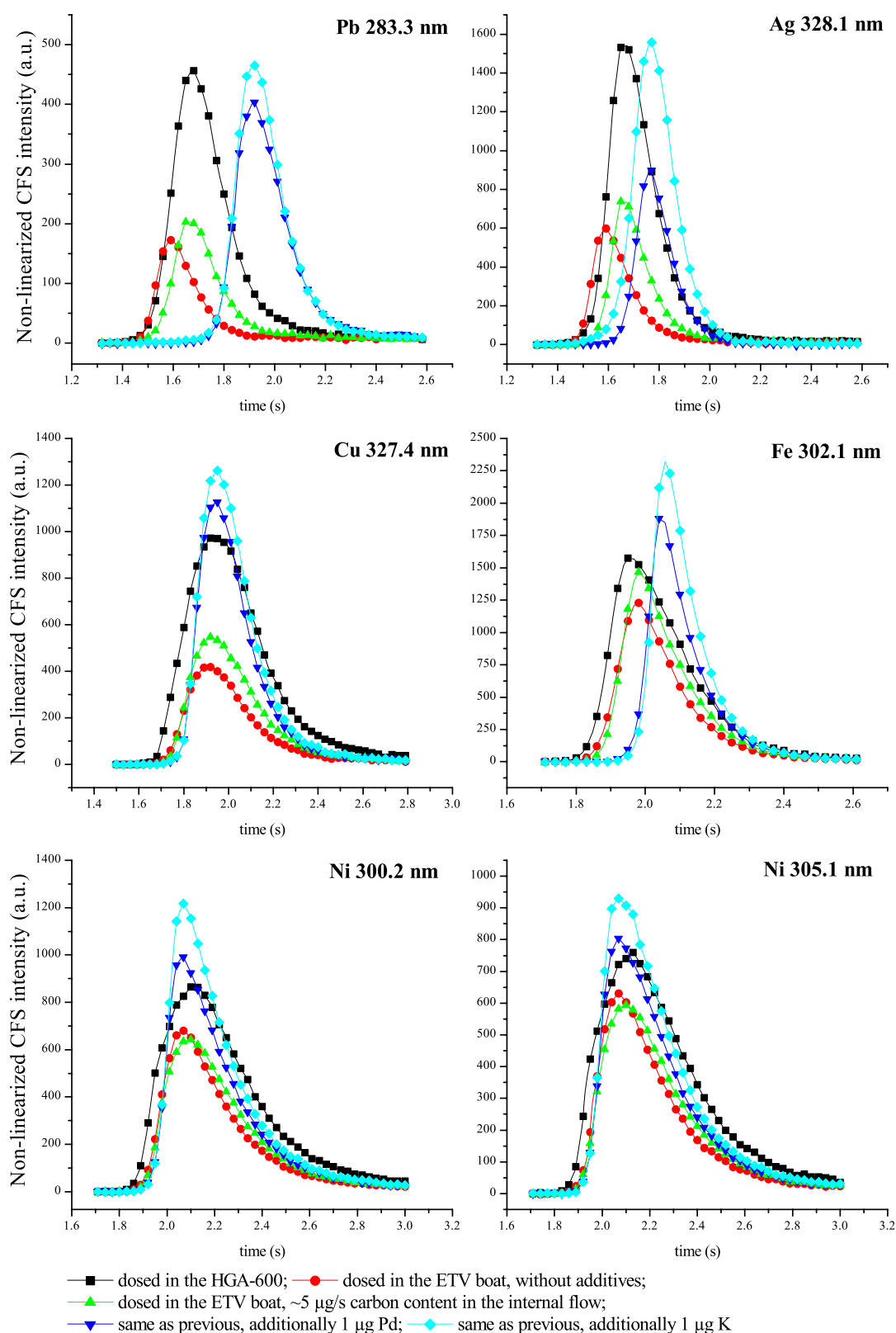


**Fig. 3.17:** Effect of  $\text{C}_6\text{H}_{12}$ ,  $\text{KNO}_3$ , and  $\text{Pd}(\text{NO}_3)_2$  modifiers addition on CS-CFS intensity profiles after background cutting off for Ag, Cu, Fe, Ni, and Pb (see Fig. 3.16 for further details).

Fig. 3.18 shows the summary of the influences of the modifiers used on the analyte TEs. The effect of cyclohexane is feebly marked only for volatile species. Probably, it is coupled with lower aerosol precipitation efficiency caused by  $H_2$  presence in the discharge. The effect of  $C_6H_{12}$ ,  $KNO_3$ , and  $Pd(NO_3)_2$  modifier combination is pronounced for all analytes. Thus, the use of these modifiers can be considered as a successful mean for ETV sampling with almost homogeneous TEs for analytes with different volatilities.

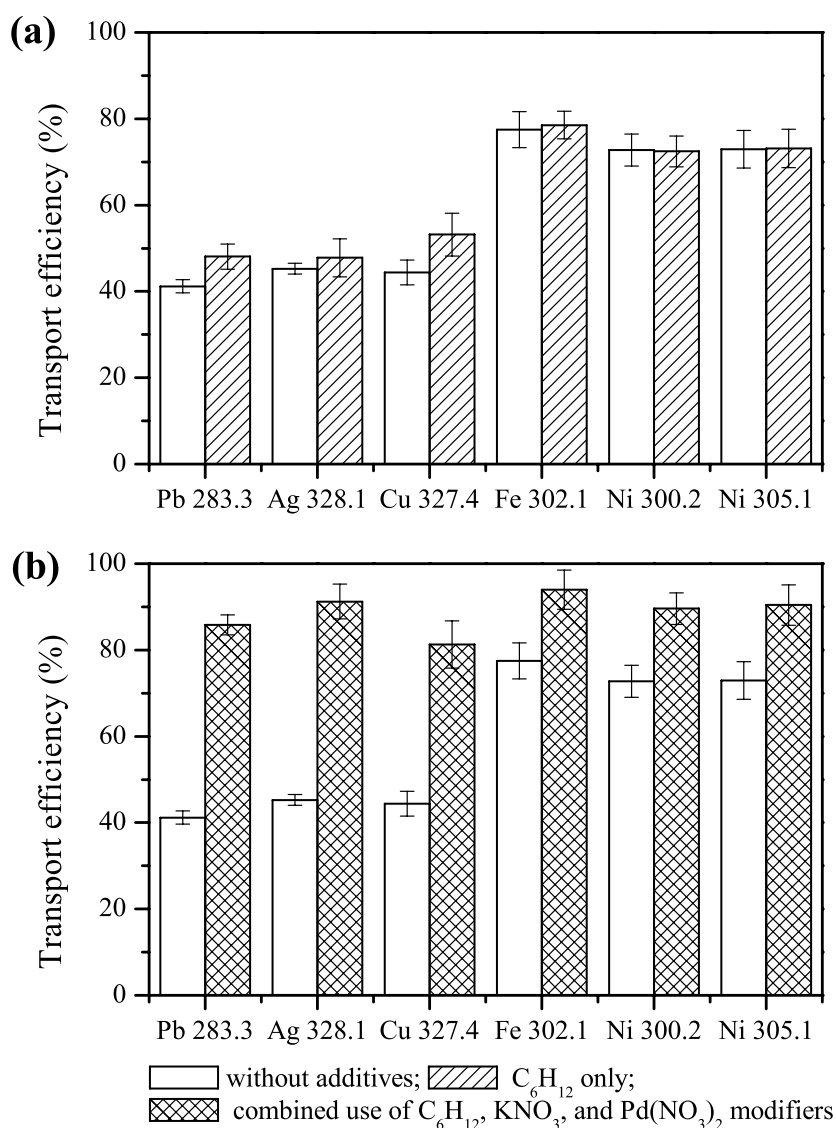


**Fig. 3.18:** Summary showing (a) the effect of  $C_6H_{12}$  addition to the ETV internal flow and (b) combination of  $C_6H_{12}$ ,  $KNO_3$ , and  $Pd(NO_3)_2$  modifiers both on TEs of 4 ng Ag, 20 ng Cu, Fe, Pb, and 100 ng Ni; obtained for carbon content in the internal flow  $\sim 5 \mu g s^{-1}$  and 1  $\mu g$  K and Pd masses; flow distribution 150/150/1200 mL  $min^{-1}$  (internal/slucie/external) with 1:9 splitting.

3.7.4 Behavior of the corona discharge current in presence of  $C_6H_{12}$ 

The corona discharge current with addition of different cyclohexane amounts into the internal flow is measured. Fig. 3.19 illustrates this dependence for “cold” ETV, i.e. without decomposition of  $C_6H_{12}$  that occurs during ETV firing. An increase of the current is observed with the enhancement of  $C_6H_{12}$  content in the furnace gas. By flow rates through the flask exceeding  $2\text{--}3\text{ mL min}^{-1}$  (corresponds to  $\sim 2\%$  of the internal flow), the discharge obtains unsteady character. Visual observations show the motion of the glowing area. At too higher concentrations, the gas ionization occurs only at the electrode tip. Under such conditions, the charging the aerosol particulates can occur with very low efficiency that results in strong decreasing analyte TEs. Too higher standard deviations obtained by determination of the flow

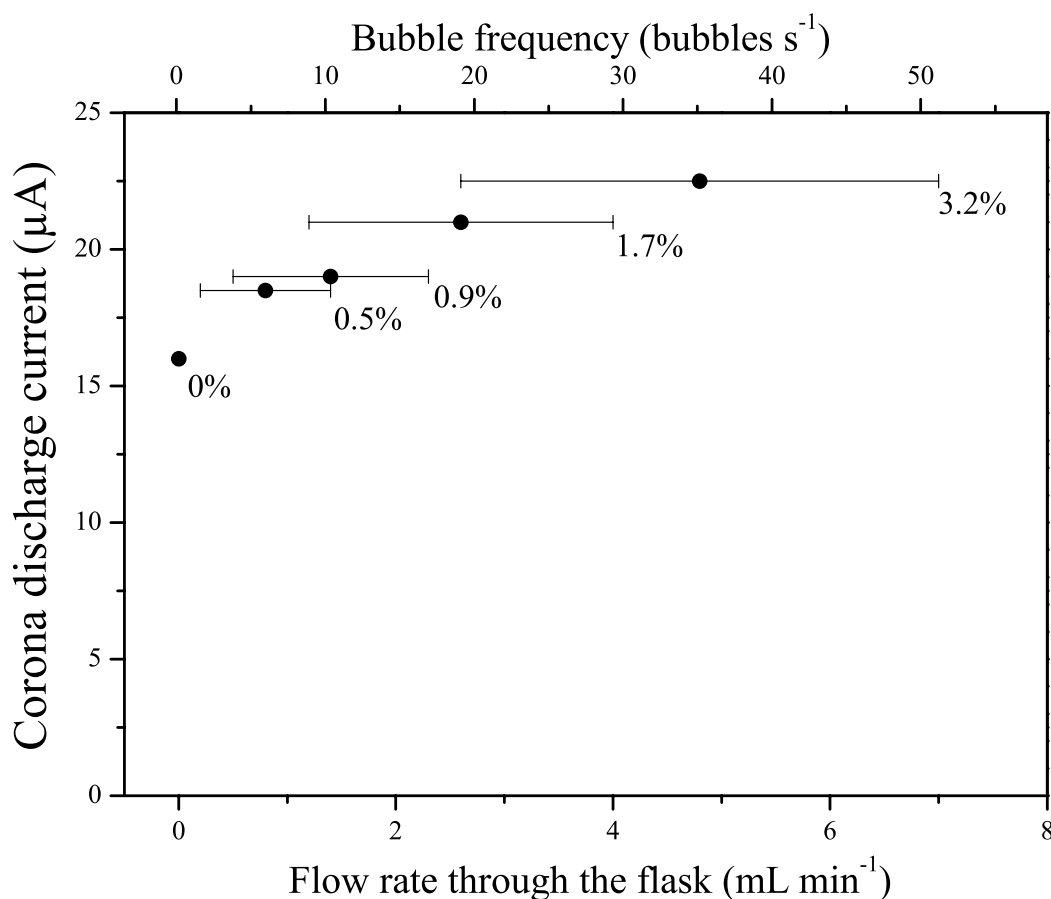


**Fig. 3.19:** Dependence of the current of negative corona discharge on the content of the  $C_6H_{12}$  vapor in the internal flow (expressed as the flow rate through the flask with cyclohexane), obtained for “cold” ETV system (i.e. cyclohexane molecules are not decomposed), flow conditions  $150/150/1200\text{ mL min}^{-1}$  (internal/sluice/external) with 1:9 flow splitting. The percentages show the part of the internal flow that passes through the flask.

through the cyclohexane flask are caused by unreliable flow measuring via bubble frequency. During further measurements, the flow is controlled using the discharge current, which shows high sensitivity to the cyclohexane amount in the Ar flow.

Fig. 3.20(a) illustrates the behavior of the corona current for the following ETV-EP operating conditions: without additives, with optimal cyclohexane content in the upstream, and with too higher cyclohexane content. Without additives, the increase of the corona current is caused by the decrease of the Ar density (these quantities are inversely proportional to each other [Manm]), when the hot gas from the ETV reaches the discharge area. Using this curve, a mean flight time of the aerosol through the transport system can be estimated, which is in this case around 3.5 s. After the end of vaporization, the corona current slowly sinks to the initial value. Addition of  $C_6H_{12}$  provides not only higher corona currents but also unsteady character of the glowing (Fig. 3.20(a),(b)). As it is clearly seen from the comparison, the dependencies measured with presence of  $C_6H_{12}$  show more noises on the curves. At lower  $C_6H_{12}$  amounts (flows up to  $2.6 \text{ mL min}^{-1}$ ), the migration of the discharge within the furnace volume cannot be visually observed but this undoubtedly has an impact on precipitation efficiency. By higher  $C_6H_{12}$  amounts in the furnace gas (flows higher than  $2.6 \text{ mL min}^{-1}$ ), the discharge demonstrates more pulsed character and the amplitude of pulses rises with the increase of the  $C_6H_{12}$  amount. The migration of the corona can be visually observed.

Fig. 3.20(c) shows the discharge behavior by ETV-EP sampling with  $KNO_3$  and  $Pd(NO_3)_2$  modifier additions. Addition of Pd has no remarkable influence on the discharge but the use of K leads to an increase of the current by  $3 \text{ }\mu\text{A}$  for approximately 4 s. It seems to be that K takes part in the electron generation process.

The above consideration shows that the corona glowing in the presence of  $C_6H_{12}$  has an unstable character. The particle collection efficiency can be reduced due to the corona migration and the current pulses. Thus, with  $C_6H_{12}$  addition, we probably obtain two competitive processes: the first is the enhancement of the condensation rate in the ETV upstream due to the carbon content of the  $C_6H_{12}$  and the second is the reduction of the charging efficiency of the aerosol particulates due to the already mentioned processes. Probably, by ETV sampling into the ICP torch, the problems with particle collection would not occur.

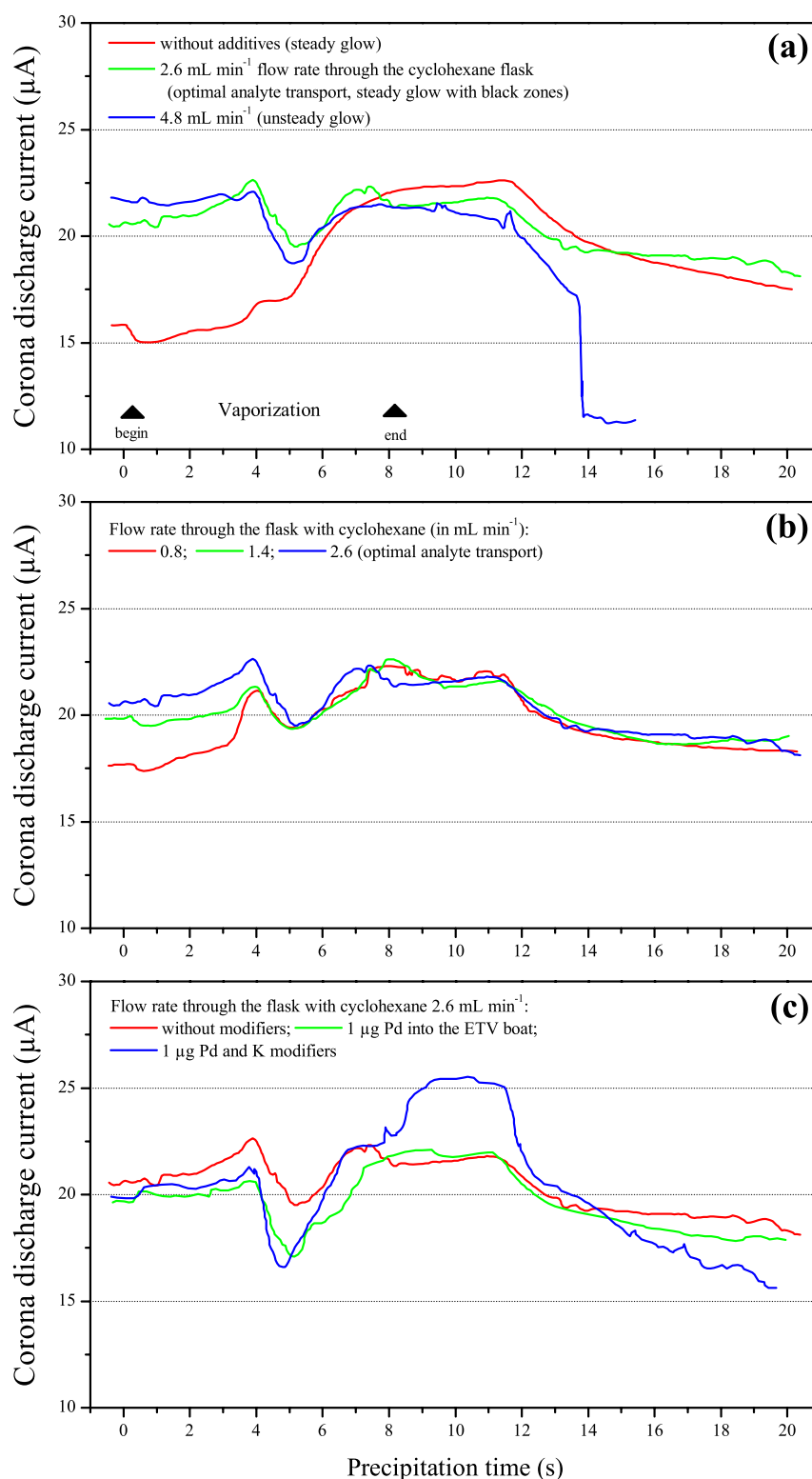


**Fig. 3.20:** Behavior of the corona discharge current in the presence of C<sub>6</sub>H<sub>12</sub> and the influence of KNO<sub>3</sub> and Pd(NO<sub>3</sub>)<sub>2</sub> modifiers: (a) behavior for steady and unsteady modes of the glowing; (b) steady glowing with different carbon contents; and (c) influence of the modifiers (see Fig. 3.16 for further details).

---

#### 4. Platform-to-platform sample transfer, dilution, distribution, and dosing via electrothermal vaporization and electrostatic deposition

---

The “Platform-to-Platform Sample Transfer, Distribution, Dilution, and Dosing System (PLASATRADIS)” is developed in the context of an international research cooperation with the groups of Prof. Dr. A. Kh. Gilmutdinov (Department of Physics, Kazan State University, Russia), Prof. Dr. W. Frech (Department of Chemistry, University of Umea, Sweden), and Prof. Dr. I. Grinshtein (Russian Research Center “Applied Chemistry”, St. Petersburg, Russia). The work has been supported by the “International Association for the Promotion of Cooperation with Scientists from the New Independent States of the Former Soviet Union (INTAS)”. Our part of investigations is reported below.

The potential of the ETV as a sample introduction tool arises from the fact that the analyte aerosol generated in the furnace can be diluted and distributed on the further transport path in pre-set ratios and then quantitatively re-collected by means of intra-furnace EP on the platform of another GF or by external EP on one or a set of platforms or other suitable substrates. The latter makes possible to produce a set of secondary platforms with equal analyte compositions from one individual primary sample. Such multitudes allow sequential multi-element determinations with single-element instrumentation or comparative measurements with different techniques. In addition, the procedure allows external thermal sample pretreatment with pyrolysis, vaporization, condensation, and re-precipitation that significantly reduces the sample matrix. Consecutive elaboration of this idea resulted in the development of “Platform-to-platform sample transfer, distribution, dilution, and dosing system (PLASATRADIS)” consisting of the following parts: (a) the ETV-AFC unit, (b) an aerosol transport and dividing system (see Sect. 2.3), and (c) a precipitation equipment consisting of one or ten equalized electrostatic precipitators. Integration of these parts into one unit provides a better way of coping with the problems associated with solid sample treatment. Furthermore, the quantitative platform-to-platform transfer allows direct determination of analyte TEs, since the primary and secondary samples can be obtained on the same types of boats that can be analyzed with the same analytical instrumentation.

#### 4.1 Precision and reproducibility of measurements

The advantages of the PLASATRADIS system in the handling of the ETV produced aerosols are applied in this thesis mainly for aerosol flow splitting in the pre-set 1:9 ratio after corresponding flow dilution in the ETV unit. The aim of this procedure is to investigate the ETV-AFC unit under higher flow conditions, which are commonly used for sampling into the ICP torch but are absolutely not suitable for the collection of aerosol particles in the corona discharge. The results of these measurements are presented in Chapter 3 of this work. From these data follows that the obtained relative standard deviation (RSD) of TE measurements with both divided and non-divided sample aerosols (e.g. see Figs. 3.1, 3.2, 3.4) does not depend on the flow conditions applied and is under 5% (for  $n=4-5$  repetitions).

Determination of the TEs for Cu, Fe, Mg, Ni, and Pb from the ETV boat to 10 secondary platforms of the 10-fold precipitation unit as a part of the PLASATRADIS system is performed. Average values of the analyte TEs are presented in Fig. 4.1(a) whereas their distributions over all secondary platforms are in Fig. 4.1(b)-(f). Determined TEs are between 42-57% with 8-12% RSD (for  $n=10$ ). Analyte compositions on secondary platforms are measured with a second ETV-EP process with intra-furnace EP. Therefore, all sample analytes have passed the ETV-EP process twice that results in higher RSD. The differences in the analyte TEs are caused by the dependence of the TEs for ETV sampling on analyte volatility (see Chapter 3).

A correlation in the TE values between the different platforms of the 10-fold precipitation unit is observed (cf. Fig. 4.1(b)-(f)). It is not caused by the scatter either of aerosol sub-flow rates through each precipitator or of corona discharge currents, but most likely by a not perfectly reproducible positioning of the graphite platform in the precipitator at the present state of the development. This may be a reason that not all discharges burn optimally during the EP process. The distributions of the sub-flows and the discharge currents over all precipitating stations are presented in Fig. 4.2(a),(b). They have mostly a uniform character. No correlation with the TEs is observed.

Blank measurements under variety of precipitating conditions show the absence of contamination at the precipitators.

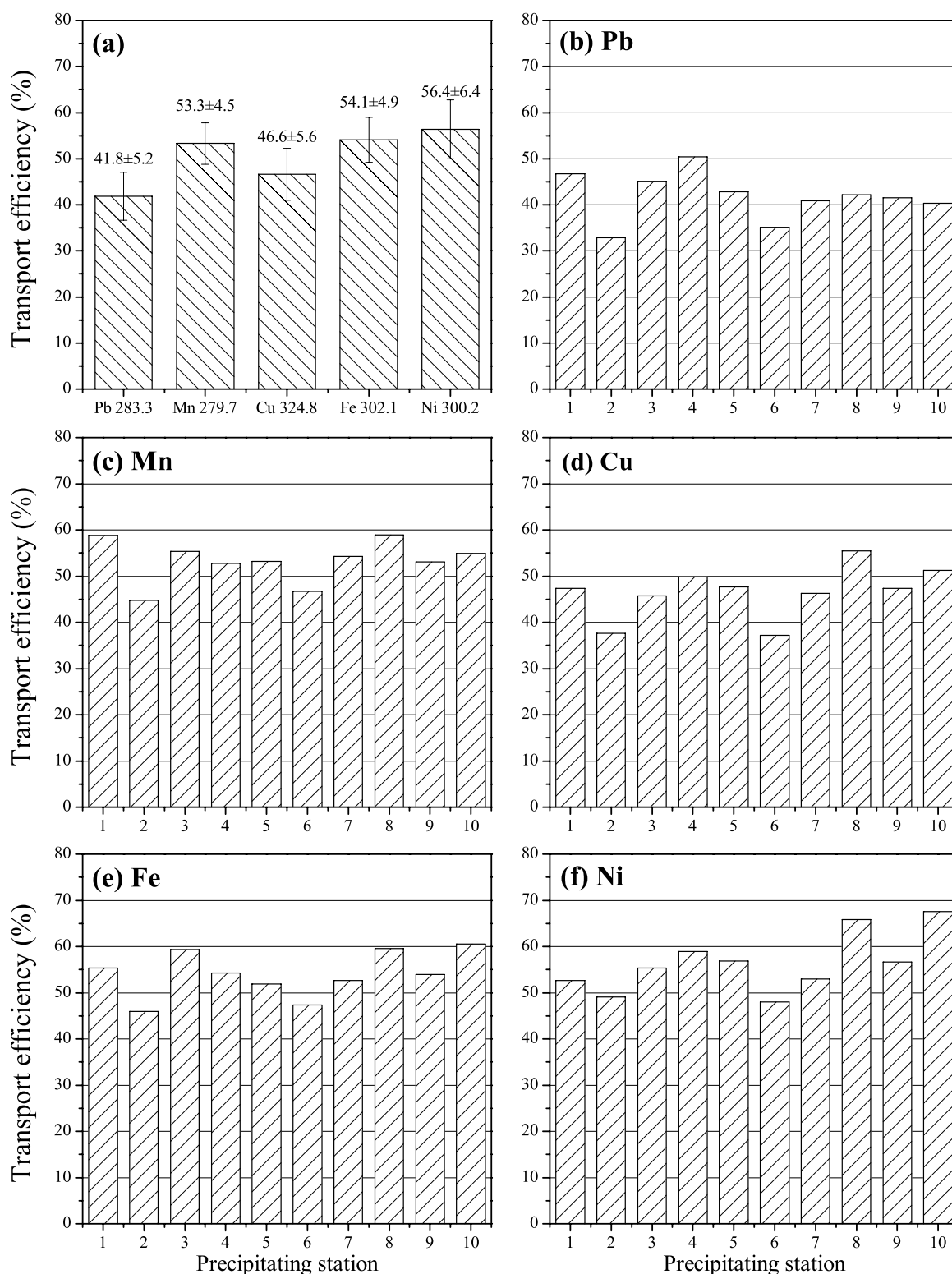


**Fig. 4.1:** Transport efficiencies for 8 ng Mn, 40 ng Cu, Fe, Pb, and 200 ng Ni dosed as a multi-element solution into the ETV boat and obtained with the external 10-fold precipitator: (a) mean values (SDs for the tandem ETV-EP procedure) and (b)-(f) TEs over all EP stations.



“Children” samples were also mailed in plastic containers into the co-authors laboratories for ICP-MS, ETAAS as well as SSAAS (Analytik Jena AG) analysis. The results indicate the high stability of the platform adsorbed samples.

## 4.2 Further applications of the 10-fold precipitation unit

After tests with model aerosols produced by the ETV, the 10-fold precipitation unit was applied to the collection of atmospheric aerosols as well as for the indoor measurements [Mat1, Mat2]. Fig. 4.3 shows measured concentrations of Al, Cu, Mn, Fe, and Pb in the ambient air by aerosol collections on the roof of I. Physical Institute and in the Workshop of the Institute. In the first case, when the wind was from the forestland to the city center, the obtained samples were considered as the “clean” ones. Higher concentrations of Al, Fe, and Pb were obtained by measuring in the Workshop.

The equipment for indoor and outdoor aerosol collection is until now in development.

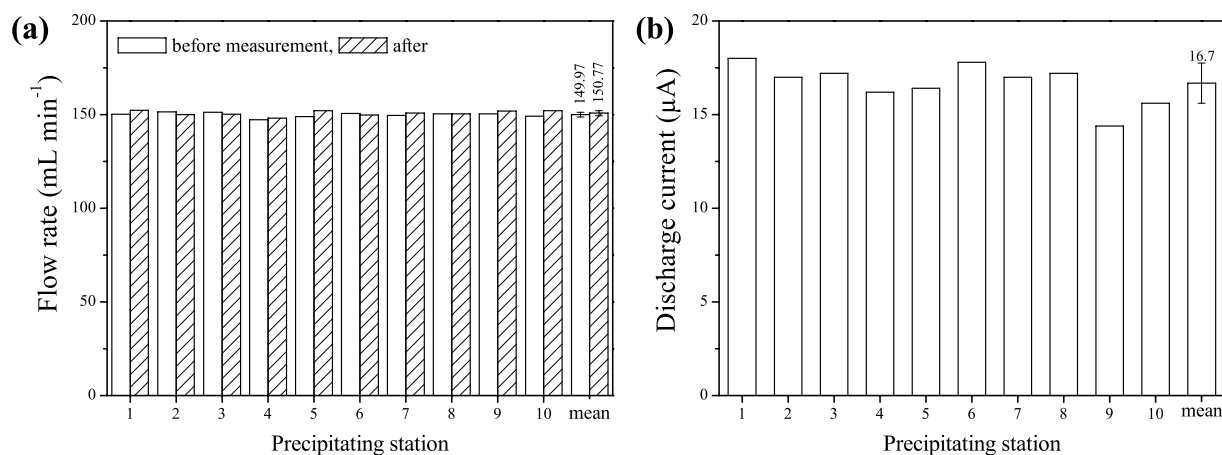


**Fig. 4.2:** Results of the adjustment of the 10-fold precipitation unit: (a) flow distribution through the precipitating stations before and after the measurement and (b) distribution of the corona discharge currents in the precipitators.

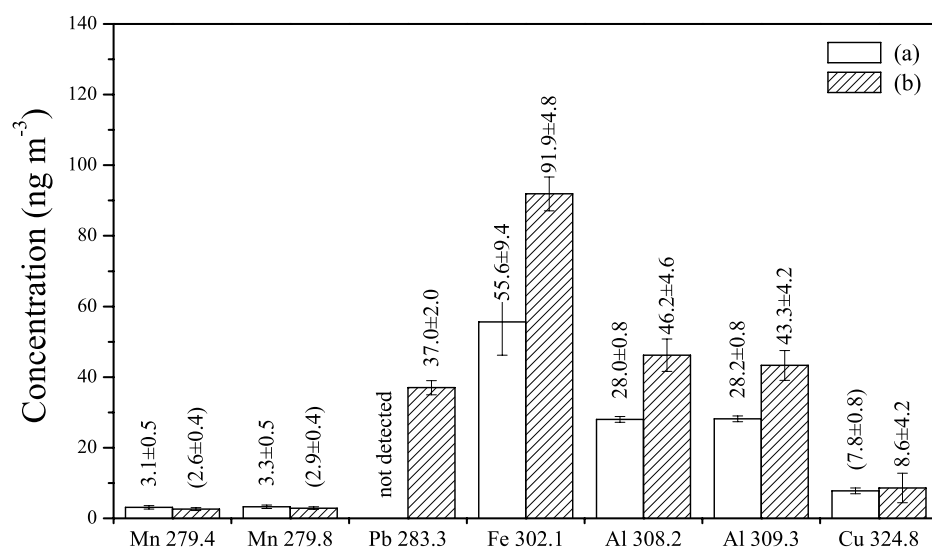


**Fig. 4.3:** Results of the collection of atmospheric aerosols using the 10-fold precipitation unit (a) on the roof of the I. Physical Institute and (b) in the Workshop of the Institute; in both cases signals of Si (288.2) and Mg (285.2) are saturated. Precipitation conditions: (a) duration 6h (54 L), wind from the forestland to the city center 7-12 km/h, cloudy, relative humidity 40-55%, temperature 8-12°C and (b) duration 3 h 15 min (29 L). Content of the secondary platforms is measured with ETV-EP CS-CFS, results taken from Ref. [Mat1, Mat2]. Values in brackets are unreliable.

---

## 5. Computer modeling of the dynamics of sample analytes and graphite furnace carbon in the axially focusing convection upstream

---

### 5.1 Condensation processes

#### 5.1.1 Homogeneous analyte condensation

A first and only existing theoretical description of the condensation of analyte vapor generated by ETV has been performed by Kántor [Kan1]. The concept was based on the formation of thermodynamically stable droplet nuclei with sizes exceeding a critical diameter, upon which further particle growth takes place. The critical diameter is derived from the Kelvin or Thompson-Gibbs equation [Hind]:

$$d_p^* = 4\sigma \frac{V_m}{kT \ln(S)}, \quad (5.1)$$

where  $d_p^*$  is the critical diameter,  $\sigma$  is the surface tension of the liquid droplet,  $V_m$  is the molecular volume of the vapor species,  $k$  is the Boltzmann constant,  $T$  is the absolute temperature, and  $S$  is the saturation ratio, defined below. At given  $S$ , droplets smaller than the critical size tend to evaporate, while larger ones, i.e. the “stable nuclei”, grow. It also follows that with larger  $S$  the size of the stable nuclei is smaller.

The saturation ratio is a measure of the magnitude of analyte vapor supersaturation and is defined as

$$S = \frac{p_{vap}}{p_s(T)}, \quad (5.2)$$

where  $p_{vap}$  is the actual partial pressure and  $p_s(T)$  is the equilibrium vapor pressure at the temperature of nucleation. The partial pressure of the analyte vapor can be approximated by the following relationship:

$$p_{vap} = \frac{N_s T_g R}{V_g t_v}, \quad (5.3)$$

where  $N_s$  is the number of moles of vapor from the evaporated sample,  $T_g$  is the initial temperature of the carrier gas in Kelvin,  $R$  is the gas constant,  $V_g$  is the flow rate at the initial temperature  $T_g$ , and  $t_v$  is the mean evaporation time.

The Eqs. 5.1-5.3 show that with the increasing the partial pressure of the analyte vapor, the saturation ratio increases too and the critical diameter becomes smaller. Consequently, the concentration of stable nuclei increases with  $S$ . On the other hand, below a certain value of the saturation ratio the formation of stable nuclei is negligible. In other words, the concentration of atoms in the gas phase is insufficient to promote self-nucleation. In this case, the analyte atoms will be mostly deposited on colder surfaces before they reach the analytical device.

To prove the applicability of Kantor's particle formation concept for the analyte condensation in ETV-AFC system, an estimate of saturation ratios for analyte densities in the upstream (see Table A.4.1) is performed. The supersaturation for most analytes studied is achieved first at temperatures under the melting point (i.e. analytes are in solid state). At the same time, the carbon originating from the GF is in a highly supersaturated state even within the furnace at vaporization temperature and can probably start to form polyatomic structures and larger carbon particulates.

### 5.1.2 Heterogeneous analyte condensation

Our measurements and the works of other authors have proven that carbon masses of about 70-80  $\mu\text{g}$  per heating shot are evaporated from the GF [Ort1, Ort2]. SEM and TEM investigations of carbon particulates in the furnace volume and in the upstream (see Sect. 3.6) confirm the hypothesis that carbon particles with nanometer sizes can be found even within the furnace. Thus, the predominant mechanism of analyte condensation is very likely the nucleated condensation of analyte atoms on the growing carbon particulates. This mechanism can probably lead to the packing of the analyte atoms into the carbon particulates that results in the observed shift of the analyte signal appearance toward later times by ETA CS-CFS analysis (see Fig. 3.17).

From the above discussion follows, that Kantor's particle formation concept [Kan1] based on the homogeneous condensation of liquid droplets is obviously not applicable for analyte amounts typically used by ETV sampling (nano- and picogram amounts). Thus, this

work concludes that the analyte condensation occurs predominantly heterogeneously through the attachment of analyte atoms at carbon particulates.

The carbon condensation begins from the nucleation. Primary nuclei can probably be formed by the following mechanisms:

- (1) evaporation of carbon multimers and growth of polyaromatic structures and
- (2) bending, folding up, and collapsing of larger polyaromatic structures to more spherical particulates.

Mechanism of particulate formation for the carbon released from the GF by vaporization is very similar to that for hydrocarbons by means of pyrolysis or incomplete combustion that has been the field of study by a large number of investigators [Donn, Mann, Lah1, Lah2, Fre1, Fre2]. The hydrocarbons produce two types of carbons [Donn]. The first type is formed by the deposition on the walls of the reactor and is known as pyrocarbon while the second type is formed in the bulk in the gaseous phase. The gaseous phase particulate matter could be termed “carbon black” or “soot”. The former is an industrially manufactured carbon material and is characterized by spherical or nearly spherical fused aggregate particulates with the range of sizes between 100 and 1000 nm. Soot, on the other hand, is a randomly formed particulate carbon, which in addition to carbon can contain a large variety of inorganic and organic impurities.

The formation of soot particles is a logical consequence of the growth of molecules through collisions. The process involves the conversion of primary molecular species, which include free radicals and ions, into relatively larger particulates containing many tens of thousands of atoms and consists of three different stages [Donn]:

- (1) nucleation or formation of soot precursors and soot inceptions, which involved the transformation of a molecular system to a particulate system;
- (2) coagulation of particles, which involves collisions between the large number of tiny particles with dimensions in the order of 1-2 nm produced by nucleation. This results in the formation of larger spherical particles with dimensions in the order of 10-50 nm; and
- (3) agglomeration of these spherical particles into chains up to 1 mm in length.

As it is shown later for the case of the GF carbon, with relevant C densities, these first nucleation steps (up to nanometer particle sizes) pass very fast, already inside the GF or within few millimeters above the GF outlet. Thus, in the modeling we can omit the nucleation and consider only coagulation of carbon particles through collisions.

In the modeling, carbon particles are considered as hard spheres with sufficient number of degrees of freedom, in which the kinetic energy of collision participants (C-C or C-Me) can be redistributed. Calculations are performed with mean parameters: the mean carbon particle density ( $n_C$ ), the mean carbon particle diameter ( $d_C$ ), and the mean carbon particle mass ( $m_C$ ).

## 5.2 Kinetic model

The kinetic model allows to estimate the influence of physico-chemical factors upon the condensation process of sample analytes in nano- and picogram amounts (ppb and ppt ranges). The proposed model takes into account (1) the condensation of carbon released from the GF surface by vaporization, (2) two-dimensional diffusion of free analyte atoms in a non-isothermal environment, (3) attachment of analyte atoms to polyatomic carbon particles, and (4) the loss of analyte atoms reaching the AFC tube wall. The model is developed for the real geometry of the ETV-AFC unit and based on the measured temperature dependences in the upstream (see Sect. 3.4).

The following basic assumptions are made:

- (1) the analyte is completely atomized in the ETV, i.e. there are only free analyte atoms at the GF outlet;
- (2) there are only longitudinal temperature gradients within the AFC tube, i.e. any given tube cross-section is isothermal;
- (3) the velocity profile of the upstream flow is considered to be rectangular, i.e. the upstream flow rate depends only on initial flow rate and flow temperature;
- (4) the carbon vapor is considered as a vapor consisting of identical particles with the particle mass equal to the mean particle mass;
- (5) analyte condensation occurs only during sticking collisions with carbon particles, other reactions (analyte-analyte, analyte-modifier etc.) have significantly lower reaction rates and are not considered.

Fig. 5.1 illustrates the notational convention used in the model. The frame of reference for the three cylindrical coordinates  $r$ ,  $\varphi$ , and  $z$  is given. The geometry of the ETV-AFC unit (GF outlet hole and AFC tube) can be completely described by three parameters: (1)  $L$ , the

length of the AFC tube; (2)  $R_{AFC\ tube}$ , the inside radius of the tube; and (3)  $R_{GF\ outlet}$ , the radius of the GF outlet hole.

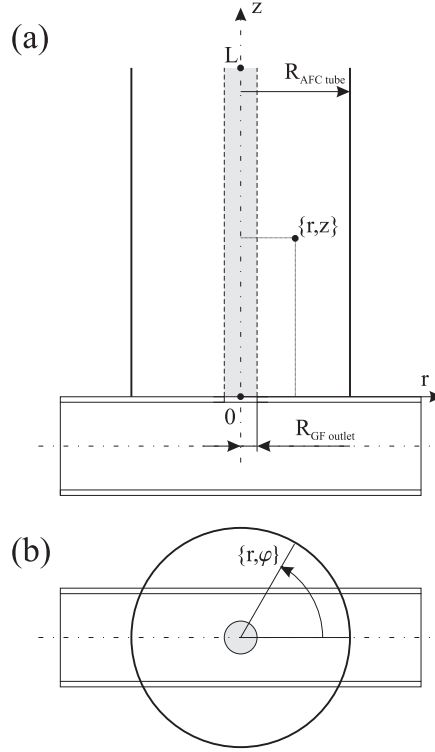


**Fig. 5.1:** Axially focusing convection tube geometry in (a) longitudinal section and (b) cross-section.

### 5.2.1 Rate of the carbon condensation process

The mechanism for the coagulation of the particles consisting of  $i$   $C_1$  atoms is suggested in the form of the following reaction:



The complete description of the rate of variation of the carbon particle density due to the coagulation process is given by:

$$\frac{dn_C}{dt} = -\sqrt{2} \left( \frac{8 k T(t)}{\pi m_C(t)} \right)^{\frac{1}{2}} \sigma_{CC}(t) n_C^2, \quad (5.6)$$

where  $\sigma_{CC}$  is the interaction cross-section ( $\sigma_{CC} = \pi d_C^2$ ),  $k$  is the Boltzmann's constant, and  $T$  is the actual gas temperature. The diffusion of heavy carbon particulates is neglected.

The general form of the solution is:

$$n_c(t) = \frac{n_{c0}}{1 + \sqrt{2} n_{c0} \int_0^t \left( \frac{8 k T(t')}{\pi m_c(t')} \right)^{\frac{1}{2}} \sigma_{cc}(t') dt'} , \quad (5.7)$$

where  $n_{c0}$  is the initial carbon particle density. The iterative formula for calculations is:

$$n_{C,t'+\Delta t} = \frac{n_{C,t'}}{1 + \sqrt{2} \left( \frac{8 k T_{t'}}{\pi m_{C,t'}} \right)^{\frac{1}{2}} \sigma_{CC,t'} n_{C,t'} \Delta t} \quad (5.8)$$

with

$$m_{C,t'} = \frac{n_{C,t'-\Delta t}}{n_{C,t'}} m_{C,t'-\Delta t} , \quad (5.9)$$

$$\sigma_{CC,t'} = \pi d_{C,t'}^2 , \text{ and} \quad (5.10)$$

$$d_{C,t'} = \sqrt[3]{\frac{6}{\pi F} \frac{m_{C,t'}}{m_a} V_a} , \quad (5.11)$$

where  $F$  is the space filling coefficient defined below,  $m_a$  and  $V_a$  are the mass and volume of the carbon atom, respectively ( $V_a = \frac{4}{3} \pi a_c^3$ ,  $a_c$  is the covalent radius for carbon). In this consideration, the carbon particles are presumably identified with the graphite and as the covalent radius for carbon  $a_c$ , a half of the typical interatomic distance between two neighboring atoms in the basal plane of the graphite lattice is used. The space filling  $F$  (for the model of hard spherical particles) is defined as a ratio between the volumes of the single atoms forming the particle to the particle volume [Weiß]. The space filling factor for the graphite structure is 0.169 [Bats]. The identifying with the graphite gives a lower estimate for the carbon particle diameters and interaction cross-sections because the particle structure is very likely closer to fractal carbon flakes with more rapid increase of the diameter with the number of C-atoms composing the particle. The values of basic parameters used in the modeling are presented in Table 5.1.



<i>Geometry</i>		
	AFC tube length	14 cm
	Diameter	13 mm
	GF outlet hole diameter	2.6 mm
<i>Upstream flow rate</i>		
	Volume flow rate (293 K)	150 mL min <sup>-1</sup>
<i>Computation</i>		
	Time increment	$\Delta t = 10^{-6}$ s
<i>Carbon</i>		
	Space filling factor [Bats]	0.169
	Initial particle size	0.5 nm
	Covalent radius [Weiß, Weas]	0.07105 nm

**Table 5.1:** Simulation conditions for the condensation of carbon in the ETV-AFC unit.

There are always some ions in the furnace gas phase at vaporization temperatures (1600-2600°C). The charged particles can serve as nucleating agents and speed up the carbon condensation. Therefore, the condensation rate given above should be considered as a lower estimate of the actual process.

### 5.2.2 Rate of the analyte condensation process

In the frames of that there are only free metal atoms at the GF outlet, we can consider the mechanism of condensation as an attachment of free analyte atoms at the carbon particles during the collision process. It is suggested in the form of the following reaction:



The complete description of the rate of variation of the analyte vapor density ( $\partial n_{Me} / \partial t$ ) due to analyte condensation process is given by the following equation:

$$\frac{\partial n_{Me}}{\partial t} = - \left( \frac{8 k T(t)}{\pi \mu_{C Me}(t)} \right)^{\frac{1}{2}} \sigma_{C Me} n_{Me} n_C(t) f(T), \quad (5.13)$$

where  $\sigma_{CMe}$  is the collision cross-section for the pair metal-carbon ( $\sigma_{CMe} = \pi(\frac{d_C}{2} + a_{Me})^2$ ),  $a_{Me}$  is the radius of the metal atom (taken as a half of the Me-Me bond length [Weas]),  $\mu_{CMe}$  is the reduced mass ( $\mu_{CMe} = m_C m_{Me} / (m_C + m_{Me})$ ),  $m_{Me}$  is the analyte atom mass), and  $f(T)$  is the attachment function defined in the following section.

The general form of the solution is given as follows:

$$n_{Me}(t) = n_{Me0} \exp \left[ - \int_0^t \left( \frac{8 k T(t')}{\pi \mu_{CMe}(t')} \right)^{\frac{1}{2}} \sigma_{CMe}(t') f(T) n_C(t') dt' \right], \quad (5.14)$$

where  $n_{Me0}$  is the initial analyte particle density. Assuming that the carbon particle density is constant during the short time increment  $\Delta t$ , we obtain the following iterative formula for calculations:

$$n_{Me,t'+\Delta t} = n_{Me,t'} \exp \left[ - \left( \frac{8 k T_{t'}}{\pi \mu_{t'}} \right)^{\frac{1}{2}} \sigma_{t'} f(T_{t'}) n_{C,t'} \Delta t \right], \quad (5.15)$$

with

$$\mu_{t'} = \frac{m_{C,t'} m_{Me}}{m_{C,t'} + m_{Me}}, \quad (5.16)$$

$$\sigma_{t'} = \pi \left( \frac{d_{C,t'}}{2} + a_{Me} \right)^2. \quad (5.17)$$

### 5.2.3 Attachment function

In order to define the attachment function  $f(T)$  of a free analyte atom to the surface of a relatively large carbon particle, we assume that the processes of adsorption and re-vaporization for the system atom plus carbon particle and for atom plus GF surface are more or less similar. Thus, the attachment function can be formulated based on the maximal pre-treatment temperature of the analyte studied in an AAS GF. Generally, at this temperature

first losses of the analyte by pretreatment are observed. These temperatures also depend on chemical modifiers applied. These data are given elsewhere [Wel2].

As the attachment probability, the following equation is used:

$$f(T) = \frac{1}{1 + \exp\left[\frac{T - \alpha T_p}{\gamma T_p}\right]}, \quad (5.18)$$

where  $T_p$  is the maximal pretreatment temperature,  $\alpha$  and  $\gamma$  are parameters ( $\alpha = 1$  and  $\gamma = 0.15$  for all analytes studied).

#### 5.2.4 Analyte distribution function

There are several mechanisms determining the analyte particle displacement during its diffusion and convective motion in the system under consideration. In the vertical direction, these are first of all the processes of convection and thermal contraction during the fast upstream cooling down. In this case, the diffusion due to weak gradients is neglected. In the radial direction, the net flux of atoms  $J$  is determined by concentration diffusion and is given in the form of Fick's first diffusion law [Hind]:

$$J = -D \frac{dn_{Me}(r)}{dr}. \quad (5.19)$$

Here,  $D$  is the diffusion coefficient for the analyte atom under consideration in the Ar environment and  $dn_{Me}(r)/dr$  is the concentration gradient. The flux  $J$  is the quantity transferred per unit time through a unit area of a cylinder surface with radius  $r$  under the influence of the concentration gradient. The temperature dependence of the diffusion coefficient is described later.

The analyte particle number distribution  $N_{Me}(r, t)$  above the GF outlet hole is approximated with the following equation:

$$N_{Me}(r, t) = \frac{3 N_{Me0}}{\pi R(t)^6} (R(t)^2 - r^2)^2, \quad (5.20)$$

where  $N_{Me0}$  is the initial particle number and  $R(t)$  is the radius of the distribution (there are no analyte atoms at  $r > R(t)$ ). An advantage of this bell-shaped function over the Gaussian

distribution is the limited range of definition  $\{-R(t), +R(t)\}$  that is suited for the modeling conditions with the GF outlet hole forming the limited particle distribution. As radius at the half height at  $t=0$ , the radius of the outlet hole is assumed for all analytes studied.

Fig. 5.2(a) illustrates the initial particle distribution together with the GF outlet hole radius ( $R_{out}(t=0) = R_{GF\ outlet}$ ). Owing to analyte atom diffusion, the time dependence of the distribution function is described with the increasing radius  $R_{out}(t)$  as follows:

$$R_{out}(t) = R_{GF\ outlet} + \int_0^t \sqrt{\frac{D(t')}{2t'}} dt'. \quad (5.21)$$

This expression takes into account the temperature dependence of the diffusion coefficient and represents the spreading out of the sample analyte atoms starting from the initial distribution shown in Fig. 5.2(a). Within the central condensation area where C-particles are presented ( $r < R_{GF\ outlet}$ ) the analyte attachment to the carbon particulates can take place.

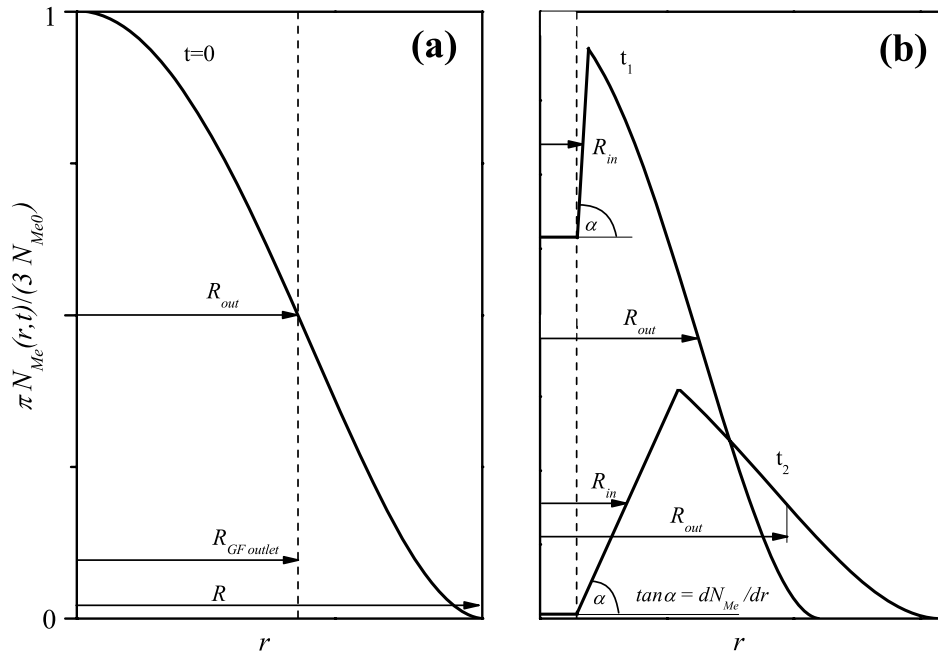


**Fig. 5.2:** Distribution function of the analyte particle number: (a) for  $t=0$ , (b) for the times  $t_1$  and  $t_2$  ( $t_1 < t_2$ ).

The distributions for the later times ( $t_1$  and  $t_2$ ) are shown in Fig. 5.2(b). Diffusion of analyte atoms into the central condensation area owing to the gradient  $dN_{Me}(r)/dr$  has to be taken into account. During the condensation process, this gradient will be estimated based on

the depth of the dip in the particle number distribution and the total number of particles transferred into the central condensation area by diffusion. An estimate of the number of analyte atoms coming into the central condensation area  $N_{in}(t)$  is done based on Fick's first law (Eq. 5.19) as follows:

$$N_{in}(t) = \int_0^t A(t) D(t) \frac{dn_{Me}}{dr} dt, \quad (5.22)$$

where  $A(t)$  is the surface of a volume element (cylindrical layer with radius  $r = R_{GF\ outlet}$ ). Thus, when the number of the condensed analyte atoms per a unit time becomes higher than that transferred from the outside by diffusion, the depth together with the gradient grows. In the opposite case, when the bottom is almost reached, they both begin to sink. The system eventually comes to equilibrium by equalizing the both rates. The gradient at the radius  $R_{in}(t)$  at the half height of the dip characterizes the analyte diffusion into the central condensation area.

The analyte losses are estimated as the number of particles outside the AFC tube according to the distribution function.

For connecting the AFC tube to the transport tubing, two different methods for the further describing the analyte and carbon particle dynamics are considered. The first is turbulent mixing of the carbon and analyte densities. In this case, a very rapid increase of the condensation rate is observed. The second is a laminar narrowing of the streaming lines without mixing. In this case, the analyte distribution function and the radius of the central condensation area are correspondingly modified. The last method is in better correspondence with our measurements.

During the transport process in the tubing, carbon particulates can be lost by sedimentation, impaction in curvatures and turbulences, as well as by electrostatic forces. The percentage of lost carbon particulates is regarded to be low because of their much higher masses. The carbon particle losses are not in consideration.

### 5.2.5 Temperature dependence of the gas phase diffusion coefficients

During the upstream cooling process, the temperature is constantly changing in time and space. The diffusion coefficient is a crucial parameter that determines the distribution of

analyte atoms inside the AFC tube. The temperature dependence of the diffusion coefficient is derived from the relation [Lvov]:

$$D(T) = D_0 \left( \frac{T}{T_0} \right)^\chi, \quad (5.23)$$

where  $D_0$  is the diffusion coefficient determined at a reference temperature  $T_0$  (typically,  $T_0 = 273.15 \text{ K}$ ) and  $\chi$  is the gas combination factor that is close to 2. Values of  $D_0$  and  $\chi$  for different elements are summarized by L'vov [Lvov] and listed in Table 5.2. The dependence of the diffusion coefficients on the longitudinal coordinate  $D(z)$  can be described using Eq. 5.23 if the temperature distribution along the longitudinal coordinate is known.

The temperatures in the AFC upstream have been measured with the rapid thermocouple (see Sect. 3.4). These results are obtained for  $200 \text{ mL min}^{-1}$  internal gas flow rate with 3 mm outlet hole diameter but they can be also applied for the model because at  $150 \text{ mL min}^{-1}$  internal gas flow and 2.6 mm hole diameter the flow velocities are very similar. The temperature profile within the AFC tube can be approximated with the following expression combining the rapid exponential temperature decay near the GF outlet and the linear sinking at the large values of  $z$ :

$$T(z) = P_1 - P_2 z + P_3 \exp(-P_4 z). \quad (5.24)$$

Here, the parameters  $P_1$ ,  $P_2$ ,  $P_3$ , and  $P_4$  are the constants of approximation determined for measured temperature dependences corresponding to the vaporization temperatures of the analytes studied [Wel2]. Fig. 5.3 shows the approximation using Eq. 5.24 for GF heating temperature of  $2500^\circ\text{C}$  (Ni vaporization). The values of these parameters along with the pre-treatment and vaporization temperatures for Ag, Cu, Fe, Mn, Ni, and Pb for the cases without and with the addition of Pd-Mg modifier are summarized in Table 5.2.

### 5.2.6 Estimation of evaporation rates for analytes and carbon

Estimates for analyte evaporation rates can be derived from the atomization peak duration in GF ETAAS. The full analyte mass dosed into the ETV boat is vaporized during about a half second.

The carbon evaporation rate at  $2500^\circ\text{C}$  is estimated based on the experimental data for GF tube mass losses (see Sect. 3.5). The rates for different analyte vaporization temperatures,

which correspond to different times of a single heating cycle, are estimated by assuming that the evaporated carbon density is proportional to the carbon saturation vapor density extracted from the saturation vapor pressures given in Ref. [Land]. Here, the carbon evaporation rate is expressed as follows:

$$\frac{dm}{dt} = P n(T) \Delta V(T) m_a, \quad (5.25)$$

where  $n(T)$  is the carbon saturation vapor density at the analyte vaporization temperature,  $\Delta V(T)$  is the volume element,  $m_a$  is the mass of the C-atom, and  $P$  is the constant of proportionality determined based on the known evaporation rate at 2500°C ( $P \approx 500$ ). The carbon evaporation rates at different times of a heating cycle and, thereby, at different analyte vaporization temperatures are tabulated in Table 5.3.

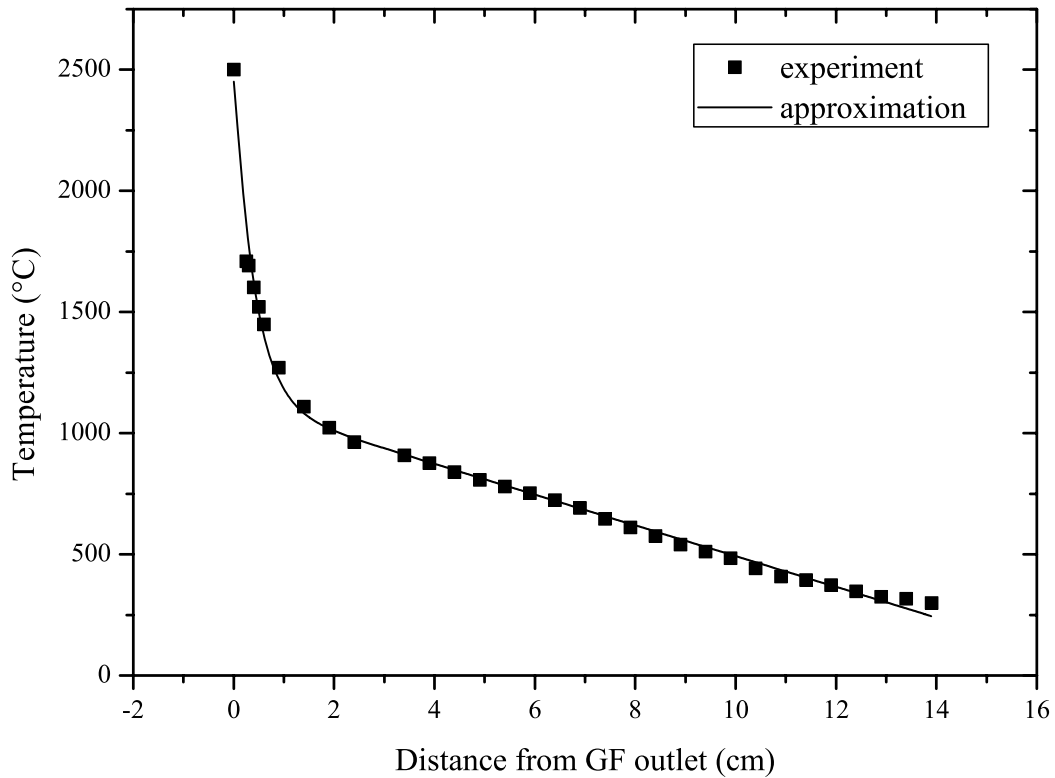


**Fig. 5.3:** Approximation of the temperature dependence in the upstream (see Fig. 3.5(d)) for the case of Ni vaporization at 2500°C.

<i>Element</i>	$D_0 \times 10^{-6} / \text{m}^2 \text{s}^{-1}$ <sup>2)</sup>	$\chi$ <sup>2)</sup>	$T_p$ <sup>3)</sup> /°C	$T_{\text{vap}}$ <sup>3)</sup> /°C	$P_1$ /°C	$P_2$ /°C cm <sup>-1</sup>	$P_3$ /°C	$P_4$ /°C cm <sup>-1</sup>
Ag	7.9	1.89	650	1600	721.6	40.62	847.4	2.47404
Cu	9.3	1.91	1000	2300	1037.2	58.40	1218.1	2.47404
Fe	7.9	1.96	1400	2400	1082.4	60.94	1271.1	2.47407
Mn	13.0	1.70	1100	2200	992.2	55.86	1165.2	2.47414
Ni	9.4	1.93	1400	2500	1127.4	63.47	1324.1	2.47407
Pb	7.9	1.84	600	1800	811.8	45.70	953.3	2.47415
Ag <sup>1)</sup>	7.9	1.89	1000	1800	811.8	45.70	953.3	2.47415
Mn <sup>1)</sup>	13.0	1.70	1400	2300	1037.2	58.40	1218.1	2.47404
Pb <sup>1)</sup>	7.9	1.84	1200	2000	902.0	50.78	1059.3	2.47413

<sup>1)</sup> with Pd-Mg modifiers

<sup>2)</sup> data from Ref. [Lvov]

<sup>3)</sup> data from Ref. [Wel2]

**Table 5.2:** Simulation conditions for the condensation of Ag, Cu, Fe, Mn, Ni, and Pb in the ETV-AFC unit.

Time /s	GF temperature /°C	Platform temperature /°C	Evaporation rate /μg s <sup>-1</sup>
2	2200	~1600	0.07
2.2	2300	~1800	0.27
2.7	2400	~2200	0.92
3.4	2500	~2350	2.92
5	2600	~2500	8.56

**Table 5.3:** Estimated carbon evaporation rates obtained with Eq 5.25 at different times from the beginning of the ETV heating cycle and, thereby, at different temperatures in the GF tube center with corresponding them platform temperatures (data from Fig. 3.3).

### 5.3 Results and discussion

Three sets of calculations are performed: the first set yields condensation of carbon particulates, the second described only analyte diffusion without condensation and the third one included the analyte condensation upon the growing carbon particulates. The calculations are performed for the laboratory-made ETV-AFC system described in Sect. 2.1. For computa-



tions, the minimum time increments necessary to obtain consistency in the results were used. Finer increments did not yield noticeable differences in the results.

The starting point of the simulation is defined by the time at which the temperature of the ETV platform is equal to the analyte vaporization temperature shown in Table 5.2. The end of the simulation is set to the time at which the total number of free analyte atoms decreases below 0.01% of the initial value.

### 5.3.1 Carbon condensation

The first result demonstrates the condensation of carbon. Fig. 5.4(a) shows the density of carbon particulates in the upstream as a function of the pathway inside the AFC tube for different carbon amounts released from the tube at different times during a heating cycle and, thereby, at different GF temperatures. For better understanding, the density profiles show the C-particle density decrease caused by volume reactions only and do not include the density increase caused by thermal gas contraction. However, the thermal contraction has been taken into account in all calculations. Very high particle formation rates are observed within a few millimeters from the GF tube outlet hole at higher vaporization temperatures. There particle density is decreased in 2-3 orders of magnitude. With decreasing the vaporization temperature, the carbon particle density and, thereby, the condensation rate becomes lower. With increasing the distance from the outlet, the density decreases hyperbolically. If the thermal volume contraction is taken into account, the curves in Fig. 5.4(a) pass a minimum and then increase again for a couple of centimeters.

The dynamic of the particle growing is presented in Fig. 5.4(b-c) as dependences of the mean number of carbon atoms composing the carbon particulate and the mean particulate diameter as functions of the pathway and time. The simulation shows a significant difference in the particle sizes for not widely differing vaporization temperatures. After only a half centimeter from the GF tube outlet the particles formed by 2500°C are 20-30 times larger and composed from  $10^4$ - $10^5$  times higher number of atoms than those released by 1600°C. With the increase of the coordinate and decreasing the upstream temperature, the condensation rate and the carbon particle density becomes lower and after a few centimeters from the outlet, the process of carbon particle formation is almost finished. Further condensation does not essentially increase the particle sizes and density.

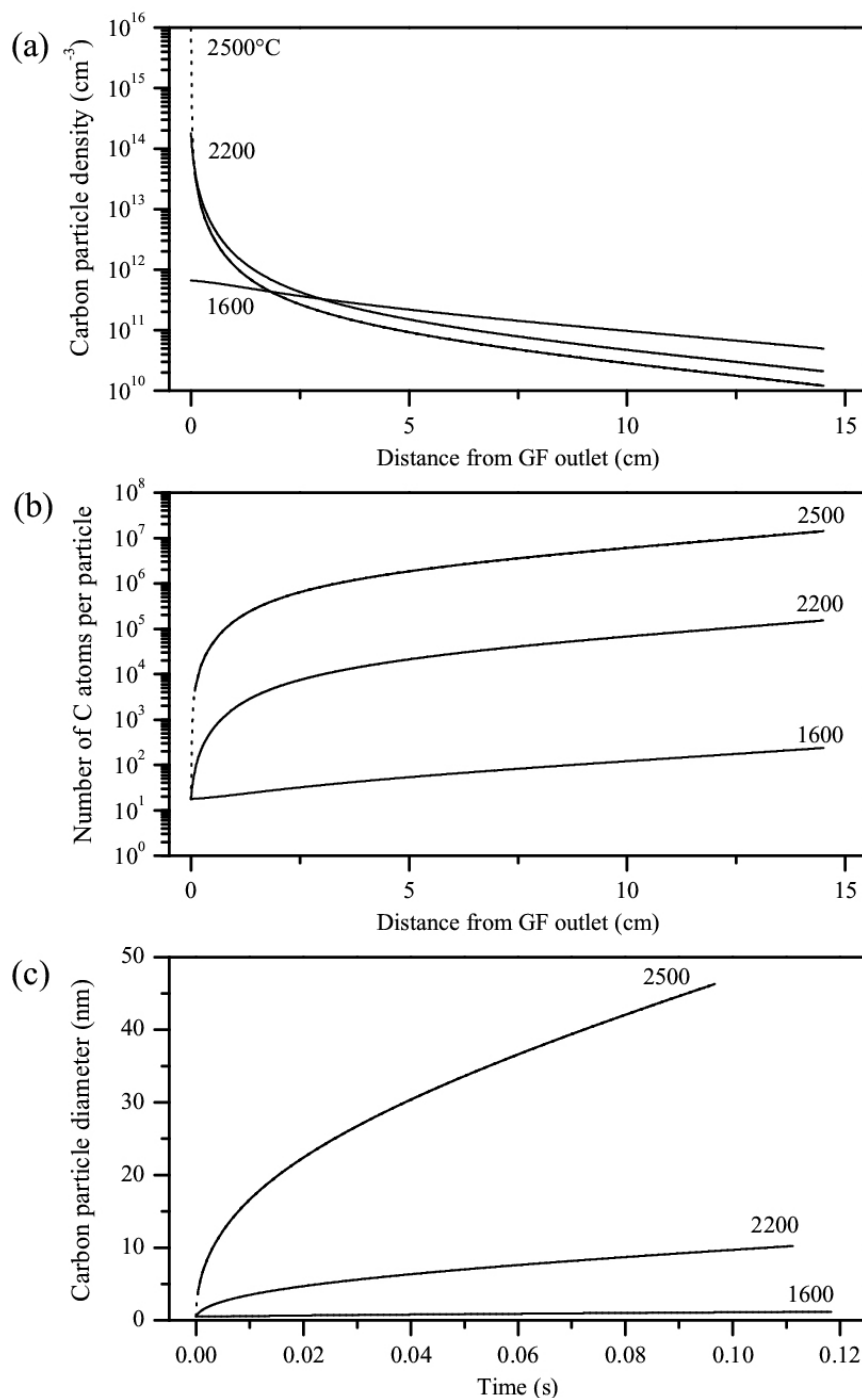


**Fig. 5.4:** Modeling of carbon condensation in the AFC upstream at different platform temperatures during the ETV heating cycle.

- (a) The particle density,
- (b) mean number of  $\text{C}_1$  atoms per a carbon particle, and
- (c) the mean diameter of carbon particles.

Results obtained for initial carbon particle diameters 0.5 nm, released carbon masses according to Table 5.3.

The carbon condensation at different vaporization temperatures explains the differences in the condensation and transport of analytes of different volatilities. The medium and low volatile analytes Fe or Ni are found from the beginning in an environment consisting of large carbon particulates with the large analyte-carbon collision cross-sections. This will support and speed up the analyte condensation process. The situation with volatile analytes Ag or Pb is different. They are evaporated at lower temperatures into an environment with a lower number of significantly smaller carbon particles. As a result, the rate of analyte condensation is much lower. Important effect of Pd modifier (see Sect. 3.7.1) is that these volatile analytes co-vaporize with significantly higher carbon densities.

The results in Fig. 5.4 show an agreement with the data of the microscopic investigation of carbon particulates in the upstream presented in Sect. 3.6. At 2.25 cm above the GF tube outlet, the simulated mean diameters of the carbon particulates are around 3.5 nm for vaporization at 2200°C and around 15 nm for vaporization at 2500°C (both the platform temperatures during the heating cycle). The TEM images (see Fig. 3.12) obtained at 2400°C (corresponds to the platform temperature slightly higher than 2200°C) for the same cut show particulates with 10 nm diameters. The SEM images (see Fig. 3.13(a)) obtained at 2600°C (platform temperature ~ 2500°C) for the same cut are not resolved. At 0.25 cm above the GF tube outlet, the simulated mean diameters are ~0.5 nm for vaporization at 1600°C, ~1.2 nm for 2200°C, and ~5 nm for 2500°C (all temperatures are the platform temperatures during the heating cycle). For higher temperatures, an extremely fast growth of the diameter is calculated that makes the starting value of the diameter (0.5 nm) almost unimportant. The SEM images (see Fig. 3.11(d)) at 0.25 cm above the outlet are also not resolved. The SEM images of thermophoretically collected particles at 2.25 cm (see Fig. 3.13(a)) and of electrostatically collected after 1 m transport path (see Fig. 3.13(b)-(d)) are very similar to each other that is also in agreement with the above calculations. Chains and web-like structures of agglomerated carbon particulates of approximately the same sizes can be well seen in the SEM images in both cases. It should be noted that the above consideration does not take into account the forces leading to formation of chains and web-like structures, which are very likely caused by polarization of carbon particulates due to ions supporting the condensation.

Fig. 5.5 shows space and time dependences of the position of a released aerosol volume element for different GF temperatures. The beginning and the ending of the curves correspond to the GF outlet and to the end of the AFC tube. As it is seen from Fig. 5.5, the flight

time through the AFC tube is about 0.1 s. For comparison, the time to transport the aerosol from the ETV to the ETA GF is about 3.5 s. The estimated flow velocity at the GF outlet is up to  $5 \text{ m s}^{-1}$ .

The results presented above were calculated based on the parameters listed in Table 5.1. The computer modeling allows modifications of all the basic parameters in order to investigate their influence. Fig. 5.6(a) is illustrating the effect of the initial diameter of carbon particles at the GF outlet on the density and diameter of carbon particulates on the subsequent path. The simulation is performed for 0.2, 0.5, 1, and 3 nm particle diameters at the GF tube outlet. This range of the initial particle diameters very likely reflects the real spectrum of the particles within the ETV furnace. As it is clearly seen from the graphs, all the data converge

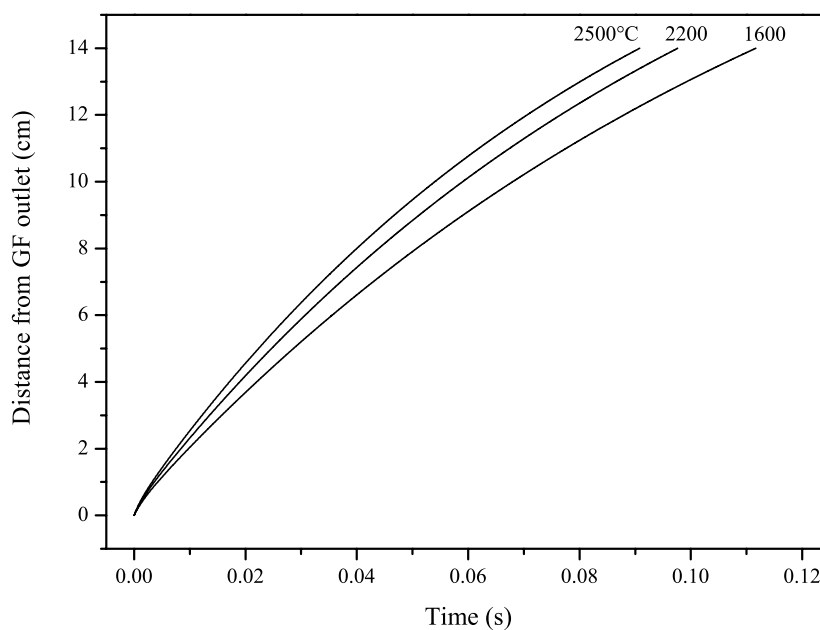


**Fig. 5.5:** Dependence of the volume element position in the AFC upstream as a function of the flight time at different platform temperatures during the ETV heating cycle, obtained for  $150 \text{ mL min}^{-1}$  internal gas flow, 0.5 nm initial carbon particle diameters; released carbon masses according to Table 5.3.

to the same values after a very short distance. Thus, it can be concluded that the initial particle diameter is not a crucial parameter for this consideration and is of less importance than the carbon mass density. It is assumed that the initial size of the carbon particles for all considerations below is 0.5 nm in diameter.

Fig. 5.6(b) shows the carbon particle density in the upstream flow for different diameters of the GF outlet hole (left) and for different gas flow rates (right). These estimations can be done by not large deviations from the given values for the outlet hole diameter and the flow rate. From the behavior of the curves, it can barely be discerned that the characteristics show higher slope when the flow rate is lower. It is also easily seen in both graphs that the maximal difference between the upper and the bottom curves at the same distance is not higher than one order of magnitude. Thus, the obtained approximation is more or less stable and has no significant variation by changing the main physical, geometrical, and experimental parameters.

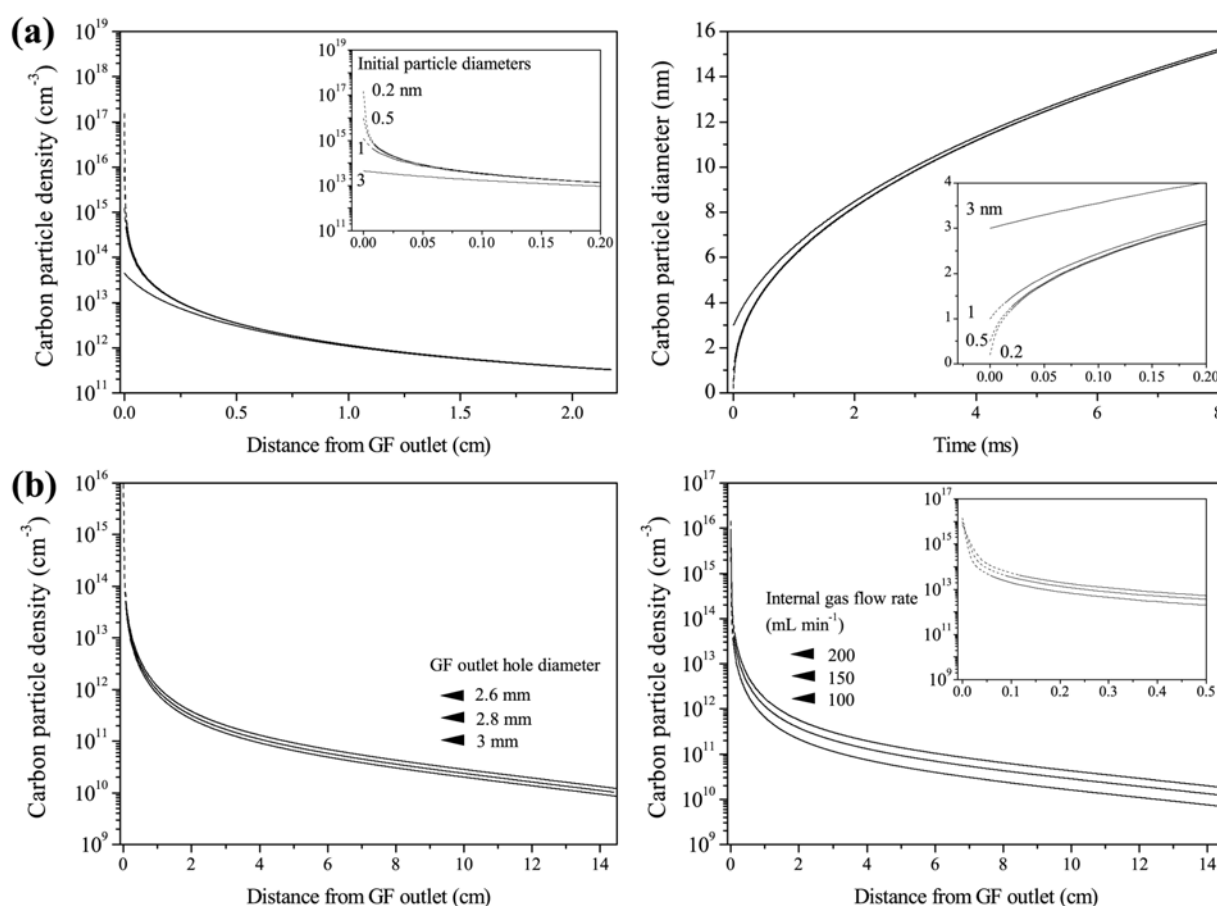


**Fig. 5.6:** Effect of physical, geometrical, and experimental parameters on the condensation process of carbon particulates.

(a) Effect of the initial diameter of carbon particles at the GF outlet on their density and mean diameters on the subsequent pathway;

(b) effect of the size of the GF outlet hole (left) and the internal gas flow rate (right).

Results obtained for 2500°C vaporization temperature,  $8.56 \mu\text{g s}^{-1}$  carbon evaporation rate and for  $150 \text{ mL min}^{-1}$  internal gas flow rate (if not otherwise denoted).

One can conclude that the vaporization temperature and the released carbon mass are the main factors, which have a remarkable influence on the behavior of the carbon condensation process and as it will be shown below on the condensation of the analyte atoms.

### 5.3.2 Analyte dynamics without condensation

The second situation calculated demonstrates the distribution of Ag, Cu, Fe, Ni, Mn, and Pb atoms in the upstream without analyte adsorption by carbon aerosol. Fig. 5.7 illustrates the longitudinal dependence of the total number, the number of free atoms in the central condensation area overlapping with the carbon particulates, and the number of atoms lost on the AFC tube wall presented as the percentage of the initial number of analyte atoms as function of the pathway from the GF tube outlet.

Very similar distributions are obtained for two groups of analytes with heavy (Ag and Pb) and with light atoms (Cu, Fe, Ni, and Mn). According to the difference in the masses that results among other factors in different diffusional properties, the light analytes faster leave the central condensation area that can be well seen in the slope of the curves. Thus, Ag and Pb remain in the central condensation area slightly longer than the other analytes studied. At the end of the AFC tube, 3-4% of light and ~5% of heavy atoms are still in the central condensation area.

The first wall losses occur after 4.5-5 cm for heavy and 3-3.5 cm for light analytes. Thus, the following losses of the initial analyte amounts at the end of the AFC tube are simulated: 17.7% for Ag, 18.1% for Pb, 32.7% for Mn, 32.6% for Cu, 30.6% for Fe, and 36.2% for Ni. These values are the maximal losses that occur within the AFC tube under given simulation conditions in the absence of analyte condensation.

### 5.3.3 Analyte dynamics with condensation

The third situation calculated takes into account the attachment of Ag, Cu, Fe, Ni, Mn, and Pb atoms to the carbon aerosol. The results of the simulation are given in Fig. 5.8, which has the same form of presentation as Fig. 5.7. Additionally to the distributions illustrated in Fig. 5.7, the percentage of the analyte atoms attached at the carbon aerosol particulates is shown.

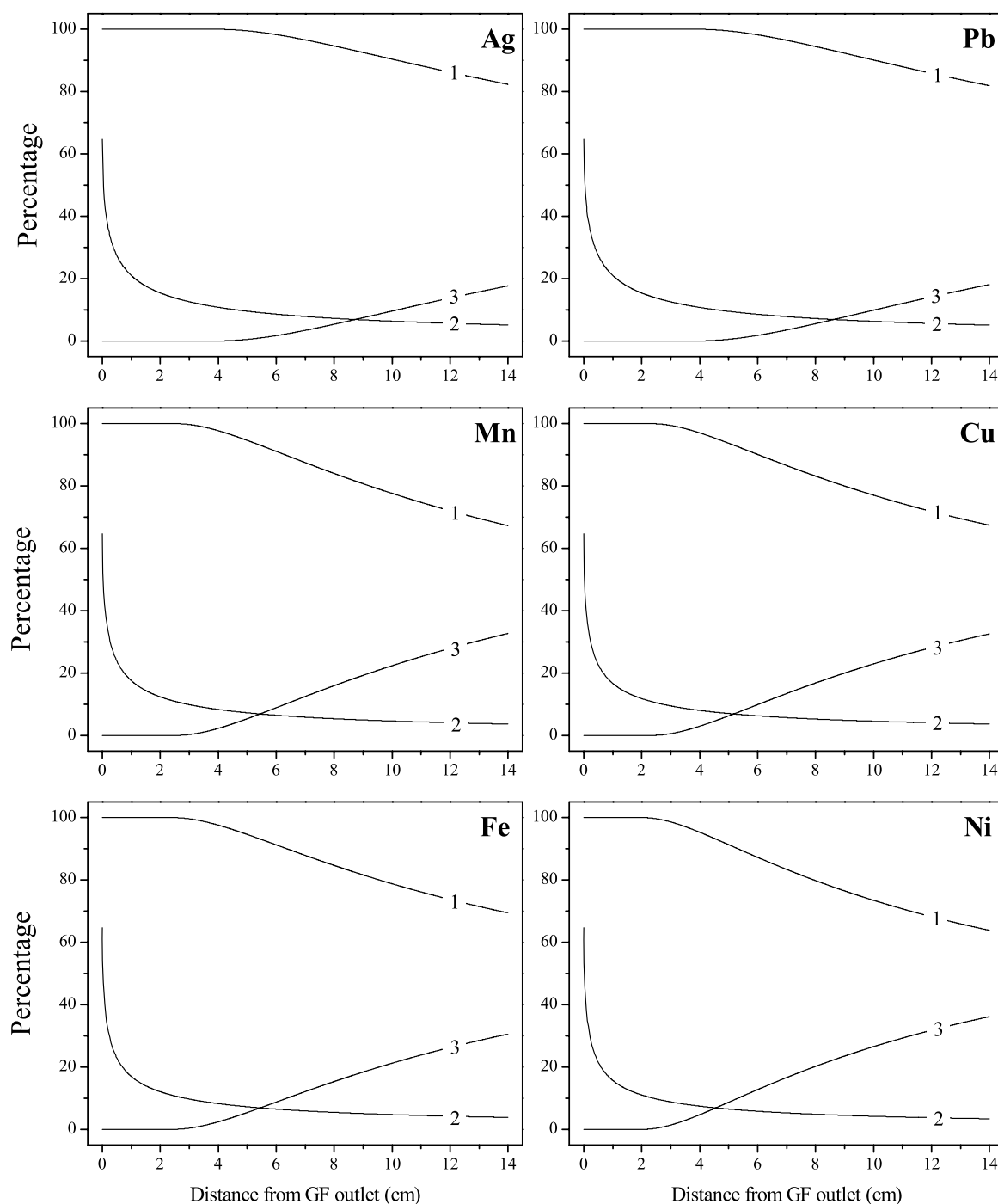


**Fig. 5.7:** Simulation results for Ag, Cu, Fe, Ni, Mn, and Pb without taking into account the attachment at carbon particles. Shown as the percentage dependences to the total number of the analyte atoms for: (1) the number of free atoms, (2) the number of free atoms in the central condensation area of present C-particles, and (3) the number of lost atoms, as functions of the pathway from the GF outlet hole. Obtained for simulation conditions according to Tables 5.1 and 5.2.

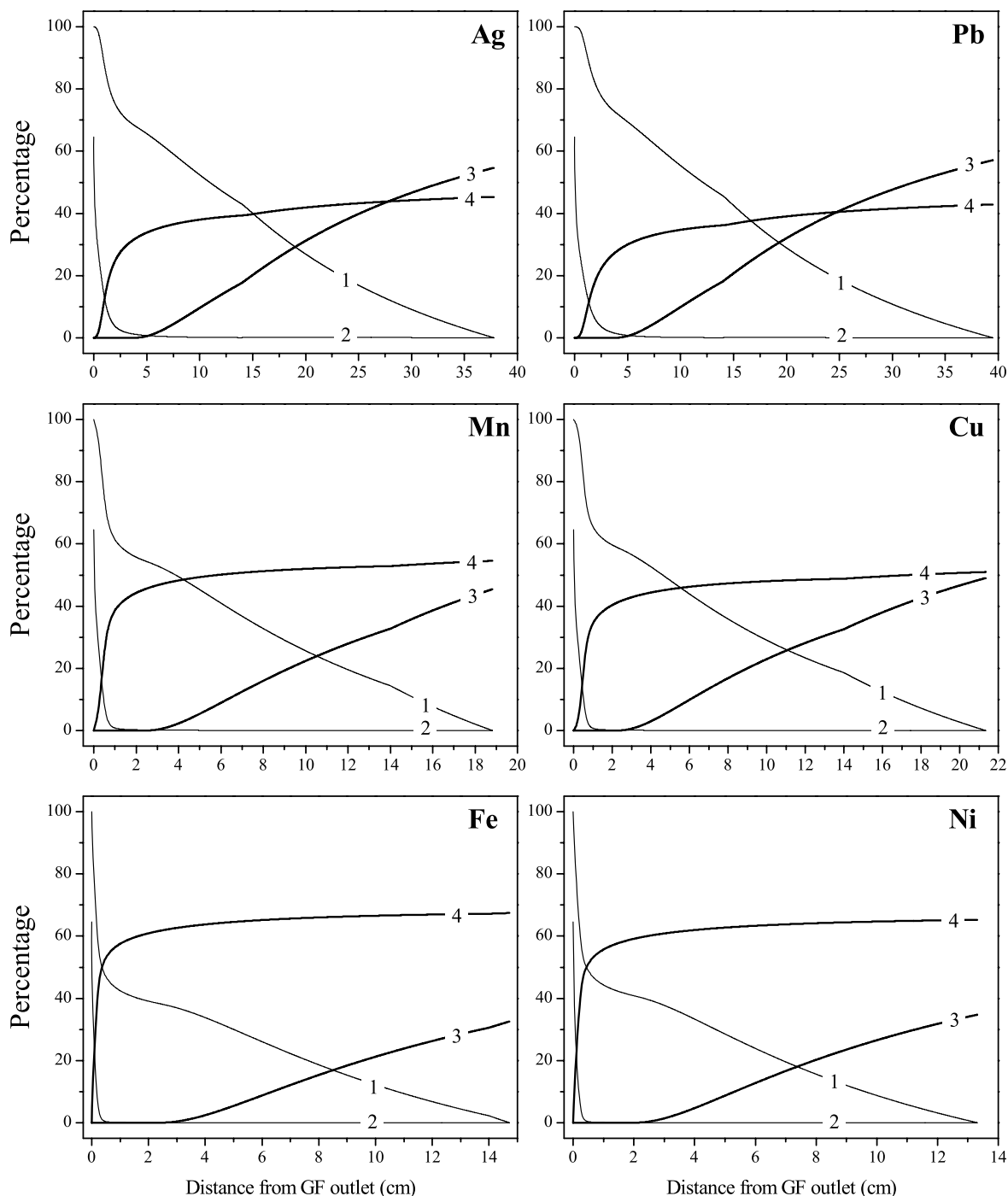


**Fig. 5.8:** Simulation results for Ag, Cu, Fe, Ni, Mn, and Pb with taking into account the attachment at carbon particles. Shown as the percentage dependences to the total number of the analyte atoms for: (1) the number of free atoms, (2) the number of free atoms in the central condensation area of present C-particles, (3) the number of lost atoms, and (4) the number of attached atoms, as functions of the pathway from the GF outlet hole. Obtained for simulation conditions according to Tables 5.1 and 5.2, parameters of the attachment function:  $\alpha = 1$  and  $\gamma = 0.15$ .



The attachment process of analyte atoms can be described with three stages of the attachment function. During the first one, the attachment rate is negligible because the re-vaporization of metal atoms prevails over their adsorption. It is well seen with the example of volatile analytes such as Ag and Pb.

During the second stage, the increase of the attachment function results in the decrease of the number of analyte atoms in the central condensation area. This decay is sharper for medium and low volatile analytes. The dip in the analyte distribution function (see Fig. 5.2) grows rapidly. Then, the analyte condensation rate decreases with the decreasing number of free metal atoms in the central condensation area. Curve 2 rapidly falls within a short distance from the GF outlet. On the other hand, the decrease of the analyte atom density leads to increasing density gradient and, thereby, to growth of the rate of the diffusion transport into the central condensation area. Finally, these rates will come to an equilibrium.

The third stage begins with the very low equilibrium when the bottom of the dip is almost reached. The further condensation is indirectly controlled by the diffusion from the outside. Owing to the decreasing number of free analyte atoms, the number of adsorbed atoms grows with a decreasing rate.

The laminar narrowing of the streaming lines at the outlet of the AFC tube results in a slight enhancement of the condensation rate due to the increased density gradient. A slight enhancement of the losses is also seen.

Compared with the data in Fig. 5.7, the density of free atoms (curves 1 and 2 in Fig. 5.8) shows a fast decrease within the first millimeters. The percentage of free atoms in the central condensation area where C-particles are presented (curve 2) approaches to 0% at ~5 cm from the GF outlet for Ag and Pb, at ~1 cm for Mn and Cu, and at ~0.5 cm for Fe and Ni. Thus, the main part of the condensation process occurs close to the GF outlet and for medium and low volatile analytes even within the radiation shielding plate.

Fig. 5.8 shows that only Ni is fully condensed within the AFC tube. Other analytes studied would need longer pathways to complete the condensation in an AFC tube of constant diameter (~20 cm for Cu and Mn and ~40 cm for Ag and Pb). They still have high amounts of free atoms at the AFC tube outlet, which are mainly lost by further transportation.

Thus, owing to this model, the following amounts of the initial analyte masses are carried by carbon aerosol to the analytical instrument: 45.3% for Ag, 42.9% for Pb, 54.6% for Mn, 50.9% for Cu, 67.4% for Fe, and 65.2% for Ni. These values can be considered as ana-

lyte TEs under the assumption that the losses of the carbon particulates along the transport path are negligible.

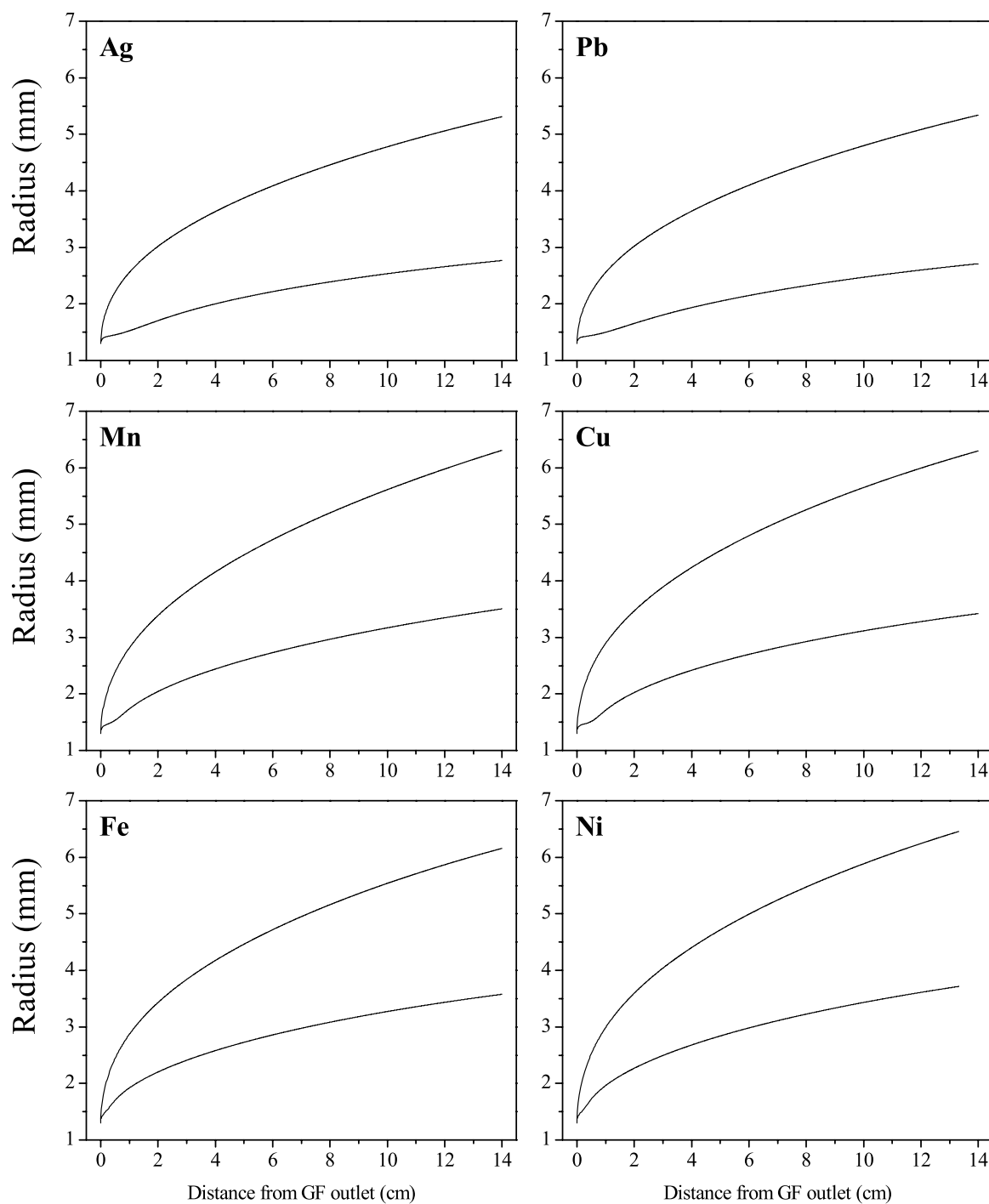
Fig. 5.9 illustrates the dependence for  $R_{out}$  and  $R_{in}$  (see Fig. 5.2) on the coordinate. Both curves ( $R_{out}$  during a whole interval and  $R_{in}$  at larger distances) show a root dependence on coordinate. At the end of the AFC tube, the radii have the following values:  $R_{out} = 5.31$  mm and  $R_{in} = 2.77$  mm for Ag, 5.34 mm and 2.71 mm for Pb, 6.31 mm and 3.51 mm for Mn, 6.3 mm and 3.42 mm for Cu, 6.15 mm and 3.58 mm for Fe, and 6.46 mm and 3.71 mm for Ni.

The results presented above were calculated for the following parameters:  $\alpha = 1$ ,  $\gamma = 0.15$  (Eq. 5.18), and carbon contents according to Eq. 5.25 and Table 5.3. Fig. 5.10 shows the results of the modifications of these parameters in order to investigate their influence on the analyte condensation. The empty (unfilled) columns in Fig. 5.10 correspond to the previously described case.

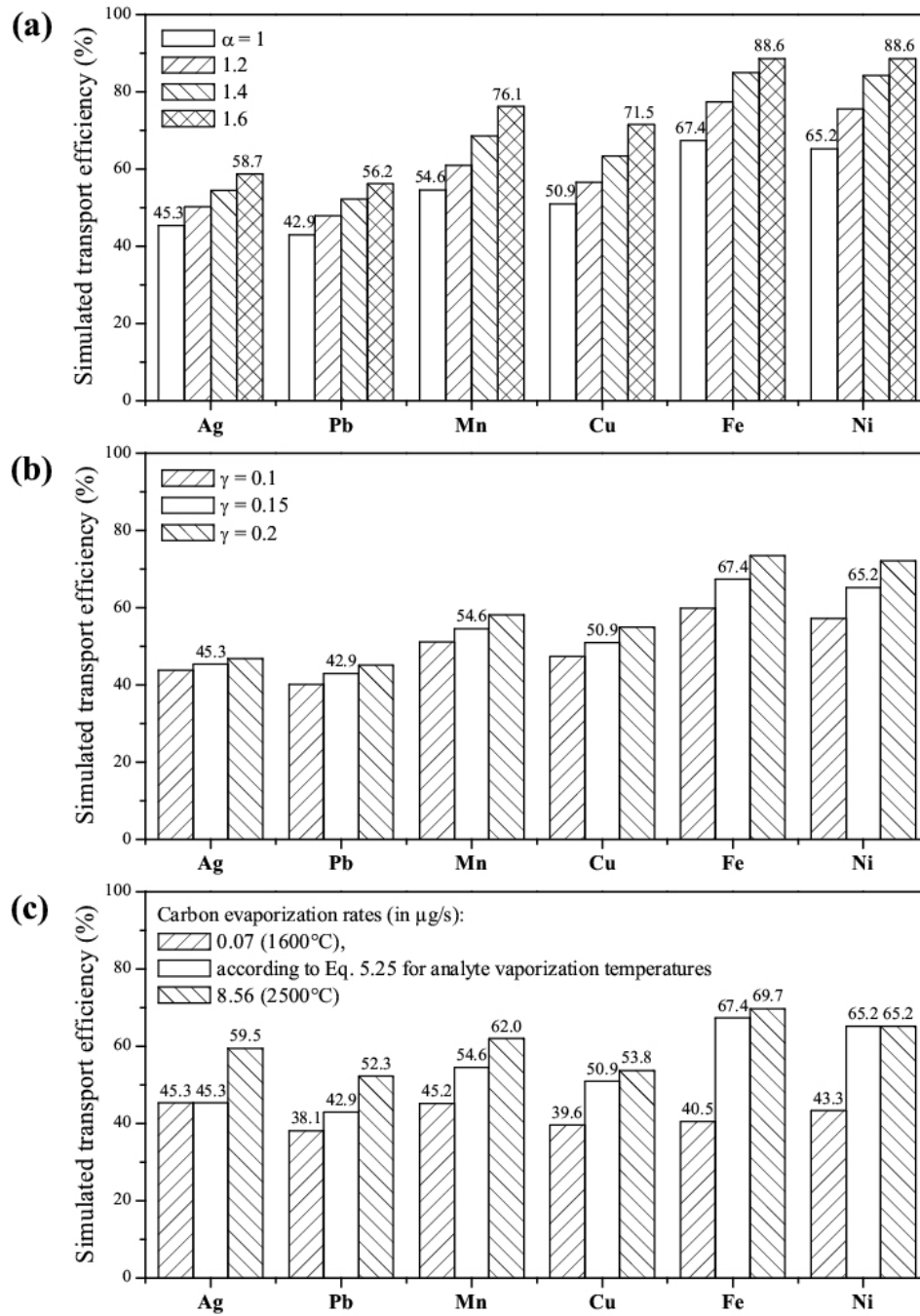
Fig. 5.10(a) shows the effect of the parameter  $\alpha$  of the attachment function on the simulated TEs. Simulations are performed for  $\alpha = 1, 1.2, 1.4$ , and  $1.6$ . The increase of  $\alpha$  results in the enhancement of the simulated TEs. For  $\alpha T_p$  close to  $T_{vap}$  as it is in the cases of Fe and Ni, the analyte TEs are approaching to maximum values. The simulations with  $\alpha = 1$  illustrate a lower estimation of the real condensation process.

Fig. 5.10(b) shows the effect of the parameter  $\gamma$ . By increasing the parameter, the attachment function becomes flatter and the analyte adsorption begins at higher temperatures. Analogously, by the decreasing, the adsorption begins at lower temperatures. The deviation of the obtained results for  $\gamma = 0.1, 0.15$ , and  $0.2$  is under 3% for Ag, Cu, Mn, and Pb and 8% for Fe and Ni.

The most interesting dependence is shown in Fig. 5.10(c) presenting the effect of the carbon evaporation rate on the TEs. Two situations when the analytes are condensed in the presence of carbon amounts released at  $1600^\circ\text{C}$  (vaporization temperature of Ag) and at  $2500^\circ\text{C}$  (vaporization temperature of Ni) are compared. The following analyte TEs are calculated for the lower carbon amounts ( $0.07 \mu\text{g s}^{-1}$ ): 45.3% for Ag, 38.1% for Pb, 45.2% for Mn,



**Fig. 5.9:** Dependences of  $R_{out}$  (upper curves) and  $R_{in}$  (bottom curves) on the distance from the GF outlet determined for Ag, Cu, Fe, Ni, Mn, and Pb. Obtained for simulation conditions according to Tables 5.1 and 5.2, parameters of the attachment function:  $\alpha = 1$  and  $\gamma = 0.15$ .



**Fig. 5.10:** Effect of the parameters of the attachment function and the carbon evaporation rates on the simulated analyte TEs.  
 (a)  $\alpha$  varied between 1 and 1.6 with  $\gamma = 0.15$  ;  
 (b)  $\gamma$  varied between 0.1 and 0.2 with  $\alpha = 1$ ; and  
 (c) the carbon evaporation rate is varied with  $\alpha = 1$  and  $\gamma = 0.15$  .  
 Obtained for simulation conditions according to Tables 5.1 and 5.2.

39.6% for Cu, 40.5% for Fe, and 43.3% for Ni. A significant decrease in the TE is observed for medium and low volatile analytes Fe and Ni (by ~25%). By Mn and Cu, the decrease is also essential (by ~10%). For the higher carbon amounts ( $8.56 \mu\text{g s}^{-1}$ ), the following TEs are obtained: 59.5% for Ag, 52.3% for Pb, 62% for Mn, 53.8% for Cu, 69.7% for Fe, and 65.2% for Ni. This time, a significant enhancement is observed for volatile analytes. The TEs of Ag, Pb, and Mn are increased by around 15%, 10%, and 8%.

#### 5.3.4 Influence of modifiers on analyte condensation

The results of the simulation of the modifier effect on the transport of more volatile analytes Ag, Cu, and Mn are presented in Fig. 5.11. The action of the Pd-Mg modifier in this simulation is considered via the attachment function given by Eq. 5.18 that denotes the temperature dependence by means of AAS pretreatment temperature. Furthermore, and more important, the volatile analytes are vaporized at higher temperatures when higher carbon density is co-evaporated.

With decreasing the volatility, the attachment of the metal atoms begins at higher temperatures than without modifier (see Fig. 5.8). This results in more rapid decrease of the density of free atoms. In the central condensation area where C-particles are presented, its relative value approaches to 0% at ~2 cm from the GF outlet for Ag and Pb and at ~0.7 cm for Mn. Thus, the main part of the condensation process occurs faster and closer to the GF outlet.

Thus, the following TEs are obtained according to this simulation: 56% for Ag, 60.9% for Pb, and 66.5% for Mn and the resulting enhancement of the simulated TEs due to the modifier effect is around 10% for Ag, 18% for Pb, and 12% for Mn.

#### 5.3.5 Comparison with experimental data

The comparison of the simulated TEs for Ag, Cu, Fe, Ni, Mn, and Pb with the experimental results is shown in Fig. 5.12(a) for the case without modifiers. The modeling shows a good agreement with the experimental data and reflects the dependence of the TEs on the analyte volatility as well.

The effect of modifiers is shown in Fig. 5.12(b) for volatile analytes Ag, Mn, and Pb. An agreement is also seen. In both cases, the discrepancies between the simulation and experiment are under 10%.

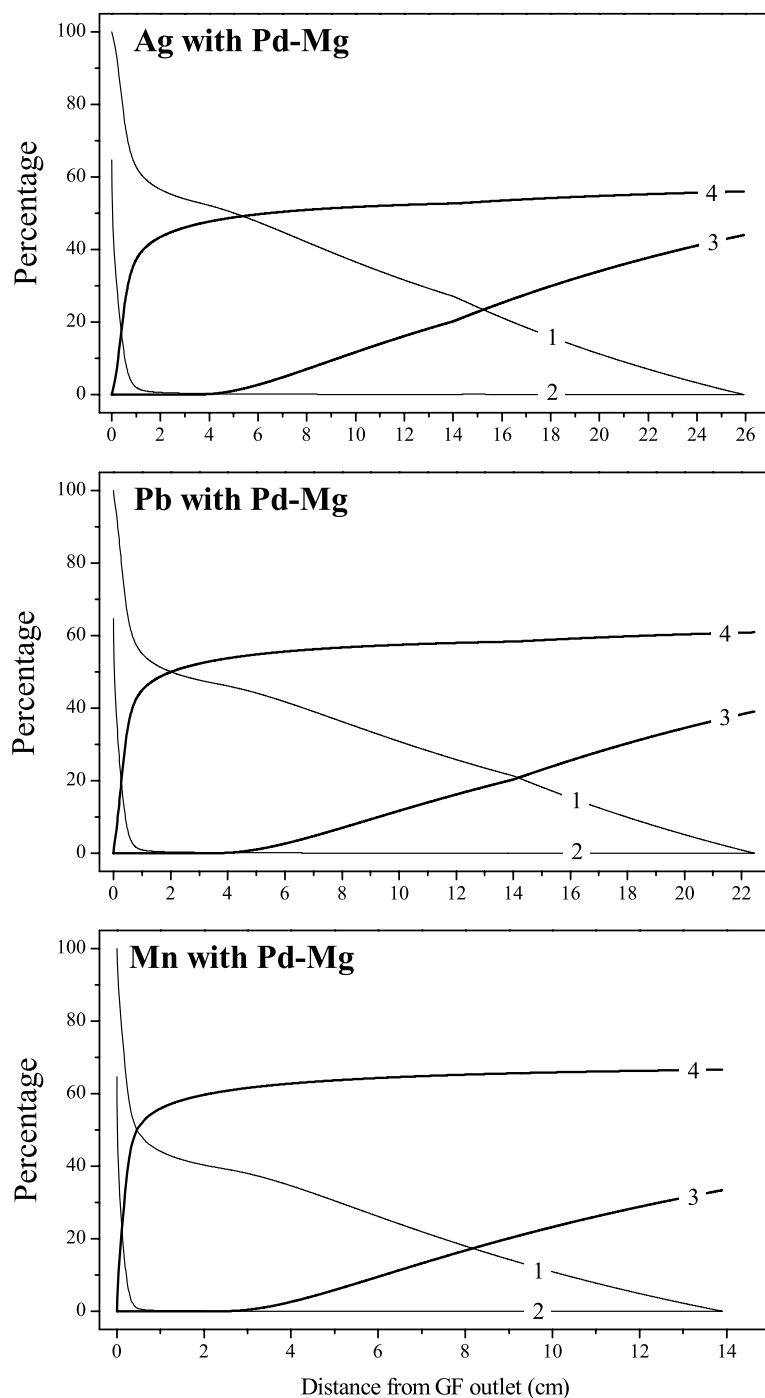


**Fig. 5.11:** Simulation results of the modifier effect for Ag, Mn, and Pb. Shown as the percentage dependences to the total number of the analyte atoms for: (1) the number of free atoms, (2) the number of free atoms in the central condensation area of present C-particles, (3) the number of lost atoms, and (4) the number of attached atoms, as functions of the pathway from the GF outlet hole. Obtained for simulation conditions according to Tables 5.1 and 5.2, parameters of the attachment function:  $\alpha = 1$  and  $\gamma = 0.15$ .

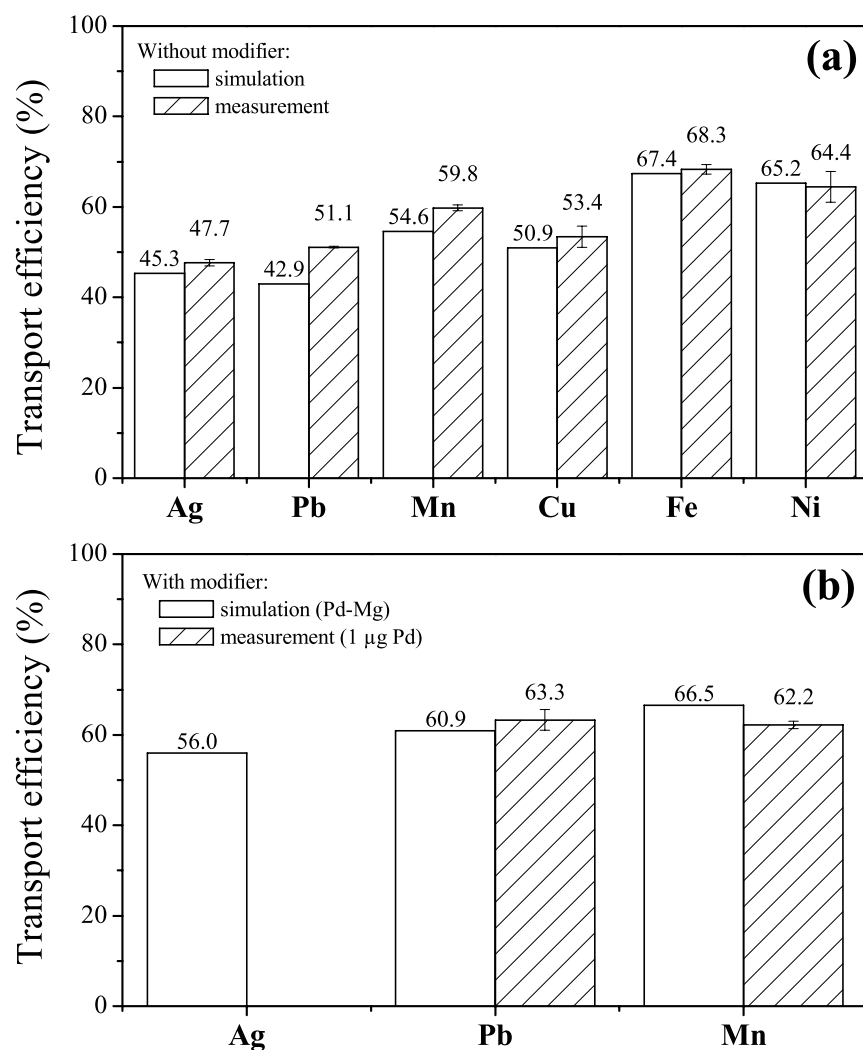


**Fig. 5.12:** Comparison of the simulated and experimentally measured TEs.

(a) Without modifier, for Ag, Cu, Fe, Ni, Mn, and Pb and

(b) with modifier, for Ag, Mn, and Pb.

The data taken from Figs. 3.14(b), 5.8, and 5.11.

---

## 6. Conclusions

---

The new ETV unit allows sampling of solid and liquid samples into analytical instruments for subsequent analysis and transporting high, medium, and low volatile analytes with higher and more homogeneous TEs to the analytical instrument. This is achieved with the formation of the axially focussing convection (AFC) zone within the vertical tube, where the condensation of sample analytes occurs in a laminar flow predominantly apart from the colder walls. Furthermore, shielding of the upstream against incandescent emission of the GF tube and surrounding with several bypass flows results in better conditions for rapid analyte condensation.

The constructed ETV-AFC system showed higher analyte TEs with more equal figures for analytes of widely differing volatilities in comparison with the previously used ETV instruments. With the copper radiation shielding plate mounted 2.5 mm above the GF tube to one of the water-cooled copper flanges, TEs up to 44% for Pb, 54% for Mn, 45% for Cu, 55% for Fe, and 59% for Ni were determined for multielement standard solutions dosed in the ETV boat. With the later constructed shielding plate with a ring slit for the admixture of the additional cold sluice gas to the upstream, more effective cooling of the upstream directly above the GF outlet was achieved. With this more sophisticated upstream surrounding below, within, and above the shielding plate, TEs up to 48% for Ag, 51% for Pb, 60% for Mn, 53% for Cu, 68% for Fe, and 64% for Ni were determined. Moreover, the sluice gas introduction reduces possible contaminations originating from the outer surface of the GF tube.

Increasing TEs with the ageing of the pyrolytically coated GF tube were observed. The effect was associated with the growing content of carbon particulates released from older tubes during analyte vaporization. The gravimetrically measured tube losses during a single heating cycle (8 s, 2600°C) were in the range of 70-120 µg and had an increase up to 250 µg by approaching to the tube lifetime. This indicated very high C-vapor supersaturation inside the GF tube at vaporization temperatures. According to SEM micrographs, the carbon is found in the form of relatively large particles already within the GF tube. At 0.25 cm above the GF outlet, SEM micrographs showed higher densities of larger C-particles. At 2.25 cm, SEM and TEM micrographs showed large amounts of fine dispersed carbon particles with diameters around 10 nm, which begin to form chains and web-like structures. The density and diameters of carbon particles decreased with decreasing vaporization temperature and,



thereby, decreasing evaporated C-masses. Thus, the analyte atoms are found in the environment of significantly larger carbon particles with higher particle densities.

Based on the estimation of analyte vapor saturations performed for typically used analyte contents (pico- and nanogram amounts), it follows that the generated analyte vapor is unsaturated under ETV-AFC operating conditions. Thus, the work concluded that the homogeneous particle formation concept often used for larger analyte contents and higher amounts of analyte vapor supersaturation [Kan1] is not applicable for this condensation problem. The condensation of the analyte atoms occurs mainly heterogeneously, i.e. by attachment of the atoms at carbon aerosol particles. The carbon particles act as adsorbents for the analytes and support their transport. Thus, due to different mechanisms, the analyte TEs depend not only on analyte element, sample composition, matrix, pretreatment and vaporization conditions etc. but also on carbon amounts evaporated at the analyte vaporization temperature and on the GF tube age.

Using the heterogeneous particle formation concept, the modeling of the influence of physico-chemical element properties, vaporization conditions, and ETV-AFC unit geometry on condensation and transport of analyte atoms was carried out for six analytes of different volatilities Ag, Cu, Fe, Ni, Mn, and Pb. The model took into account the condensation of the carbon released from the GF tube at analyte vaporization temperatures as well as the attachment of analyte atoms at carbon particulates during sticking collisions. The attachment function describing the probability that a colliding analyte atom sticks to the carbon particle has been formulated as a function of the pretreatment temperature used in GFAAS (e.g. tabulated in Ref. [Wel2]) with a statistical broadening of 15%.

The modeling of the carbon condensation showed an agreement with SEM and TEM investigations. Owing to the simulation, a rapid growth of carbon particles (with only a very slight dependence on the initial particle diameter) can be seen within first millimeters above the GF outlet. At 2.25 cm above the outlet, approximately the same particle sizes in the range of 10-15 nm can be found from both the results of our modeling and the micrographs. On the further pathway, the particle diameter increases significantly slower that is also in agreement with the micrographs showing very similar structures of the particles collected thermophoretically in the AFC upstream at 2.25 cm above the GF and electrostatically precipitated after one meter of transport path through the subsequent tubing. The obtained results were considered as a lower estimate of the carbon condensation process because of the mechanisms, which can

speed up the condensation such as a presumed presence of impurities and charged particles in the upstream as well as more rapid increase of the C-C interaction cross-sections due to the fractal structure of the particles (carbon flakes), were not involved in the calculations.

The calculated analyte TEs were: 45% for Ag, 43% for Pb, 54.6% for Mn, 50.9% for Cu, 67.4% for Fe, and 65.2% for Ni. The model shows good agreement with the experimental data and reflects the dependence on the analyte volatility. With taking into account the modifier effect, an enhancement of the calculated TEs for the analytes of higher volatility was observed: 56% for Ag, 61% for Pb, and 67% for Mn. In both cases, the discrepancies between the simulation and experiment were less than 10%.

The simulated TEs showed a strong dependence on the reference temperature in the analyte attachment function (with  $\alpha = 1$ , the analyte pretreatment temperature in GFAAS). The increase of the parameter  $\alpha$  led to analyte condensation at higher temperatures and, thereby, to higher TEs. For  $\alpha = 1.6$ , the TEs up to 59% for Ag, 56% for Pb, 76% for Mn, 72% for Cu, 89% for Fe and Ni were calculated.

Moreover, the modeling showed a high content of free analyte atoms of more volatile species at the AFC tube outlet. Thus, the AFC tube in the experiments should be longer to provide full condensation under AFC conditions.

Sample/carrier modifier effects on analyte TEs were investigated employing the ETV-AFC instrumentation. The use of K and Pd modifiers in microgram amounts in nitric acid solutions had a positive influence mainly on the TEs of volatile species.  $K^+$  ions and compounds may speed up the nucleated condensation of carbon that leads to earlier formation of particulates. The influence of K as an analyte carrier by itself is less probable because the K-vapor achieves supersaturation and begins to form condensation nuclei under ETV-AFC conditions at temperatures below 300°C when most analytes studied are attached at carbon aerosol particulates. With addition of  $Pd(NO_3)_2$  modifier, the analytes are vaporized at higher temperatures when higher carbon density is co-evaporated. Better co-vaporization and faster formation of particulates resulted in more uniform TEs for analytes with different volatilities: 63% for Pb, 62% for Mn, 70% for Fe, and 64% for Ni. The combined use of  $KNO_3$  and  $Pd(NO_3)_2$  modifiers with  $C_6H_{12}$  (cyclohexane) added to the internal flow of the ETV unit resulted in significant enhancement of the TEs: 91% for Ag, 86% for Pb, 81% for Cu, 94% for Fe, and 90% for Ni.

The PLASATRADIS system that was developed in the context of an international research cooperation combined the potential of the ETV-AFC as a sample pretreatment and introduction tool with possibilities of diluting, distributing, and dosing of the generated aerosols like gas carried slurries, and quantitative re-collection of aerosols on one or a set of secondary graphite platforms. The system provides a better way of coping with the problems associated with solid sampling and has the following advantages. Primary solid samples can be weighed into the ETV boat in higher amounts to reduce dosing errors and effects caused by non-homogeneities of the sample, and thereby, to obtain higher precision of the measurements. Due to the controlled dividing of the aerosol, the analyzed amount can be adapted to the dynamic range of the spectrometer. Using the highly symmetric aerosol flow splitter, a set of platforms with equal analyte compositions from the same individual primary sample can be produced. RSD of the measurements with aerosol dividing into two sub-flows in 1:9 ratio was less than 5% (for  $n=4-5$  repetitions). Using the 10-fold precipitation unit with the 10-fold aerosol splitter, the overall RSD for the TEs measurements was less than 12% ( $n=10$  platforms). Analyte compositions on secondary platforms are measured with a second ETV-EP process with intra-furnace EP. Therefore, all sample analytes have passed the ETV-EP process twice that results in the higher RSD given above.

---

## Appendix

---

### A.1 List of figures

<b>Fig. 2.1:</b>	Principle of the axially focusing of the upstream flow used in the development of the new ETV-AFC setup [Her8].	24
<b>Fig. 2.2:</b>	A novel laboratory constructed electrothermal vaporization unit with an axially focusing convection tube (ETV-AFC): (a) schematic representation and (b) photograph.	25
<b>Fig. 2.3:</b>	Principle of the upstream shielding against incandescent radiation of the GF during ETV firing; the arrows show directions of internal, external, and sluice gas flows.	26
<b>Fig. 2.4:</b>	Diagram of the external generator of gaseous additives to the internal flow of the GF.	28
<b>Fig. 2.5:</b>	Experimental arrangement for sample introduction into continuum source coherent forward scattering spectrometer (CS-CFS) using electrothermal vaporization with internal electrostatic precipitation (ETV-EP). Based on the idea of T. Buchkamp [Buc2].	29
<b>Fig. 2.6:</b>	Principle of CFS with a Voigt configuration and a continuum source [Her2].	30
<b>Fig. 2.7:</b>	Principle of aerosol transport, dividing, and dosing: (a) transport with internal/external EP dosing; (b) transport and dividing with internal/external EP; and (c) transport and dividing with external EP onto a set of sample collectors.	34
<b>Fig. 2.8:</b>	Technical realization of internal EP directly onto the L'vov platform of the ETA furnace (HGA-600) with the AS-60 autosampler. The autosampler cap can be easily rotated by 180° between two pre-adjusted positions for sampling of aqueous solutions and ETV aerosols.	35
<b>Fig. 2.9:</b>	Technical realization of external EP onto GF boats [Her1]: (a) laboratory constructed external electrostatic precipitator; (b) electrostatic precipitator in open state; and (c) EP onto different platform types.	36
<b>Fig. 2.10:</b>	Technical realization of (a) an external 10-fold precipitator and (b) a highly-symmetric 10-fold aerosol splitter [Her1].	37
<b>Fig. 2.11:</b>	Principle and capabilities of electrostatic sampling.	38
<b>Fig. 2.12:</b>	Schematic presentation of the measuring cycle for the cases of (a) ETV-EP solid sample introduction and (b) aqueous sample introduction.	41
<b>Fig. 2.13:</b>	Calibration curve for PtRh-PtRh thermocouple used for temperature measurements on the upstream axis.	43

- Fig. 3.1:** Effect of upstream shielding against incandescent GF tube radiation on TEs for Cu, Fe, Mn, Ni, and Pb dosed as liquid solutions into the ETV boat. Analyte masses: 64 ng Cu, Fe, Pb, and 640 ng Ni (ETV without radiation shielding) and 4 ng Mn, 20 ng Cu, Fe, Pb, and 100 ng Ni (ETV with radiation shielding); flow conditions 200/1300 mL min<sup>-1</sup> (internal/external flow) with 1:9 splitting; standard deviations for n=5. \_\_\_\_\_ 46
- Fig. 3.2:** ETV-EP analyte TEs for high, medium, and low volatile elements with end-on flow-through ETV and ETV-AFC, determined simultaneously, calibrated against aqueous standard solutions dosed into ETA-CFS furnace. Sample for end-on flow-through ETV measurements: 2 ng Ag, 6.4 ng Al, Cu, Fe, Pb, and 64 ng Cd, Ni; total flow: 150 mL min<sup>-1</sup> [Ber2]; sample for ETV-AFC measurements: 0.4 ng Mn, 2 ng Al, Cu, Fe, Pb, and 10 ng Ni; total flow 220 mL min<sup>-1</sup>. \_\_\_\_\_ 48
- Fig. 3.3:** Optimization and controlling of the ETV vaporization conditions: (a) pyrometrically (longitudinal observation through the housing side window) and (b) by means of a photodiode (transversal observation) for applied GFs of larger size; 2600°C vaporization temperature, 8 s hold time. Influence of the maximal power step on the ramp time, presentation of the “platform effect”. \_\_\_\_\_ 50
- Fig. 3.4:** Influence of the ETV flow conditions on analyte transport: (a) normalized CS-CFS temporal peak areas as a function of ETV flow conditions; (b) TEs with and without additional sluice gas. Analyte masses dosed into ETV boat: 4 ng Mg, 20 ng Pb, Cu, Fe, and 100 ng Ni. \_\_\_\_\_ 52
- Fig. 3.5:** Temperature dependences on the axis of the AFC tube during the ETV firing and subsequent cool-down steps: (a-c) temporal and (d) spatial. The plots (a) and (d) corresponds to the optimal flow conditions and the plot (b) for turbulent behavior in the upstream (noise on the curves). Obtained for the same vaporization temperature (2600°C) and flow distributions 200/1300 mL min<sup>-1</sup> (internal/external), for different distances between the radiation shield and the AFC tube (*h*) and for different vertical coordinates (*z*) with the beginning at the GF outlet (at *z*=0). \_\_\_\_\_ 53
- Fig. 3.6:** Temporal temperature dependences on the axis of the AFC tube for the ETV mode with direct platform-to-platform sampling without splitting: (a) for different distances from the GF outlet hole with optimized on the maximum of the TE flow distributions 80/140 mL min<sup>-1</sup> (internal/external) and (b) for different ETV flow distributions; both obtained for the same vaporization temperature 2600°C. \_\_\_\_\_ 55
- Fig. 3.7:** Comparison of (a) spatial and (b) temporal temperature distributions on the axis of the AFC tube obtained by different ETV flow distributions: 80/140 mL min<sup>-1</sup> and 200/1300 mL min<sup>-1</sup> (internal/external). All the curves correspond to the 7<sup>th</sup> s of the vaporization

step. The flight times obtained for the GF outlet diameter 3 mm; vaporization temperature 2600°C. \_\_\_\_\_ 56

**Fig. 3.8:** (a) Differential and accumulative mass losses of the GF with incomplete protection against ambient air and (b-f) respective TEs for 4 ng Mn, 20 ng Pb, Cu, Fe, and 100 ng Ni, both as functions of the GF tube age. Flow conditions: 200/200/1100 mL min<sup>-1</sup> (internal/sluidce/external). \_\_\_\_\_ 58

**Fig. 3.9:** TEs for two different tubes from the same series and in the same analytical age (15-35 furnace shots); analyte masses: 4 ng Ag, 20 ng Pb and Fe, 100 ng Ni; improved sluidce gas inlet. Flow conditions: 200/200/1100 mL/min (internal/sluidce/external), 1:9 splitting. \_ 60

**Fig. 3.10:** Monitoring of the GF tube characteristics during the tube ageing: (a) dissipation power and (b) differential mass loss of the GF (with sufficient inert gas protection) both as functions of the tube ageing and (c) tube mass increase during weighing in ambient air; obtained without sample introduction, vaporization temperature 2600°C. Additional information see in the Text. \_\_\_\_\_ 61

**Fig. 3.11:** SEM images of carbon particles released from the ETV furnace by different vaporization temperatures during 6 s vaporization time and thermophoretically collected on silicon wafers (a-c) inside the GF, flows 150/0/0 mL min<sup>-1</sup> (internal/sluidce/external) and (d) directly above the GF outlet hole, flows 150/150/1200 mL min<sup>-1</sup>. \_\_\_\_\_ 63

**Fig. 3.12:** TEM images of carbon particles released from the ETV furnace during vaporization and thermophoretically collected at 2.25 cm above the GF outlet hole on nickel nets (400 mesh, 3.05 mm diameter, with carbon coating), obtained by vaporization temperature 2400°C (6 s hold time) with flows 150/150/1200 mL min<sup>-1</sup> (internal/sluidce/external).\_\_ 64

**Fig. 3.13:** SEM images of carbon particulates released from the ETV furnace by vaporization at 2600°C during 6 s and collected on silicon wafers (a) thermophoretically 2.25 cm above the GF outlet hole and (b-d) electrostatically in different areas of the precipitation spot; flows 150/150/1200 mL min<sup>-1</sup> (internal/sluidce/external), 1:9 flow splitting prior to particle collection. \_\_\_\_\_ 65

**Fig. 3.14:** Effect of KNO<sub>3</sub>, Pd(NO<sub>3</sub>)<sub>2</sub>, and Mg(NO<sub>3</sub>)<sub>2</sub> modifiers on TEs of Pb, Mn, Cu, Fe, and Ni for different ETV-AFC operating conditions: (a) flow distribution 80/140/0 mL min<sup>-1</sup> (internal/sluidce/external) without dilution, sample: 0.4 ng Mn, 2 ng Cu, Fe, Pb, and 10 ng Ni; and (b) 200/200/1100 mL min<sup>-1</sup> with 1:9 flow splitting, sample: 4 ng Mn, 20 ng Cu, Fe, Pb, and 100 ng Ni. Obtained by GF tube ages 150–180 shots, carbon loss ~ 100 µg shot<sup>-1</sup>. \_\_\_\_\_ 67

**Fig. 3.15:** Effect of C<sub>6</sub>H<sub>12</sub> (cyclohexane) addition to the ETV internal flow on TEs of 4 ng Ag, 20 ng Cu, Fe, Pb, and 100 ng Ni, obtained by ETV flow conditions 150/150/1200 mL min<sup>-1</sup> (internal/sluidce/external) with 1:9 splitting. GF tube ages are 50–90 shots. \_\_\_\_\_ 69

- Fig. 3.16:** Effect of combined use of  $C_6H_{12}$  added to the ETV internal flow,  $KNO_3$  and  $Pd(NO_3)_2$  modifiers to the ETV boat on TEs of 4 ng Ag, 20 ng Cu, Fe, Pb, and 100 ng Ni, obtained by flow distribution 150/150/1200 mL min<sup>-1</sup> (internal/sluidce/external) with 1:9 splitting, GF tube ages 50–90 shots. \_\_\_\_\_ 71
- Fig. 3.17:** Effect of  $C_6H_{12}$  and K/ $Pd(NO_3)_2$  modifiers addition on CS-CFS intensity profiles after background cutting off for Ag, Cu, Fe, Ni, and Pb (see Fig. 3.16 for further details). \_\_\_\_ 73
- Fig. 3.18:** Summary showing (a) the effect of  $C_6H_{12}$  addition to the ETV internal flow and (b) combination of  $C_6H_{12}$ , K, and  $Pd(NO_3)_2$  modifiers both on TEs of 4 ng Ag, 20 ng Cu, Fe, Pb, and 100 ng Ni; obtained for carbon content in the internal flow ~5 µg s<sup>-1</sup> and 1 µg K/Pd masses; flow distribution 150/150/1200 mL min<sup>-1</sup> (internal/sluidce/external) with 1:9 splitting. \_\_\_\_\_ 74
- Fig. 3.19:** Dependence of the current of negative corona discharge on the content of the  $C_6H_{12}$  vapor in the internal flow (expressed as the flow rate through the flask with cyclohexane), obtained for “cold” ETV system (i.e. cyclohexane molecules are not decomposed), flow conditions 150/150/1200 mL min<sup>-1</sup> (internal/sluidce/external) with 1:9 flow splitting. The percentage ratios show the part of the internal flow that passes through the flask. \_\_\_\_\_ 75
- Fig. 3.20:** Behavior of the corona discharge current in the presence of  $C_6H_{12}$  and the influence of K and Pd modifiers: (a) behavior for steady and unsteady modes of the glowing; (b) steady glowing with different carbon contents; and (c) influence of the modifiers (see Fig. 3.16 for further details). \_\_\_\_\_ 77
- Fig. 4.1:** Transport efficiencies for 8 ng Mn, 40 ng Cu, Fe, Pb, and 200 ng Ni dosed as a multi-element solution into the ETV boat and obtained with the external 10-fold precipitator: (a) mean values (SDs for the tandem ETV-EP procedure) and (b)-(f) TEs over all EP stations. \_\_\_\_\_ 80
- Fig. 4.2:** Results of the adjustment of the 10-fold precipitation unit: (a) flow distribution through the precipitating stations before and after the measurement and (b) distribution of the corona discharge currents in the precipitators. \_\_\_\_\_ 81
- Fig. 4.3:** Results of the collection of atmospheric aerosols using the 10-fold precipitation unit (a) on the roof of the I. Physical Institute and (b) in the Workshop of the Institute; in both cases signals of Si (288.2) and Mg (285.2) are saturated. Precipitation conditions: (a) duration 6h (54 L), wind from the forestland to the city center 7-12 km/h, cloudy, relative humidity 40-55%, temperature 8-12°C and (b) duration 3 h 15 min (29 L). Content of the secondary platforms is measured with ETV-EP CS-CFS, results taken from Ref. [Mat1, Mat2]. Values in brackets are unreliable. \_\_\_\_\_ 82

- Fig. 5.1:** Axially focusing convection tube geometry in (a) longitudinal section and (b) cross-section. \_\_\_\_\_ 87
- Fig. 5.2:** Distribution function of the analyte particle number: (a) for  $t=0$ , (b) for the times  $t_1$  and  $t_2$  ( $t_1 < t_2$ ). \_\_\_\_\_ 92
- Fig. 5.3:** Approximation of the temperature dependence in the upstream (see Fig. 3.5(d)) for the case of Ni vaporization at 2500°C. \_\_\_\_\_ 95
- Fig. 5.4:** Modeling of carbon condensation in the AFC upstream at different platform temperatures during the ETV heating cycle. (a) The particle density, (b) mean number of C<sub>1</sub> atoms per a carbon particle, and (c) the mean diameter of carbon particles. Results obtained for initial carbon particle diameters 0.5 nm, released carbon masses according to Table 5.3. \_\_\_\_\_ 98
- Fig. 5.5:** Dependence of the volume element position in the AFC upstream as a function of the flight time at different platform temperatures during the ETV heating cycle, obtained for 150 mL min<sup>-1</sup> internal gas flow, 0.5 nm initial carbon particle diameters; released carbon masses according to Table 5.3. \_\_\_\_\_ 100
- Fig. 5.6:** Effect of physical, geometrical, and experimental parameters on the condensation process of carbon particulates. (a) Effect of the initial diameter of carbon particles at the GF outlet on their density and mean diameters on the subsequent pathway; (b) effect of the size of the GF outlet hole (left) and the internal gas flow rate (right). Results obtained for 2500°C vaporization temperature, 8.56 µg s<sup>-1</sup> carbon evaporation rate and for 150 mL min<sup>-1</sup> internal gas flow rate (if not otherwise denoted). \_\_\_\_\_ 101
- Fig. 5.7:** Simulation results for Ag, Cu, Fe, Ni, Mn, and Pb without taking into account the attachment at carbon particles. Shown as the percentage dependences to the total number of the analyte atoms for: (1) the number of free atoms, (2) the number of free atoms in the central condensation area of present C-particles, and (3) the number of lost atoms, as functions of the pathway from the GF outlet hole. Obtained for simulation conditions according to Tables 5.1 and 5.2. \_\_\_\_\_ 103
- Fig. 5.8:** Simulation results for Ag, Cu, Fe, Ni, Mn, and Pb with taking into account the attachment at carbon particles. Shown as the percentage dependences to the total number of the analyte atoms for: (1) the number of free atoms, (2) the number of free atoms in the central condensation area of present C-particles, (3) the number of lost atoms, and (4) the number of attached atoms, as functions of the pathway from the GF outlet hole. Obtained for simulation conditions according to Tables 5.1 and 5.2, parameters of the attachment function:  $\alpha = 1$  and  $\gamma = 0.15$ . \_\_\_\_\_ 104
- Fig. 5.9:** Dependences of  $R_{out}$  (upper curves) and  $R_{in}$  (bottom curves) on the distance from the GF outlet determined for Ag, Cu, Fe, Ni, Mn, and Pb. Obtained for simulation conditions



according to Tables 5.1 and 5.2, parameters of the attachment function:  $\alpha = 1$  and  $\gamma = 0.15$ . \_\_\_\_\_ 107

**Fig. 5.10:** Effect of the parameters of the attachment function and the carbon evaporation rates on the simulated analyte TEs. (a)  $\alpha$  varied between 1 and 1.6 with  $\gamma = 0.15$ ; (b)  $\gamma$  varied between 0.1 and 0.2 with  $\alpha = 1$ ; and (c) the carbon evaporation rate is varied with  $\alpha = 1$  and  $\gamma = 0.15$ . Obtained for simulation conditions according to Tables 5.1 and 5.2. \_\_\_\_ 108

**Fig. 5.11:** Simulation results of the modifier effect for Ag, Mn, and Pb. Shown as the percentage dependences to the total number of the analyte atoms for: (1) the number of free atoms, (2) the number of free atoms in the central condensation area of present C-particles, (3) the number of lost atoms, and (4) the number of attached atoms, as functions of the pathway from the GF outlet hole. Obtained for simulation conditions according to Tables 5.1 and 5.2, parameters of the attachment function:  $\alpha = 1$  and  $\gamma = 0.15$ . \_\_\_\_\_ 110

**Fig. 5.12:** Comparison of the simulated and experimentally measured TEs. (a) Without modifier, for Ag, Cu, Fe, Ni, Mn, and Pb and (b) with modifier, for Ag, Mn, and Pb. The data taken from Figs. 3.14(b), 5.8, and 5.11. \_\_\_\_\_ 111

**Fig. A.3.1:** Multi-element spectrum measured simultaneously with ETA-CS-CFS spectrometer. Analyte contents in the dosed solution: 0.4 ng Ag and Mn, 2 ng Al, Cu, Fe and Pb, and 10 ng Ni. \_\_\_\_\_ 122

**Fig. A.3.2:** Approximation of the spectrum near a resonance line with determination of the line position and subtraction of the background on the examples of (a) Pb single line, (b) non-resolved Mn doublet, (c) partially resolved Cu and Ag lines, and (d) partially resolved Al doublet and Ni lines. \_\_\_\_\_ 124

**Fig. A.3.3:** Approximation of the growth and the decay of the line profile after the subtraction of the background on the example of the resonance line of Fe 302.1 nm. \_\_\_\_\_ 124

## A.2 List of tables

**Table 2.1:** Temperature programs for (a) ETV and (b) HGA-600. \_\_\_\_\_ 39

**Table 5.1:** Simulation conditions for the condensation of carbon in the ETV-AFC unit. \_\_\_\_\_ 89

**Table 5.2:** Simulation conditions for the condensation of Ag, Cu, Fe, Mn, Ni, and Pb in the ETV-AFC unit. \_\_\_\_\_ 96

**Table 5.3:** Estimated carbon evaporation rates obtained with Eq 5.25 at different times from the beginning of the ETV heating cycle and, thereby, at different temperatures in the GF tube center with corresponding them platform temperatures (data from Fig. 3.3). \_\_\_\_\_ 96

**Table A.4.1:** Saturation ratios obtained from Eq. A.4.1 for analytes, modifiers, and carbon densities under analytical conditions at different cool-down temperatures. \_\_\_\_\_ 125

### A.3 CS-CFS spectra evaluation software

Fig. A.3.1 shows a typical raw spectrum of resonance lines corresponding to a multi-element solution measured with the CS-CFS spectrometer at two different positions of the 50 nm spectral window (50 nm wavelength interval corresponds to 728 channels of the detector).

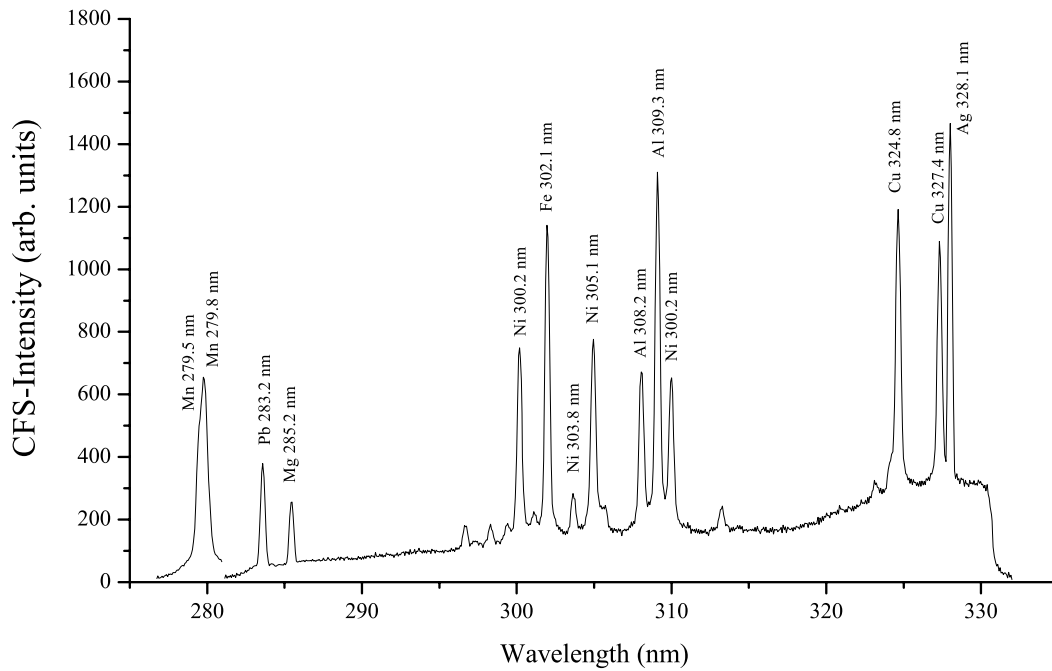


**Fig. A.3.1:** Multi-element spectrum measured simultaneously with ETA-CS-CFS spectrometer. Analyte contents in the dosed solution: 0.4 ng Ag and Mn, 2 ng Al, Cu, Fe and Pb, and 10 ng Ni.

First, the positions ( $\lambda_0$ ) and the half-widths ( $\Delta\omega$ ) of the resonance lines are determined by approximation of the raw spectrum at the temporal cutoffs corresponding to the maximal line intensity with the following function:

$$F(\lambda) = B(\lambda) + \sum_{i=1}^3 L_i(I_0, \lambda_0, \Delta\omega), \quad (\text{A.3.1})$$

where  $B(\lambda)$  is the fitting function for the background:

$$B(\lambda) = a\lambda + b, \quad (\text{A.3.2})$$

and  $L(I_0, \lambda_0, \Delta\omega)$  is the Lorentz function:

$$L(I_0, \lambda_0, \Delta\omega) = \frac{I_0 \Delta\omega^2}{4(\lambda - \lambda_0)^2 + \Delta\omega^2}, \quad (\text{A.3.3})$$

where  $I_0$  is the maximum line intensity at the temporal cutoff. The resonance line of an analyte element is approximated together with one line from the left and one from the right if they exist within the range of 30 channels. The raw spectrum is fitted within the range beginning from 20 channels before the left line and ending at 20 channels after the right one (i.e. for a single line, the interval is 40 channels and for several lines is 40 plus the distances between the neighboring lines). Fig. A.3.2 shows some examples of the resonance line fitting for the cases of a single line, a non-resolved doublet as well as two and three partially resolved lines. The fitting allows to obtain the positions and the half-widths of the lines. A mean value of the line half-widths is then used. Based on these data, temporal profiles  $I_0(t)$  of the resonance lines are determined. During this procedure, the line background is cut off.

Fig. A.3.3 shows the temporal profile for the Fe line (302.1 nm). The growth and the decay of the line profile are approximated with the exponential functions. The CFS intensity is determined as the sum of the areas under the exponential functions and the rest of the profile with taking into account a factor of linearization  $\alpha$ . The linearized form of the CFS signals ( $S$ ) is formed as follows:

$$S = \frac{A_1^\alpha}{\alpha\beta_1} \exp(\alpha\beta_1(t - t_{01})) + \sum_{t=t_1}^{t_2} I(t)^\alpha + \frac{A_2^\alpha}{\alpha\beta_2} \exp(-\alpha\beta_2(t - t_{02})), \quad (\text{A.3.3})$$

where  $A_1$ ,  $A_2$ ,  $\beta_1$ ,  $\beta_2$ ,  $t_{01}$ , and  $t_{02}$  are the parameters of the exponential fits shown in Fig. A.3.3. The factor  $\alpha$  is determined based on the linearity of analytical calibration curves. Typical value of  $\alpha$  are between 0.6 and 0.8. The linearization of the CFS signals arises due to the quadratic dependence of the transmitted CFS intensity on the atomic density [Her2, Her4].

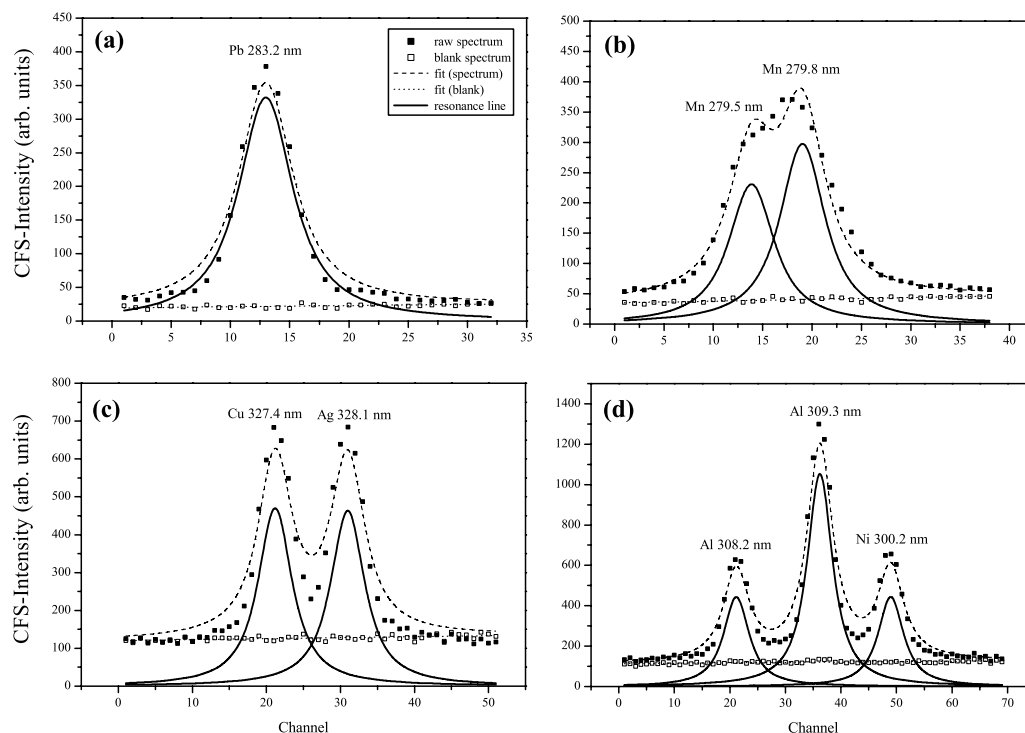


**Fig. A.3.2:** Approximation of the spectrum near a resonance line with determination of the line position and subtraction of the background on the examples of (a) Pb single line, (b) non-resolved Mn doublet, (c) partially resolved Cu and Ag lines, and (d) partially resolved Al doublet and Ni lines.

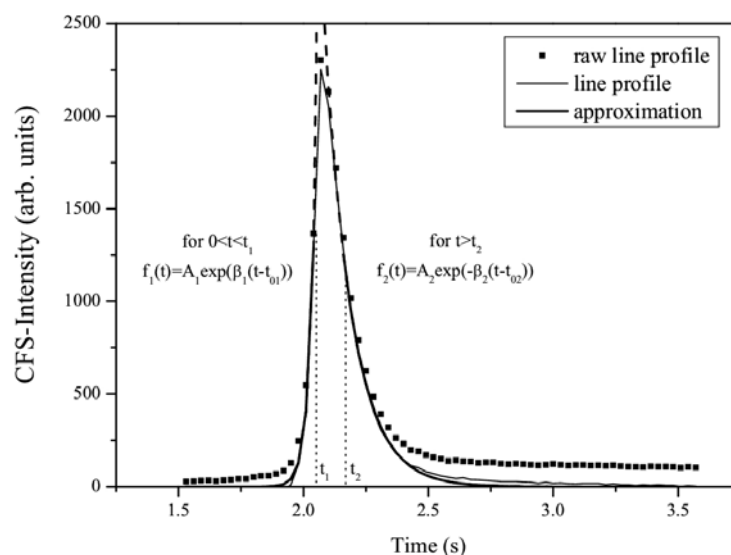


**Fig. A.3.3:** Approximation of the growth and the decay of the line profile after the subtraction of the background on the example of the resonance line of Fe 302.1 nm.

#### A.4 Estimations of analyte, modifier, and carbon vapor saturations

The saturation ratio [Hind] is defined as:

$$S = \frac{p}{p_s}, \quad (\text{A.4.1})$$

where  $p$  is the actual partial pressure and  $p_s$  is the saturation vapor pressure at the gas temperature. The saturation ratios for different temperatures during cool-down obtained with vapor pressure parameters given in Ref. [Land] are listed in Table A.4.1. The data are calculated for the monoatomic densities produced by vaporization of analytes, matrix modifiers, and GF carbon into Ar flow ( $200 \text{ mL min}^{-1}$ ) during one second. No reduction of vapor density either by condensation, chemical reactions, or by gas mixing is considered.

The supersaturation of the carbon vapor at the vaporization temperature shows that the carbon can be obtained in the form of polyatomic particulates even within the GF. Except for the high volatile analyte Pb and the elements in higher concentrations (K and Pd), self-nucleation, if this term is applicable, would be occur as a desublimation (gas-to-solid) process.

T, °C	500	750	1000	1250	1500	1750	2600	T <sub>sat</sub> , °C <sup>1)</sup>	T <sub>MP</sub> , °C <sup>2)</sup>
Pb <sup>3)</sup>	2.0E+00	1.5E-03	2.0E-05	1.1E-06	1.5E-07	3.3E-08		518	327.5
Mn		6.2E+00	1.0E-02	1.5E-04	9.8E-06	1.3E-06		810	1244
Cu			1.2E+00	1.2E-02	3.3E-04	2.4E-05	5.2E-08	1009	1083.4
Fe			1.1E+02	2.5E-01	3.3E-03	1.5E-04	1.2E-07	1184	1535
Ni			1.6E+02	3.2E-01	3.8E-03	1.6E-04	1.1E-07	1197	1453
K (1 µg)	4.6E-03	2.1E-04	3.4E-05					274	63.25
Pd (1 µg)					9.3E+00	4.0E-01	4.0E-04	1669	1554
C (7.1 µg) <sup>4)</sup>					3.2E+10	8.3E+07	7.2E+01	3288	3652 (sub)

<sup>1)</sup> temperature of saturation, extracted from Eq. A.4.1

<sup>2)</sup> data from Ref. [Weas]

<sup>3)</sup> for 1 ng of each analyte

<sup>4)</sup> ~½ GF mass loss per 1 s (see Sect. 3.5.1)

**Table A.4.1:** Saturation ratios obtained from Eq. A.4.1 for analytes, modifiers, and carbon densities under analytical conditions at different cool-down temperatures.

---

## References

---

- [Andr] J. C. de Andrade, F.C. Strong, and N. J. Martin, "*Rapid determination of zinc and iron in foods by flow-injection analysis with flame atomic-absorption spectrophotometry and slurry nebulization*", *Talanta* **37** (1990) 711-718.
- [Bats] S. Batsanov, "*Structural chemistry. Book of facts*", Dialog-MGU (2000).
- [Ber1] J. Bernhardt, T. Buchkamp, G. Hermann, G. Lasnitschka, "*Transport efficiencies and analytical determinations with electrothermal vaporization employing electrostatic precipitation and electrothermal atomic spectrometry*", *Spectrochim. Acta Part B* **54** (1999) 1821-1829.
- [Ber2] J. Bernhardt, T. Buchkamp, G. Hermann, G. Lasnitschka, "*Sample transport efficiency with electrothermal vaporization and electrostatic deposition technique in multi-element solid sample analysis of plant and cereal materials*", *Spectrochim. Acta Part B* **55** (2000) 449-460.
- [Buc1] T. Buchkamp, A. Garbrecht, G. Hermann, B. Kling, "*Size and distribution of particles deposited electrostatically onto the platform of a graphite furnace obtained using laser ablation sampling*", *Spectrochim. Acta Part B* **52** (1997) 1525-1533.
- [Buc2] T. Buchkamp and G. Hermann, "*Solid sampling by electrothermal vaporization in combination with electrostatic deposition for electrothermal atomization multi-element analysis*", *Spectrochim. Acta, Part B* **54** (1999) 657-668.
- [Buc3] T. Buchkamp, Dissertation, I. Physikalisches Institut der Justus-Liebig-Universität Giessen, in Arbeit.
- [Carn] G.R. Carnrick, B.K. Lomas and W.B. Barnett, "*Analysis of solid samples by graphite furnace atomic absorption spectrometry using Zeeman background correction*", *J. Anal. At. Spectrom.* **1** (1986) 443-447.
- [Chan] C.-C. Chang and S.-J. Jiang, "*Determination of copper, cadmium and lead in biological samples by electrothermal vaporization isotope dilution inductively coupled plasma mass spectrometry*", *J. Anal. At. Spectrom.* **12** (1997) 75-80.
- [Corn] A. Corney, B.P. Kibble and G.W. Series, "*The forward scattering of resonance radiation, with special reference to double resonance and level-crossing experiments*", *Proc. Roy. Soc. London A* **293** (1966) 70-93.
- [Dam1] S. Boonen, P. Verrept, L. Moens and R. Dams, "*Use of the simplified generalized standard additions method for calibration in solid sampling electrothermal*

- vaporization inductively coupled plasma atomic emission spectrometry", *J. Anal. At. Spectrom.* **8** (1993) 711-714.
- [Dam2] L. Moens, P. Verrept, S. Boonen, F. Vanhaecke and R. Dams, "Solid sampling electrothermal vaporization for sample introduction in inductively coupled atomic emission spectrometry and inductively coupled plasma mass spectrometry", *Spectrochim. Acta, Part B* **50** (1995) 463-475.
- [Dam3] F. Vanhaecke, S. Boonen, L. Moens and R. Dams, "Solid sampling electrothermal vaporization inductively coupled plasma mass spectrometry for the determination of arsenic in standard reference materials of plant origin", *J. Anal. At. Spectrom.* **10** (1995) 81-87.
- [Dam4] F. Vanhaecke, S. Boonen, L. Moens and R. Dams, "Isotope dilution as a calibration method for solid sampling electrothermal vaporization inductively coupled plasma mass spectrometry", *J. Anal. At. Spectrom.* **12** (1997) 125-130.
- [Davi] L.A. Davis, J.D. Winefordner, "Evaluation of a Voigt effect coherent forward scattering atomic spectrometer", *Anal. Chem.* **59** (1987) 309-312.
- [Donn] J.-B. Donnet, R.C. Bansal, M.-J. Wang, "Carbon Black. Science and Technology", Second Edition, Marcel Dekker, New York, USA (1993).
- [Edig] R.D. Ediger and S.A. Beres, "The role of chemical modifiers in analyte transport loss interferences with electrothermal vaporization ICP-mass spectrometry", *Spectrochim. Acta, Part B* **47** (1992) 907-922.
- [Fre1] A. Kazakov, H. Wang, and M. Frenklach, "Detailed modeling of soot formation in laminar premixed ethylene flames at a pressure of 10 bar", *Combustion and Flame* **100** (1995) 111-120.
- [Fre2] H. Wang and M. Frenklach, "A detailed kinetic modeling study of aromatics formation in laminar premixed acetylene and ethylene flames", *Combustion and Flame* **110** (1997) 173-221.
- [Fri1] R. S. Flagan and S. Friedlander, *Particle formation in pulverized coal combustion – a review*. Chap. 2 in D. T. Shaw, Ed., *Recent developments in Aerosol Science*, Wiley, New York (1978).
- [Fuch] N. A. Fuchs and A. G. Stutugin, *Highly dispersed aerosols*, Ann Arbor Science, London (1970).

- [Full] C. W. Fuller, R. C. Hutton and B. Preston, "*Comparison of flame, electrothermal and inductively coupled plasma atomisation techniques for the direct analysis of slurries*", *Analyst* **106** (1981) 913-920.
- [Gafu] M. Gafurov, SPECVIEW 3.0 for Windows, Program help, (2004).
- [Gre1] M.M. Lamoureux, D.C. Grégoire, C.L. Chakrabarti, and D.M. Goltz, "*Modification of a commercial electrothermal vaporizer for sample introduction into an inductively coupled plasma mass spectrometer. 1. Characterization*", *Anal. Chem.* **66** (1994) 3208-3216.
- [Good] Ph. Goodall, M.E. Foulkes and L. Ebdon, "*Slurry nebulization inductively coupled plasma spectrometry – the fundamental parameters discussed*", *Spectrochim. Acta Part B* **48** (1993) 1563-1577.
- [Gre2] D.C. Grégoire and R.E. Sturgeon, "*Analyte transport efficiency with electrothermal vaporization inductively coupled plasma mass spectrometry*", *Spectrochim. Acta Part B* **54** (1999) 773-786.
- [Gre3] D.M. Hughes, C.L. Chakrabarti, D.M. Goltz, D.C. Grégoire, R.E. Sturgeon and J.P. Byrne, "*Seawater as a multi-component physical carrier for ETV-ICP-MS*", *Spectrochim. Acta, Part B* **50** (1995) 425-440.
- [Gre4] M.W. Hinds, D.C. Grégoire and E.A. Ozaki, "*Direct determination of volatile elements in nickel alloys by electrothermal vaporization inductively plasma mass spectrometry*", *J. Anal. At. Spectrom.* **12** (1997) 131-135.
- [Hass] J. Hassler, A. Detcheva, O. Förster, P. Perzl, K. Flórian, "*Working with a modern ETV-device and an ICP-CID spectrometer*", *Annali di Chimica*, **89** (1999) 827-836.
- [Hind] W.C. Hinds, "*Aerosol Technology*", John Wiley & Sons, New York, USA (1982).
- [Hir1] I. Hirano, "*Magneto-optical spectra of the Cs D<sub>2</sub> line*", *J. Phys. B: At. Mol. Opt. Phys.* **26** (1993) 3479-3494.
- [Hir2] I. Hirano, "*Forward scattering magneto-optical spectra of the Cs D<sub>2</sub> line*", *Phys. Rev. A* **50** (1994) 4650-4656.
- [Hir3] I. Hirano, "*Forward-scattering magneto-optical effects*", *Phys. Rev. A* **52** (1995) 3594-3600.
- [Hir4] M. Namiki and K. Hirokawa, "*Coherent forward scattering spectrometry of rare earth elements using excitation by a continuum spectrum source*", *Fresenius Z. Anal. Chem.* **316** (1983) 795-796.



- [Hir5] K. Hirokawa, *"State of the art of coherent forward scattering spectroscopy"*, Fresenius Z. Anal. Chem. **324** (1986) 612-617.
- [Her1] G.Hermann, M.Gafurov, R.Matz, A.Trenin, W.Frech, E.Bjorn, A.Gilmutdinov, K.Nagulin, I.Grinshtein, L.Vasilieva, *"Platform-to-platform analyte transfer and handling system with sample pretreatment, splitting and micro-dosing via electrothermal vaporization and electrostatic re-precipitation"*, CSI-XXXIII, Coloquim Spectroscopicum Internationale (7.-12. September 2003, Granada, Spain) TH-P-39, 643-644
- [Her2] G. Hermann, *"Coherent Forward Scattering Spectroscopy (CFS): Present status and future perspectives"*, CRC Crit. Rev. Anal. Chem. **19** (1988) 323-377.
- [Her3] G. Hermann, M. Jung, G. Lasnitschka, R. Moder, A. Scharmann and X. Zhou, *"Multi-element determination on strong and weak lines by coherent forward scattering spectroscopy with continuum sources"*, Spectrochim. Acta, Part B **45** (1990) 763-768.
- [Her4] G. Hermann, *"Coherent forward scattering atomic spectrometry"*, Anal. Chem. **64** (1992) 571A-579A.
- [Her5] G. Hermann, *"ET-AAS oder CFS mit dem Kontinuumstrahler? - Chancen und Grenzen"*, Proc. Colloquium Analytische Atomspektroskopie, CANAS '95, Ed. B. Welz, Konstanz (1996) 61-67.
- [Her6] G. Hermann, *"Multi-element analysis with continuum source coherent forward scattering atomic spectrometry"*, oral presentation, XIVth Seminar on Atomic Spectrochemistry, September, 7-11, 1998, High Tatras - Podbánske, Slovak Republic.
- [Her7] W. Grimm, G. Hermann, M. Jung, R. Krüger, G. Lasnitschka, A. Scharmann and M. Seib, *"Coherent forward scattering spectrometry by means of a commercial furnace electromagnet unit "*, Spectrochim. Acta, Part B **43** (1988) 1269-1272.
- [Her8] G. Hermann, J. Bernhardt, T. Buchkamp, and G. Lasnitschka, *"Measurements employing electrothermal vaporization with electrostatic precipitation on the L'vov platform and the concept of a new axially focused convection vaporizer"*, XIVth Seminar on Atomic Spectrochemistry, September, 7-11, 1998 High Tatras - Podbánske, Slovak Republic.
- [Hol1] C.M. Sparks, J.A. Holcombe and T.L. Pinkston, *"Particle size distribution of sample transported from an electrothermal vaporizer to an inductively coupled plasma mass spectrometer"*, Spectrochim. Acta, Part B **48** (1993) 1607-1615.

- [Hol2] C.M. Sparks, J.A. Holcombe and T.L. Pinkston, "*Sample retention in the transport tubing between an electrothermal vaporizer and an inductively coupled plasma mass spectrometer*", Appl. Spectrosc. **50** (1996) 86-90.
- [Hol3] J.D. Venable, J.A. Holcombe, "*Signal enhancements produced from externally generated 'carrier' particles in electrothermal vaporization-inductively coupled plasma mass spectrometry*", Spectrochim. Acta, Part B **55** (2000) 753-766.
- [Hol4] D. Langer and J.A. Holcombe, "*Thermophoretic collection and analysis of submicrometer Ag particles emitted from a graphite tube-type electrothermal vaporizer*", Anal. Chem. **71** (1999) 582-588.
- [Iup1] IUPAC, Analytical Chemistry Division, Commission on Spectrochemical and Other Optical Procedures for Analysis, "*Nomenclature, symbols, units, and their usage in spectrochemical analysis: Part II. Data Interpretation*", Pure Appl. Chem. **45** (1976) 99-103.
- [Iup2] IUPAC, Analytical Chemistry Division, Commission on Spectrochemical and Other Optical Procedures for Analysis, "*Nomenclature, symbols, units, and their usage in spectrochemical analysis: Part III. Analytical Flame Spectroscopy and Associated Non-Flame Procedures*", Pure Appl. Chem. **45** (1976) 105-123.
- [Ito] M. Ito, "*Continuum spectrum source excited coherent forward scattering spectrometry for detection of elements*", Anal. Chem. **52** (1980) 1592-1595.
- [Jac1] M. W. Hinds, K. W. Jackson and A. P. Newman, "*Electrothermal atomisation atomic-absorption spectrometry with the direct introduction of slurries. Determination of trace metals in soil*", Analyst **110** (1985) 947-950.
- [Jac2] K. W. Jackson, "*Electrothermal Atomization for Analytical Atomic Spectrometry*", Wiley-VCH Verlag, Weinheim, Germany, 1999.
- [Kan1] T. Kántor, "*Interpreting some analytical characteristics of thermal dispersion methods used for sample introduction in atomic spectrometry*", Spectrochim. Acta, Part B **43** (1988) 1299-1320.
- [Kan2] T. Kántor, Gy. Záray, "*Graphite furnace for alternative combination with d. c. arc or inductively coupled plasma*", Fresenius J. Anal. Chem. **342** (1992) 927-935.
- [Kan3] T. Kántor and G. Záray, "*Improved design and optimization of an electrothermal vaporization system for inductively coupled plasma atomic emission spectrometry*", Microchem. J. **51** (1995) 266-277.

- [Kan4] G. Záray and T. Kántor, "*Direct determination of arsenic, cadmium, lead and zinc in soils and sediments by electrothermal vaporization and inductively coupled plasma excitation spectrometry*", Spectrochim. Acta, Part B **50** (1995) 489-500.
- [Kan5] T. Kántor, "*Optimization of the electrothermal vaporization conditions for inductively coupled plasma excitation spectrometry: Selective volatilization versus covolatilization approaches*", Fresenius Z. Anal. Chem. **355** (1996) 606-614.
- [Kan6] T. Kántor, Ş.Güçer, "*Efficiency of sample introduction into inductively coupled plasma by graphite furnace electrothermal vaporization*", Spectrochim. Acta Part B **54** (1999) 763-772.
- [Kan7] T. Kántor, "*Sample introduction with graphite furnace electrothermal vaporization into an inductively coupled plasma: effects of streaming conditions and gaseous phase additives*", Spectrochim. Acta, Part B **55** (2000) 431-448.
- [Kara] V. Karanassios, M. Abdullah and G. Horlick, "The application of chemical modification in direct sample insertion-inductively coupled plasma-atomic emission spectrometry", Spectrochim. Acta, Part B **45** (1990) 119-129.
- [Keit] Keithley Instruments Inc., "*DAS-1600 HC Series, User's Guide*" (1994).
- [Ker1] A.D. Kersey, J.B. Dawson and D.J. Ellis, "*The contributions of magnetically induced dichroism and the resonant Voigt effect to the detection of silver by atomic spectroscopy*", Spectrochim. Acta, Part B **35** (1980) 865-873.
- [Ker2] A.D. Kersey and J.B. Dawson, "*Comparison of detection limits in magnetically induced optical rotation and atomic-absorption spectroscopy*", Anal. Proc. R. Soc. Chem. **18** (1981) 187-189.
- [Kita] K. Kitagawa, T. Shigeyasu and T. Takeuchi, "*Application of the atomic Faraday effect to the trace determination of elements (Cd, Ag, and Cu) - effect of the hyperfine structure on the Zeeman splitting and line-crossing*", Spectrochim. Acta, Part B **34** (1979) 389-413.
- [Kri1] M. Hornung and V. Krivan, "*Determination of trace impurities in high-purity tungsten by direct solid sampling electrothermal atomic absorption spectrometry using a transversely heated graphite furnace*", Anal. Chem. **70** (1998) 3444-3451.
- [Kri2] K.-C. Friese and V. Krivan, "*A solid-sampling system for a transversely heated graphite furnace and its application to trace element analysis of high-purity tantalum powders by atomic absorption spectrometry*", Spectrochim. Acta, Part B **53** (1998) 1069-1078.

- [Kri3] M. Lucic and V. Krivan, *"Solid sampling electrothermal atomic absorption spectrometry for analysis of aluminium oxide powders"*, J. Anal. At. Spectrom. **13** (1998) 1133-1139.
- [Kri4] H.M. Dong, V. Krivan, B. Welz and G. Schlemmer, *"Determination of trace impurities in titanium dioxide by slurry sampling electrothermal atomic absorption spectrometry"*, Spectrochim. Acta, Part B **52** (1997) 1747-1762.
- [Kri5] M. Lucic and V. Krivan, *"Slurry sampling electrothermal atomic absorption spectrometry for the analysis of aluminum-based ceramic powders"*, Appl. Spectrosc. **52** (1998) 663-672.
- [Kri6] U. Schäffer and V. Krivan, *"A graphite furnace electrothermal vaporization system for inductively plasma atomic emission spectrometry"*, Anal. Chem. **70** (1998) 482-490.
- [Kri7] U. Schäffer and V. Krivan, *"Multielement analysis of graphite and silicon carbide by inductively coupled plasma atomic emission spectrometry using solid sampling and electrothermal vaporization"*, Anal. Chem. **71** (1999) 849-854.
- [Kur1] U. Kurfürst, *"Instrumental requirements, analytical performance and characteristics for the analysis of solid samples by GF-AAS"*, Fresenius Z. Anal. Chem. **328** (1987) 316-318.
- [Kur2] U. Kurfürst, *"Solid Sample Analysis: Direct and Slurry Sampling using GF-AAS and ETV-ICP"*, Springer-Verlag, Berlin, Heidelberg, New York (1998).
- [Kur3] U. Kurfürst, *"Statistical treatment of ETA-AAS (electrothermal atomisation - atomic absorption spectrometry) solid sampling data of heterogeneous samples"*, Pure Appl. Chem. **63** (1991) 1205-1211.
- [Lah1] J. Lahaye, *"Particulate carbon from the gas phase "*, Carbon **30** (1992) 309-314.
- [Lah2] J. Lahaye and F. Ehrburger-Dolle, *"Mechanism of carbon black formation. Correlation with the morphology of aggregates"*, Carbon **32** (1994) 1319-1324.
- [Lam] K.K.K. Lam and W.T. Chan, *"Novel laser sampling technique for inductively coupled plasma atomic emission spectrometry"*, J. Anal. At. Spectrom. **12** (1997) 7-12.
- [Land] Landolt-Börnstein, 6. Aufl. Bd. II/2a, Gleichgewichte Dampf-Kondensat und osmotische Phänomene, Eigenschaften der Materie in ihren Aggregatzuständen, Springer Verlag, Berlin (1960).

- [Lie1] T. Liebner und R. Buchhold, "*Datenstruktur für Parameter und Spektren des Multi 2 Programmpakets*", interne Dokumentation (1994).
- [Lie2] T. Liebner, "*Softwareentwicklung für die Steuerung eines Spektrometers zur Spurenanalyse mit kohärenter Vorwärtsstreuung und Linearisierung der Meßsignale*", Diplomarbeit, I. Physikalisches Institut der Universität Giessen (1994).
- [Lie3] T. Liebner, "*Das Auswerteprogramm des Multi2 Programmpakets*", interne Dokumentation (1995).
- [Lvov] B.V. Lvov, "*Recent advances in absolute analysis by graphite furnace atomic absorption spectrometry*", Spectrochim. Acta Part B **45** (1990) 633-655.
- [Lück] E. Lück, W. Kreuzer and C. Busche, "*Feststoffanalytik mit Autoprobe-GFAAS; Teil I. Zertifizierte und laborinterne standardisierte Referenzmaterialien*", Fresenius Z. Anal. Chem. **335** (1989) 176-188.
- [Mann] D.M. Mann, "*A possible first step in carbon particle formation*", J. Appl. Phys. **49** (1978) 3485-3489.
- [Manm] Manmatha Kumar Das, "*Die Entladung an der Spitze-Platte-Strecke in extrem reinen Edelgasen und deren Gemischen sowie mit Zusätzen elektronegativer Gase*", Zeitschrift für angewandte Physik **13** (1961) 410-415.
- [Mat1] R. Matz, G. Hermann, A. Trenin, "*Direct solid sampling analysis of atmospheric aerosols by employing electrostatic precipitation on graphite boats*", Coloquim Spectroscopicum Internationale CSI-XXXIII, Sept. 2003, p. 619.
- [Mat2] G. Hermann, R. Matz, A. Trenin, M. Gafurov, "*Electrostatic collection of atmospheric aerosols on graphite platforms for direct solid analysis*", Coloquim Spectroscopicum Internationale CSI-XXXIII, March 2005, p. 123.
- [Merm] P. Allain, L. Jaunault, Y. Mauras, J. M. Mermet, T. Delaporte, "*Signal enhancement of elements due to the presence of carbon-containing compounds in inductively coupled plasma mass spectrometry*", Anal. Chem. **63** (1991) 1497-1498.
- [Mil1] N.J. Miller-Ihli, "*Slurry sample preparation for simultaneous multi-element graphite furnace atomic absorption spectrometry*", J. Anal. At. Spectrom. **3** (1988) 73-81.
- [Mil2] N.J. Miller-Ihli, "*Graphite furnace atomic absorption spectrometry for the analysis of biological materials*", Spectrochim. Acta, Part B **44** (1989) 1221-1227.
- [Mil3] N.J. Miller-Ihli, "*Solids analysis by GFAAS*", Anal. Chem. **64** (1992) 965A-968A.

- [Mil5] R.W. Fonseca and N.J. Miller-Ihli, "*Analyte transport studies of aqueous solutions and slurry samples using electrothermal vaporization ICP-MS*", Appl. Spectrosc. **49** (1995) 1403-1410.
- [Mil6] R.W. Fonseca, N.J. Miller-Ihli, C. Sparks, J.A. Holcombe and B. Shaver, "*Effect of oxygen ashing on analyte transport efficiency using ETV-ICP-MS*", Appl. Spectrosc. **51** (1997) 1800-1806.
- [Moch] T. Mochizuki, A. Sakashita, H. Iwata, Y. Ishibashi, and N. Gunji, "*Application of slurry nebulization to trace elemental analysis of some biological samples by inductively coupled plasma mass spectrometry*", Analytical and Bioanalytical Chemistry **339** (1991) 889-894.
- [Moen] L. Moenke-Blankenburg, "*Laser-ICP-spectrometry*", Spectrochim. Acta Rev. **15** (1993) 1-37.
- [Moor] A.W. Moore, "*Highly oriented pyrolytic graphite and its intercalation compounds*", Chemistry and Physics of Carbon **17** (1981).
- [Mül1] G. Brunner, F. Korneck, G. Müller-Vogt, W. Wendl and W. Send, "*The application of sputtering as a new sampling technique in graphite furnace atomic absorption spectrometry*", Spectrochim. Acta, Part B **47** (1992) 1097-1105.
- [Mül2] G. Müller-Vogt, A. Huwe and W. Wendl, "*The use of sputtering as a solid sampling technique in graphite furnace atomic absorption spectrometry*", Spectrochim. Acta, Part B **51** (1996) 1191-1196.
- [Ort1] H.M. Ortner, E. Bulska, U. Rohr, G. Schlemmer, S. Weinbruch, and B. Welz, "*Modifiers and coatings in graphite furnace atomic absorption spectroscopy – mechanisms of action (A tutorial review)*", Spectrochim. Acta, Part B **57** (2002) 1835-1853.
- [Ort2] H. M. Ortner, U. Rohr, P Brückner, R. Lehmann, G. Schlemmer, U. Völlkopf, B. Welz und G. Feucht, "*Untersuchungen zur Graphitkorrosion mittels Gravimetrie und ETV-ICP-MS (Investigations of graphite tube corrosion by gravimetry and ETV-ICP-MS)*", CANAS'95 Colloquium Analytische Atomspektroskopie, Bodenseewerk Perkin-Elmer GmbH, 1996.
- [Per1] PerkinElmer Life and Analytical Sciences, "*Guide to Inorganic Analysis from the Leaders in AA, ICP-OES and ICP-MS*", PerkinElmer, Inc. USA (2004).
- [Per2] Bodenseewerk Perkin-Elmer GmbH, "*Zeeman/3030 Atomabsorptions-Spektrometer, Gerätehandbuch*" (1985).

- [Rus1] R.E. Russo, "*Laser Ablation*", Appl. Spectrosc. **49** (1995) 14A-28A.
- [Rus2] X.L. Mao, O.V. Borisov and R.E. Russo, "*Enhancements in laser ablation inductively coupled plasma-atomic emission spectrometry based on laser properties and ambient environments*", Spectrochim. Acta, Part B **53** (1998) 731-739.
- [Rus3] X.L. Mao, A.C. Ciocan and R.E. Russo, "*Preferential vaporization during laser ablation inductively coupled plasma atomic emission spectrometry*", Appl. Spectroscopy **52** (1998) 913-918.
- [Sato] T. Nakamura, H. Oka, H. Morikawa, and J. Sato, "*Determination of lithium, beryllium, cobalt, nickel, copper, rubidium, cesium, lead and bismuth in silicate rocks by direct atomization atomic absorption spectrometry*", Analyst **117** (1992) 131-135.
- [Sne1] J. Sneddon, "*Sample Introduction in Atomic Spectroscopy*", Elsevier, Amsterdam, The Netherlands (1990).
- [Sne2] J. Sneddon, "*Electrostatic precipitation atomic absorption spectrometry*", Appl. Spectroscopy **44** (1990) 1562-1565.
- [Sne3] J. Sneddon, "*Direct and near-real-time determination of lead, manganese and mercury in laboratory air by electrostatic precipitation-atomic absorption spectrometry*", Anal. Chim. Acta **245** (1991) 203-206.
- [Ste1] J. Kankare and R. Stephens, "*The calculation of absolute intensities observed due to magneto-optic rotation in atomic vapors*", Appl. Spectrosc. **34** (1980) 590-594.
- [Ste2] J. Kankare and R. Stephens, "*Signal-to-noise ratio characteristics of the atomic Voigt effect*", Spectrochim. Acta, Part B **38** (1983) 1301-1309.
- [Tor1] R. Torge, Project Report Fa, Carl Zeiss Oberkochen, 1980.
- [Tor2] Personal communication, 1997.
- [Tors] G. Torsi and F. Palmisano, "*Particle collection mechanism and efficiency in electrostatic accumulation furnace for electrothermal atomic spectrometry*", Spectrochim. Acta, Part B **41** (1986) 257-264.
- [Wann] B. Wanner, P. Richner, B. Magyar, "*The role of modifiers in electrothermal vaporization inductively coupled plasma mass spectrometry (ETV-ICP-MS) for the determination of B, La and U*", Spectrochim. Acta, Part B **51** (1996) 817-827.
- [Weas] R.C. Weast, "*CRC Handbook of Chemistry and Physics*", 67<sup>th</sup> Edition, CRC Press, Inc., Boca Raton, USA (1987).

- [Weis] G. L. Weissner, "*Positive and negative Point-to-Plane Corona in Pure and Impure Hydrogen, Nitrogen, and Argon*", *Physical Review* **63** (1943) 96-107.
- [Weiß] Ch. Weißmantel, C. Hamann, "*Grundlagen der Festkörperphysik*", 4. bearb. Auflage, Barth Verlag, Heidelberg (1995).
- [Wel1] U. Voellkopf, Z. Grobanski, R. Tamm and B. Welz, "*Solid sampling in graphite furnace AAS using the central probe technique*", *Analyst* **10** (1985) 573-577.
- [Wel2] B. Welz, M. Sperling, "*Atomabsorptionsspektrometrie*", 4. Neubearb. Aufl., Wiley-VCH, Weinheim, Germany (1997).
- [Win1] L.A. Davis, R.J. Krupa and J.D. Winefordner, "*Evaluation of a laser excited Voigt effect coherent forward scattering atomic spectrometer*", *Spectrochim. Acta, Part B* **41** (1986) 1167-1174.
- [Win2] S.A. Baker, B.W. Smith and J.D. Winefordner, "*Laser ablation inductively coupled plasma mass spectrometry with a compact laser source*", *Appl. Spectrosc.* **51** (1997) 1918-1921.
- [Yam1] M. Yamamoto and S. Murayama, "*Analysis of resonant Voigt effect*", *J. Opt. Soc. Am.* **69** (1979) 781-786.
- [Yam2] M. Yamamoto, J. Hanari and Y. Takubo, "*Analytical detection sensitivity of the laser-probed resonant Voigt effect*", *J. Opt. Soc. Am. B* **3** (1986) 1245-1250.



---

## List of publications

---

### Referenced journals

1. G. Hermann, G. Lasnitschka, R. Matz, A. Trenin, W. Moritz, “*Sampling of atmospheric aerosols by electrostatic precipitation for direct analyses*”, Environmental Science and Pollution Research, Special Issue **4** (2002) 83-91.
2. G. Hermann, A. Trenin, R. Matz, M. Gafurov, A. Gilmutdinov, K. Nagulin, W. Frech, E. Björn, I. Grinshtein, L. Vasilieva, “*Platform-to-platform sample transfer, distribution, dilution, and dosing via electrothermal vaporization and electrostatic deposition*”, Spectrochim. Acta Part B **59** (2004) 737-748.
3. A. Trenin, M. Gafurov, A.Kh. Gilmutdinov, G. Hermann, “*Electrothermal vaporization with axially focusing convection upstream: effects of graphite furnace carbon,  $KNO_3$  and  $Pd(NO_3)_2$  modifiers on analyte transport*”, Spectrochim. Acta Part B (in preparation).
4. A. Trenin, G. Hermann, “*Modeling of the condensation process of sample analytes and graphite furnace carbon in the axially focusing convection upstream of the electrothermal vaporization unit*”, Spectrochim. Acta Part B (in preparation).

### Conference proceedings in journals

1. A. Trenin, K.Yu. Nagulin, A.Kh. Gilmutdinov, “*Development of a software package for the flame atomic absorption spectrophotometer SA-10MP (AO KOMZ)*”, Kogerentnaja Optika i Opticheskaja Spektroskopija (Coherent Optics and Optical Spectroscopy), Kazan, Russia (1998) 55-60 (in Russian).
2. A. Trenin, G. Hermann, A.Kh. Gilmutdinov, K.Yu. Nagulin, R. Matz, “*Analytical performance of an electrothermal vaporization unit with particle condensation inside an axially focusing convection zone*”, Kogerentnaja Optika i Opticheskaja Spektroskopija (Coherent Optics and Optical Spectroscopy), Kazan, Russia (2001) 69-76 (in Russian).
3. A. Trenin, G. Hermann, A.Kh. Gilmutdinov, K.Yu. Nagulin, “*An electrothermal vaporization instrument as a dosing tool for analysis of solid samples*”, Kogerentnaja Optika i Opticheskaja Spektroskopija (Coherent Optics and Optical Spectroscopy), Kazan, Russia (2001) 193-198 (in Russian).

## Conference proceedings

### 1999:

1. G. Hermann, T. Buchkamp, J. Bernhardt, K.Yu. Nagulin, A. Trenin, A.Kh. Gilmudinov, I. Grinsteyn, L. Vasilieva, E. Bjorn and W. Frech, “*Platform-to-platform sample transfer, distribution, dilution and dosing via electrothermal vaporization and deposition*”, Colloquium Spectroscopicum Internationale CSI XXXI, Sept. 1999, Ankara, Turkey.
2. K.Yu. Nagulin, A.Trenin, A.Kh.Gilmudinov, G.Hermann, “*Electrothermal vaporization and electrostatic deposition for pretreatment of solid samples*”, Colloquium Spectroscopicum International CSI XXXI, Sept. 1999, Ankara, Turkey.

### 2000:

3. T. Buchkamp, T. Dippel, G. Hermann, W. Krüger, G. Lasnitschka, R. Matz, A.Kh. Gilmudinov, K.Yu. Nagulin, A. Trenin, I. Grinsteyn, L. Vasilieva, E. Bjorn, W. Frech, “*Sample transfer and dosing with electrothermal vaporization and electrostatic precipitation on platforms for analytical spectroscopy*”, 6-th Rio Conference on Atomic Spectroscopy, Dec. 2000, Concepcion, Brazil.
4. T. Buchkamp, G. Hermann, W. Krüger, G. Lasnitschka, K.Yu. Nagulin, A. Trenin, A.Kh. Gilmudinov, I. Grinsteyn, L. Vasilieva, E. Björn and W. Frech, “*Platform-to-platform sample transfer, pretreatment and dosing system employing electrothermal vaporization and deposition*”, 4-th European Furnace Symposium (EFS), June 2000, Podbanske, Slovakia.

### 2001:

5. T. Buchkamp, G. Hermann, W. Krüger, G. Lasnitschka, R. Matz, W. Frech, E. Bjorn, A. Gilmudinov, K. Nagulin, A. Trenin, I. Grinsteyn, L. Vasilieva, “*Proben transfer und – dosierung mit elektrothermischer Verdampfung und elektrostatischer Abscheidung auf Grafit-Plattformen zur Analytischen Spektroskopie*”, Colloquium Analytische Atomspektroskopie CANAS '01, March 2001, Freiberg, Germany.
6. G. Hermann, T. Dippel, W. Krüger, G. Lasnitschka, R. Matz, A. Trenin, “*Analytik mit elektrostatisch abgeschiedenen Aerosolen*“, Colloquium Analytische Atomspektroskopie CANAS '01, March 2001, Freiberg, Germany.

**2002:**

7. G. Hermann, G. Lasnitschka, W. Krüger, R. Matz, A. Trenin, B. Höflich, H. Ortner, “*Analyses of atmospheric aerosols with electrostatically collected particulates*”, 7-th Rio Conference on Atomic Spectroscopy, April 2002, Florianopolis, Brazil.
8. G. Hermann, M. Gafurov, R. Matz, A. Trenin, W. Frech, E. Björn, A. Gilmutdinov, K. Nagulin, I. Grinshtein, L. Vasilieva, “*Micro-dosing of solids to GF platforms by means of electrostatic precipitation for solid sampling GF AAS (SSAAS)*”, 7-th Rio Conference on Atomic Spectroscopy, April 2002, Florianopolis, Brazil.
9. G. Hermann, M. Gafurov, R. Matz, A. Trenin, “*Diagnostics and improvement of electrothermal vaporization (ETV)*”, 7-th Rio Conference on Atomic Spectroscopy, Florianopolis, April 2002, Florianopolis, Brazil.
10. G. Hermann, M. Gafurov, R. Matz, A. Trenin, “*Diagnostics of particulates and transport efficiencies with a new construction and improvement of electrothermal vaporization (ETV)*”, 16-th Slovak Spectroscopic Conference, June 2002, Košice, Slovakia.
11. G. Hermann, M. Gafurov, R. Matz, A. Trenin, W. Frech, E. Björn, A. Gilmutdinov, K. Nagulin, I. Grinshtein, L. Vasilieva, “*Pretreatment, splitting, and micro-dosing of solid samples with electrothermal vaporization and electrostatic re-precipitation*”, 16-th Slovak Spectroscopic Conference, June 2002, Košice, Slovakia.
12. G. Hermann, G. Lasnitschka, W. Krüger, R. Matz, A. Trenin, B. Höflich, H. Ortner, “*Electrostatic sampling and analysis of atmospheric aerosols*”, 16-th Slovak Spectroscopic Conference, June 2002, Košice, Slovakia.
13. G. Hermann, M. Gafurov, R. Matz, A. Trenin, “*Investigation and improvement of an electrothermal vaporization system (ETV) by means of electrostatic precipitation of the particulates*”, 5-th European Furnace Symposium and 10-th International solid Sampling Colloquium with Atomic Spectroscopy, Sept. 2002, Blagoevgrad, Bulgaria.
14. G. Hermann, M. Gafurov, R. Matz, A. Trenin, W. Frech, E. Björn, A. Gilmutdinov, K. Nagulin, I. Grinshtein, L. Vasilieva, “*Platform-to-platform analyte transfer and handling system with sample pretreatment, splitting, and micro-dosing via electrothermal vaporization and electrostatic re-precipitation*”, 5-th European Furnace Symposium and 10-th International solid Sampling Colloquium with Atomic Spectroscopy, Sept. 2002, Blagoevgrad, Bulgaria.

15. G. Hermann, G. Lasnitschka, W. Krüger, R. Matz, A. Trenin, B. Höflich, H. Ortner, “*Electrostatic collection of atmospheric aerosols for analyses*”, 5-th European Furnace Symposium and 10-th International solid Sampling Colloquium with Atomic Spectroscopy, Sept. 2002, Blagoevgrad, Bulgaria.

**2003:**

16. G. Hermann, R. Matz, A. Trenin, “*Test und Optimierung einer elektrothermischen Verdampfungseinrichtung mit Hilfe eines elektrostatischen Partikelsammlers*“, Colloquium Analytische Atomspektroskopie CANAS '03, March 2003, Konstanz, Germany.
17. G. Hermann, M. Gafurov, R. Matz, A. Trenin, “*Elektrostatische Sammlung Atmosphärischer Aerosole auf Graphite Plattformen für die direkte Feststoffanalyse*“, Colloquium Analytische Atomspektroskopie CANAS '03, March 2003, Konstanz, Germany.
18. G. Hermann, M. Gafurov, R. Matz, A. Trenin, “*Investigation and improvement of electrothermal vaporization unit by means of electrostatic precipitation of the particulates*“, Colloquium Spectroscopicum Internationale CSI-XXXIII, Sept. 2003, Granada, Spain (invited lecture).
19. R. Matz, G. Hermann, A. Trenin, “*Direct solid sampling analysis of atmospheric aerosols by employing electrostatic precipitation on graphite boats*“, Colloquium Spectroscopicum Internationale CSI-XXXIII, Sept. 2003, Granada, Spain.
20. G. Hermann, M. Gafurov, R. Matz, A. Trenin, W. Frech, E. Bjorn, A. Gilmutdinov, K. Nagulin, I. Grinshtein, L. Vasilieva, “*Platform-to-platform analyte transfer and handling system with sample pretreatment, splitting and micro-dosing via electrothermal vaporization and electrostatic re-precipitation*“, Colloquium Spectroscopicum Internationale CSI-XXXIII, Sept. 2003, Granada, Spain.
21. A. Trenin, G. Hermann, M. Gafurov, R. Matz, B. Höflich, H. Ortner, “*Development and Characterization of a New Electrothermal Vaporization Unit Based on Condensation in an Axially Focusing Convection Flow*“, Colloquium Spectroscopicum Internationale CSI-XXXIII, Sept. 2003, Granada, Spain.
22. A. Trenin, G. Hermann, M. Gafurov, R. Matz, “*Investigation and optimization of a new electrothermal vaporization unit with analyte vapor condensation in an axially focusing upstream convection zone*“, 30th Annual Meeting of Federation of Analytical Chemistry and Spectroscopy Societies (FACSS), Oct. 2003, Ft. Lauderdale, FL, USA (oral presentation).

23. A. Trenin, G. Hermann, R. Matz, A. Gilmutdinov, K. Nagulin, W. Frech, E. Björn, *“Platform-to-platform sample transfer and handling system with distribution, dilution, and micro-dosing via electrothermal vaporization and electrostatic re-precipitation”*, 30th Annual Meeting of Federation of Analytical Chemistry and Spectroscopy Societies (FACSS), Oct. 2003, Ft. Lauderdale, FL, USA (poster presentation).

**2004:**

24. A. Trenin, M. Gafurov, R. Matz, G. Hermann, *“A new upstream electrothermal vaporization unit: effects of carbon-containing compounds and matrix/carrier modifiers on analyte transport efficiency”*, Analytica Conference, May 2004, Munich, Germany (poster presentation).
25. G. Hermann, R. Matz, A. Trenin, M. Gafurov, *“Analyses of atmospheric aerosols by employing electrostatic precipitation on the graphite boats in a portable box”*, 6-th European Furnace Symposium (EFS), June 2004, Balatonföldvár, Hungary.
26. A. Trenin, M. Gafurov, R. Matz, G. Hermann, *“Electrothermal vaporization: effects of carbon-containing compounds and sample/carrier modifiers on analyte transport efficiency”*, 6-th European Furnace Symposium (EFS), June 2004, Balatonföldvár, Hungary.
27. G. Hermann, A. Trenin, *“Design and properties of electrothermal vaporization equipment”*, 8-th Rio Conference on Atomic Spectroscopy, August 2004, Paraty, Rio de Janeiro, Brazil (invited lecture).
28. G. Hermann, R. Matz, A. Trenin, M. Gafurov, *“Portable equipment for electrostatic collection of atmospheric aerosols on graphite platforms for direct analysis”*, 8-th Rio Conference on Atomic Spectroscopy, August 2004, Paraty, Rio de Janeiro, Brazil.
29. G. Hermann, A. Trenin, *“A new electrothermal vaporization unit with high transport efficiencies of low dependence on analyte element and matrix”*, 8-th Rio Conference on Atomic Spectroscopy, August 2004, Paraty, Rio de Janeiro, Brazil.
30. A. Trenin, M. Gafurov, R. Matz, G. Hermann, *“Effects of carbon-containing compounds and matrix/carrier modifiers on analyte transport efficiency for electrothermal vaporization”*, 8-th Rio Conference on Atomic Spectroscopy, August 2004, Paraty, Rio de Janeiro, Brazil.

31. A. Trenin, M. Gafurov, and G. Hermann, “*An electrothermal vaporization device with more equal analyte transport efficiencies*”, XVIIth Slovak Spectroscopic Conference, Sept. 2004, The High Tatras, Slovakia.
32. G. Hermann, R. Matz, A. Trenin, and M. Gafurov, “*Analyses of atmospheric aerosols with electrostatic precipitation of particulates*”, XVIIth Slovak Spectroscopic Conference, Sept. 2004, The High Tatras, Slovakia.

**2005:**

33. A. Trenin, M. Gafurov, G. Hermann, “*ETV with axially focusing convection upstream and effects of GF carbon and modifiers on analyte transport*”, Colloquium Analytische Atomspektroskopie CANAS '05, March 2005, Freiberg, Germany.
34. G. Hermann, R. Matz, A. Trenin, M. Gafurov, “*Electrostatic collection of atmospheric aerosols on graphite platforms for direct solid analysis*”, Colloquium Analytische Atomspektroskopie CANAS '05, March 2005, Freiberg, Germany.
35. A. Trenin, M. Gafurov, G. Hermann, “*A newly developed upstream electrothermal vaporization device for direct solid sampling*”, Beijing Conference and Exhibition on Instrumental Analysis BCEIA, Oct. 2005, Beijing, China (invited lecture).
36. G. Hermann, R. Matz, A. Trenin, M. Gafurov, “*Electrostatic collection of atmospheric aerosols for direct solid sampling analyses*”, Beijing Conference and Exhibition on Instrumental Analysis BCEIA, Oct. 2005, Beijing, China.

**2006:**

37. A. Trenin, G. Hermann, “*A new upstream electrothermal vaporization (ETV) device – properties and understanding of analyte condensation and transport*”, International Congress on Analytical Sciences (ICAS), June 2006, Moscow, Russia (in preparation) (invited lecture).
38. A. Trenin, G. Hermann, “*Modeling of the condensation process in an AFC upstream electrothermal vaporization (ETV) device*”, International Congress on Analytical Sciences (ICAS), June 2006, Moscow, Russia (in preparation).
39. G. Hermann, A. Trenin, “*Understanding and optimization of the process of aerosol generation in ETV system*”, 7<sup>th</sup> European Furnace Symposium Atomic Absorption Spectrometry (EFS) and 12<sup>th</sup> Solid Sampling Colloquium with Atomic Spectrometry (SSC), July 2006, St. Petersburg, Russia (in preparation) (invited lecture).

---

## Curriculum Vitae

---

### Angaben zur Person:

Name: Alexander Trenin  
Geburtsdatum, Ort: 08.03.1977 in Kasan, Russische Föderation  
Familienstand: verheiratet, ein Sohn, 4 J. alt  
Staatsangehörigkeit: Russische Föderation

### Ausbildung:

Schule	Grund- und Oberschule in Kasan,	1984 – 92
	Gymnasium bei der Staatlichen Universität Kasan,	1992 – 94
Hochschule	Studium an der Staatlichen Universität Kasan,	1994 – 99
	Fachrichtungen: Physik, Mathematik und Informatik	
	Schwerpunkte: Radiophysik und Elektronik, Optik und Spektroskopie, mathematische Modellierung, Programmiersprachen	
Abschluss	am 11.06.1999, Master Diplom mit Auszeichnung	

### Weiterbildung:

01.11.99 – 28.02.01	Aspirantur bei der Staatlichen Universität Kasan
01.08.00 – 31.07.01	DAAD-Jahresstipendium für Forschungsstudium am I. Physikalischen Institut der Justus-Liebig-Universität Gießen, BRD
01.06.01 – 31.05.06	Wissenschaftlicher Mitarbeiter am I. Physikalischen Institut Thema der Doktorarbeit: „Entwicklung, Untersuchung und Optimierung einer elektrothermischen Verdampfungseinrichtung mit einer axial - fokussierenden Aufwärtsströmung für die Analyse von Spurenelementen“
Juni 2006	voraussichtliche Promotion

### Berufserfahrung:

01.11.98 – 31.07.00	Informatiklehrer im Gymnasium, Kasan
---------------------	--------------------------------------

---

## Danksagung

---

Die vorliegende Arbeit wurde an der Physikalischen Fakultät der Staatlichen Universität Kasan angefangen und am I. Physikalischen Institut der Justus-Liebig-Universität Gießen fortgesetzt und anschließend angefertigt.

Ich danke besonders meinen verehrten Lehrern, dem Leiter der Abteilung „Optische Spektroskopie“ am I. Physikalischen Institut, Herrn Prof. Dr. Gerd Hermann und dem Leiter der Abteilung „Analytische Atomspektroskopie“ beim Departement der Allgemeinen Physik an der Physikalischen Fakultät, Herrn Prof. Dr. Albert Kh. Gilmudinov, für die zahlreichen, wertvollen und aufschlussreichen Diskussionen und fruchtbaren Anregungen während der Durchführung der Arbeit sowie für die Bereitstellung der benötigten finanziellen und technischen Mitteln.

Mein besonderer Dank gebührt den Mitglieder der Abteilung von Herrn Prof. Dr. G. Hermann, Herrn Dr. M. Gafurov, Herrn R. Matz und Herrn Dr. G. Lasnitschka, sowie die Mitglieder der Abteilung von Herrn Prof. Dr. A.Kh. Gilmudinov, Herrn Dr. K.Yu. Nagulin und Herrn Dr. Yu.N. Zakharov, für die zahlreichen Ratschläge und hilfreichen Diskussionen im Laufe dieser Arbeit sowie für die Unterstützungen und das gute und produktive Arbeitsklima.

Mein besonderer Dank gebührt der Sekretärin der Abteilung „Optische Spektroskopie“ am I. Physikalischen Institut, Frau S. Hofmann, für ein gemütliches und häusliches Klima in der Abteilung.

Besonders möchte ich mich beim Geschäftsführenden Direktor des I. Physikalischen Instituts, Herrn Prof. Dr. Bruno K. Meyer, sowie bei den Institutsmitgliedern, Herrn Dr. E. Pitt, Herrn Dr. A. Hofstaetter, Herrn Dr. M. Böhm, Herrn H.P. Jorde, und bei allen Institutsangehörigen bedanken.

Zu höchstem Dank bin ich meinem Doktorvater, Herrn Prof. Dr. Gerd Hermann und seiner Ehefrau Inge Hermann, verpflichtet, die mich und meine Familie während unseres Aufenthalts in Deutschland bei allen wichtigen Episoden unseres Lebens immer unterstützt haben.

Zu höchstem Dank bin ich außerdem meiner Ehefrau Irina und meiner Mutter Eugenia verpflichtet, die mich immer sehr unterstützt haben.



Ich versichere, dass ich die vorliegende Arbeit selbständig verfasst und keine anderen als die angegebenen Quellen und Hilfsmittel verwendet habe. Diese Arbeit hat in gleicher oder ähnlicher Form noch keiner anderen Prüfungsbehörde vorgelegen.

Gießen, im Juni 2006

---

Alexander Trenin, M.Sc. (Physik)